TWO NEW, SINGLE-ISOMER, SULFATED β-CYCLODEXTRINS FOR USE AS

CHIRAL RESOLVING AGENTS FOR ENANTIOMER SEPARATIONS IN

CAPILLARY ELECTROPHORESIS

A Dissertation

by

MICHAEL BRENT BUSBY

Submitted to the Office of Graduate Studies of
Texas A&M University
in partial fulfillment of the requirements for the degree of

DOCTOR OF PHILOSOPHY

May 2005

Major Subject: Chemistry

TWO NEW, SINGLE-ISOMER, SULFATED β-CYCLODEXTRINS FOR USE AS

CHIRAL RESOLVING AGENTS FOR ENANTIOMER SEPARATIONS IN

CAPILLARY ELECTROPHORESIS

A Dissertation

by

MICHAEL BRENT BUSBY

Submitted to the Office of Graduate Studies of
Texas A&M University
in partial fulfillment of the requirements for the degree of

DOCTOR OF PHILOSOPHY

Approved as to style and content by:

_____
Gyula Vigh
(Chair of Comittee)

_____
Frank Raushel
(Member)

_____
David Ford
(Member)

_____
Manuel Soriaga
(Member)

_____
Emile Schweikert
(Head of Department)

May 2005

Major Subject: Chemistry

ABSTRACT

Two New, Single-Isomer, Sulfated β Cyclodextrins for Use as Chiral Resolving Agents

for Enantiomer Separations in Capillary Electrophoresis. (May 2005)

Michael Brent Busby, B.S., University of Texas at Tyler; M.S., Texas A&M University

Chair of Advisory Committee: Dr. Gyula Vigh

Two novel, single-isomer, sulfated cyclodextrins, the sodium salts of heptakis(2-*O*-methyl-3-*O*-acetyl-6-*O*-sulfo)cyclomaltoheptaose (HMAS) and heptakis(2-O-methyl-6-O-sulfo)cyclomaltoheptaose (HMS) were used as chiral resolving agents in both aqueous and non-aqueous electrophoretic separation of a set of pharmaceutically active weak base enantiomers. Enantiomers of twenty one of the twenty four weak bases were baseline resolved in one or more of the background electrolytes (BGE's) used.

An eight-step synthetic method was used to produce, on a large scale, the title compounds in greater than 97% purity. The purity of the synthetic intermediates and the final products were characterized by HPLC-ELSD and indirect UV-detection capillary electrophoresis (CE), respectively. X-ray crystallography, MALDI-TOF mass spectrometry and ^{1}H as well as ^{13}C NMR spectroscopy allowed for unambiguous characterization of the structure of each intermediate and the final product.

To my wife, Carol, whom I love with all my heart and to my children, Mackenzie, Krista and Paula. They bring me endless joy.

ACKNOWLEDGMENTS

TABLE OF CONTENTS

LIST OF FIGURES

FIGURE   Page

LIST OF TABLES

CHAPTER I

INTRODUCTION

1.1 Cyclodextrins as Chiral Resolving Agents

Cyclodextrin-based enantiomer separations are of continued interest to the

separation science community. Cyclodextrin-based enantiomer separations can be

accomplished by gas chromatography [1], liquid chromatography, including normal [2]

and reversed phase [3] and ion-chromatography [4], as well as electrophoretic techniques

including, capillary electrophoresis (CE) [5] , capillary isotachophoresis [6], free-flow

electrophoresis [7], and isoelectric focusing [8,9]. Compared to other enantiomer

separation technologies, CE is of the greatest importance to the pharmaceutical industry

where a large percentage of target molecules are chargeable, basic or acidic compounds.

For analytical application, CE is lowest in materials consumption and is less susceptible

to the various band broadening mechanisms that are inherent to gas chromatography

(GC) and high performance liquid chromatography (HPLC) [10]. CE does not require the

presence of a stationary phase to accomplish separation, unlike GC and HPLC, and only

a background electrolyte (BGE) containing dissolved buffer components and a chiral

selector, need to be prepared.

Cyclodextrins (CDs) serve as chiral complexing agents in CE where the

differences in the charge-to-mass ratio of the diastereomeric complexes can be

———————

This dissertation follows the style of *Electrophoresis*.

distinguished. Cyclodextrins used for CE enantiomer separations include the native species as well as those modified with various ionizable and non-ionizable functional groups. Neutral cyclodextrins include native α-, β- and γ-CDs and those functionalized with either methyl, acetyl or hydroxypropyl groups. Derivatives of β-CD are commonly used for CE because of lower cost, greater commercial availability and higher aqueous solubility compared to α-CD, γ-CD or their derivatives. Also, native CDs exhibit lower aqueous solubilities than their functionalized derivatives: the solubility of β-CD is only 16-mM [11,12]. For these reasons, 2,6-dimethyl-β-CD, 2,3,6-trimethyl-β-CD and hydroxypropyl-β-CD are among the most popular neutral cyclodextrin-based chiral resolving agents.

Neutral CDs are not applicable for the analysis of neutral enantiomers. Charged cyclodextrins are cyclodextrins modified to have either weakly or strongly acidic or basic functionalies. Charged CDs extend the applicability of CE to uncharged enantiomers. Typical examples of the weakly acidic and weakly basic functionalized CDs are carboxylic acid and trialkylamine derivatives, respectively. The charge state of the weakly acidic and basic CDs is pH dependent as is separation selectivity. The result is more difficult method development than what is available with strongly acidic and basic CDs [13]. The strongly acidic and strongly basic CDs are permanently charged over the entire working pH range (pH 2-12) of CE and include sulfated CDs and those with quaternary ammmonium functionalities, respectively. Use of the permanently charged CDs allows for development of more robust separations where the conditions do not have to be modified to suit the charge-state of the chiral resolving agent [14].

Sulfated CDs are often more desirable for use in CE than those with quaternary ammonium functional groups. Positively charged CDs have been shown to produce a low efficiency mix of CE and open tube liquid chromatography due to adsorption of the CD to the capillary wall. A model proposed by O'Keefe et al. [15] considers that the CD is tightly bound to the fused silica capillary wall yielding an overall fixed positive charge at the capillary surface. The result is increased band broadening due to chromatographic retention of the analytes and reversal of the electroosmotic flow (EOF) to a positive value. Polyacrylamide coatings have been employed to reduce the effects of chromatographic band broadening due to wall adsorption of the positively charged chiral additive [16]. Anionic CDs do not exhibit the same wall coating tendency characteristic of basic CDs so that capillary coatings are not required to prevent decreases in separation efficiency [17].

All CDs thus far mentioned are commercially available as random mixtures of isomers, characterized by their average degree of substitution. The composition of the randomly substituted material varies from batch to batch, in both the population of the various charged species and their relative proportions. Use of these cyclodextrins introduces a significant degree of uncertainty into any analysis, since the mobility [18, 19], resolution [20] and indeed, the order of migration [21-25] of the enantiomers is dependent on the molecular interaction of the enantiomers and the cyclodextrin additive. Inhomogeneous materials received from the manufacturer result in run-to-run variations. The only solution to this problem is the use of a consistently well characterized material. The best solution to this is the use of single-isomer, sulfated cyclodextrins (SISCDs).

1.2 Synthesis of Single-Isomer, Sulfated Cyclodextrins

Four different synthetic strategies for producing fully functionalized single-isomer cyclodextrins have been reported in the literature: i) one-step exhaustive per-functionalization; ii) four step bi-functionalization of all hydroxy groups at the C2 and C3 positions with identical functionality but different from that of the C6 position; iii) five step bi-functionalization of all hydroxy groups at the C3 and C6 with identical functionality but different from that of the C2 position; iv) five step functionalization at the C2, C3 and C6 positions with all different groups. Attempts to produce a single-isomer per-sulfated cyclodextrin using a one-step synthesis have thus far proven unsucccessful [26]. Development of conditions using silyl-ether protecting groups for selective modification [27-32] of CD's first heralded access to strategies ii) and iii) and since has been successfully used to produce 10 different SISCD's [14, 33-52] useful for CE enantiomer separations. Numerous asymmetrically substituted CD derivatives have been produced using strategy iv). None are of the sulfated type and all offer low yields since they typically use poorly regioselective reaction conditions to functionalize the C2 hydroxy group in the presence of an unprotected C3 hydroxy group [31, 53]. An alternative to this strategy is to protect the C2 position as a silyl-ether that can be removed without concurrent deprotection of the already protected C6 position. Functionalization of the C2 position can then be conducted using a suitable electrophile like iodomethane in the presence of sodium hydride. This allows desired functionalization of the C2 position via an intra-glucosidic silyl-ether migration mechanism [53-57]. Subsequent deprotection steps can then be conducted to allow

functionalization of the C3 and C6 positions, independently of one another. This strategy uses highly regioselective reaction conditions to potentially produce the first unsymmetrically substituted SISCD in yields that are significantly higher than those previously reported.

1.3 Use of SISCD's for Enantiomer Separations by CZE

SISCDs have been proven to be reliable, effective means for robust CE enantiomer separations methods [14,33]. Several SISCDs have been used to screen sets of structurally similar chiral acids, bases, neutrals and ampholytics under variable CD concentrations and pH conditions in aqueous [34-37] and methanolic [38-42] background electrolytes (BGE's) as well as in hydro-organic media [43]. Heptakis(2,3-di-*O*-acetyl-6-*O*-sulfo)cyclomaltoheptaose (HDAS) [36] and the corresponding dimethyl, HDMS [46], and dihydroxy, HS [37], homologs were the first SISCDs used for such chiral separations. Further research led to development of the analogous α- [34,44,45] and γ-CD [47-50] derivatives. Another, heptakis(2-*O*-methyl-3,6-di-*O*-sulfo)cyclomaltoheptaose (HMDS) [51,52], has also been shown to be effective the for separation of pharmaceutically active weak bases and is thus far the only SISCD unsymmetrically substituted at the 2- and 3-position of the CD backbone.

Observed migration of an enantiomer is the sum of the enantiomers effective mobility (μ^{eff}) and the non-discriminate electroosmotic flow (μ^{eo}):

$$\mu^{obs} = \mu^{eff} + \mu^{eo} \tag{1}$$

where μ^{obs} is the observed mobility and defined as the constant of proportionality

between the velocity (v) of an ion in an applied electric field (E).

$$v^{obs} = \mu^{obs}E^{appl} \tag{2}$$

According to Stokes, mobility is a function of the ratio of ionic charge (z) to hydrodynamic radius (a) and viscosity (η) of the BGE.

$$\mu = ze_o/6\pi\eta a \tag{3}$$

where e_o is the elementary charge constant.

Critical to rational method development for enantiomer separations is the relationship between the effective mobility of the enantiomer and the concentration of the SISCD. The Wren and Rowe model of enantiomer separations by CE showed that, in the case of neutral cyclodextrins, there exists an optimum CD concentration equal to the inverse root of the multiple of the two enantiomer-CD binding constants [58-61].

$$[C]^{opt} = (K_1K_2)^{-\frac{1}{2}} \tag{4}$$

where K_1 and K_2 are CD binding constants for the two enantiomers. At the optimum CD concentration the enantiomers exhibit a maxima in the mobility difference vs. concentration plot. Initial trials using native β-CD and randomly methylated β-CD showed good agreement with the predictions of the model. However, the model is overly simplified and asserts that the mobilities of enantiomer-CD complexes are equal. Also, the model is limited since it does not take into consideration the effects of other parameters including pH, electric field strength or electroosmotic mobility.

A more inclusive model proposed by Rawjee et al. takes into account the effect of pH on separation selectivity [62-64]. This model proposes that there are three distinct types of enantiomer separations: ionoselective, desionoselective and duoselective

enantiomer separations. In each case, separation selectivity is a function of the infinite

dilution ionic mobilities of the free and complexed enantiomers, the equilibrium binding

constants, the acid dissociation constant of the enantiomers, the pH and the cyclodextrin

concentration. The model shows that categorizing separations of weakly acidic or weakly

basic enantiomer pairs in this manner aids the selection of the optimum pH conditions

and CD concentration of the BGE .

1.3.1 The Greater Significance of the Electroosmotic Flow

In CE, electroosmotic flow is the bulk flow of the BGE in the presence of an

electric field due to a potential at the surface of the fused silica capillary referred to as

the zeta potential (ζ). The potential arises from an immobile net negative charge at the

capillary surface due to dissociation of the silanol groups formed in the hydrolysis of

fused silica . According to the Stern model [65,66], the magnitude of the surface

potential is greatest at the capillary surface and decays logarithmically with increasing

distance from the capillary surface. The same model proposes a shear plane between a

very tightly bound layer of solvated counterions immediately adjacent to the capillary

wall, referred to as the Helmholtz plane, and a diffuse layer of solvated counterions with

an unbalanced surplus of mobile cations that extends radially from the capillary wall.

Under the influence of an applied electric field, the cationic counterions in the diffuse

layer migrate to the cathode. As they do, they drag with them their waters of hydration

resulting in a plug-like bulk flow toward the cathode with a velocity that is proportional

to the charge density at the shear plane (σ), the vacuum permittivity (ε_o), the applied

electric field (E), and the BGE's dielectric constant (ε), ionic strength (I), temperature (T), and viscosity (η),

$$v^{EOF} = E\ (\sigma/\eta)(\varepsilon_o\ \varepsilon RT/IF^2)^{1/2} \qquad (5)$$

where v_{EOF} is the velocity of the EOF and R and F are the gas law and Faraday's constants, respectively . This relation illustrates the importance of temperature control over the time course of a separation.

The greater significance of the EOF as pertains to enantiomer separations lies with the idea that if the electroosmotic mobility is equal in magnitude but opposite in direction to the mobility of the more slowly migrating enantiomer then infinite resolution of the enantiomers is possible. This notion was first incorporated in what is today known as the charged chiral resolving agent migration model [67-71] or CHARM for short. Predictions of CHARM are that enantiomer resolution increases with increasing applied electric field (E), increasing capillary length (l), decreasing temperature (T) and as separation selectivity (α) diverges away from unity,

$$Rs = \sqrt{\frac{Ele_o}{8kT}}\ \frac{(|a-1|)\sqrt{(a+b)}\sqrt{z_1^{eff}}\sqrt{z_2^{eff}}}{\sqrt{|(a+b)^3|}\sqrt{z_1^{eff}} + \sqrt{|a||(1+b)^3|}\sqrt{z_2^{eff}}} \qquad (6)$$

where k is the Boltzman constant, e_o is the fundamental charge and z^{eff} is the effective charge of the analyte. Here, separation selectivity (α) is defined as the ratio of the effective mobilities of the two enantiomers,

$$\alpha = \mu_1^{eff} / \mu_2^{eff} \qquad (7)$$

where subscripts one and two refer to the faster and slower enantiomers, respectively and β is the electroosmotic mobility normalized to the effective mobility of the slower

enantiomer,

$$\beta = \mu^{EO} / \mu_2^{eff} \qquad (8)$$

The resolution equation reflects that at constant α and z^{eff}, resolution approaches infinity

as the β value approaches -1 so that as long as α does not equal 1, resolution is possible.

Capillary coatings and BGE viscosity modifiers like hydroxymethylcellulose are used to

optimize the electroosmotic mobility for separations with α values that are very close to

unity.

1.3.2 Impact of Ionic Strength Effects on SISCD Enantiomer Separations

An appreciation of ionic strength effects in CE can be gained through an

understanding of the Debye-Huckel-Onsager theory and the model from which it is

derived. The model uses as its basis the Debye-Huckel theory of point charges. The

model is taken a step beyond in that it applies an electric field to the point charge and

observes that the spherical ionic cloud around the reference ion is distorted due to an

incomplete formation of the cloud in front of the migrating ion and an incomplete decay

of the ionic cloud behind the migrating ion. The result is an egg-shaped cloud with

charge center a finite distance behind the migrating ion. The deformed cloud exerts a

drag on the migrating ion in what is referred to as the relaxation effect. The result is that

mobilities decrease with increasing ionic strength. An empirical expression proposed by

Reijenga et al. [72-75] allows for use of CZE to measure directly the effect of ionic

strength on ionic mobility. The expression takes the form,

$$\mu = \mu_o \, \varepsilon \xi \pi (-\alpha(\zeta I)^{0.5}) \qquad (9)$$

where μ_o is the infinite dilution mobility, z is the charge and a is a constant that takes the

value a = 0.5 when z = 1 and a = 0.77 when z > 2. This equation was found to be valid in

the range 1 < I < 100mM for monovalent ions and the range 0 < I < 1 mM for

multivalent ions up to z = 6. Here, ionic strength is defined in the classic Lewis sense,

$$I = 0.5 \Sigma c_i \, z_i^2 \tag{10}$$

The Reijenga equation was used to explain an unexpected mobility trend observed when

a 14-charged SISCD was used for the separation of weakly basic, pharmaceutically

active enantiomers [51]. The observation was that at zero SISCD concentration the

effective mobility of weakly basic enantiomers in a low pH BGE was positive and that

with increasing SISCD concentration the mobilities of the enantiomers became less

cationic until at some concentration a cationic mobility minima was passed. Further

increase in the SISCD concentration resulted in an increase in the cationic mobility of

the enantiomers over the SISCD concentration range used. Extrapolation of the model

showed that at higher concentrations the mobility will be depressed to zero mobility. The

same study showed that when the enantiomer binding constant is large (i.e. > 500) that

there is a local anionic mobility maximum that decreases on further increase in the

SISCD concentration until at some point the mobility can become very slightly cationic

and finally approach a zero mobility. The findings of this study suggest that without

further expansion of treatments like the Reijenga model to include more highly charged

species such as SISCD's (z > 6), equilibrium binding constants cannot be accurately

measured.

1.4 Solvent Effects in CE

The BGE solvent should satisfy numerous criteria including i) liquid over a

suitable temperature range; ii) acceptably low viscosity; iii) solubility for electrolyte

components; iv) low to moderate volatility; v) chemical stability; vi) low UV-cutoff; vii)

sufficiently high dielectric constant; vii) compatibility with instrumentation. Water, of

course, satisfies all of these but so do numerous other solvents [76-78]. Other, somewhat

common, CE solvents are methanol [79-81], acetonitrile [82] and, to a lesser extent,

formamide [83]. There is much interest in the use of solvents other than water for CE

enantiomer separations since other solvents can provide higher solubility for

hydrophobic pharmaceuticals and effect differences in both mobilty [84-86] and

separation selectivity [87,88] compared to aqueous BGE's.

In CE, the primary role of the BGE is to buffer the pH of the separation medium

from change due to production of hydronium and hydroxide at the anode and cathode,

respectively, and to provide a conductive medium for separations [88]. When a potential

is applied to a BGE filled capillary, the current generated produces Joule heat that results

in greater band broadening and is counterproductive to separation. This catch-22

situation is worsened with high electric fields, a condition that favors enantiomer

resolution, since the temperature gradient across the capillary is proportional to the

square of both the electric field strength(E) and the capillary inner diameter (r),

$$T_{diff} = E^2 \kappa_{ave} r^2 / 4k_{sol} \qquad (11)$$

where κ_{ave} is the electrical conductivity of the BGE averaged over the capillary radius

and k_{sol} is the thermal conductivity of the solvent [89,90]. It seems that the lower thermal

conductivity of non-aqueous solvents, namely methanol ($k_{sol} = 0.2$ WK^{-1}m^{-1}), might be disadvantageous compared to water ($k_{sol} = .61$ WK^{-1}m^{-1}) in CE. However, thermal band broadening has been found to be negligible when the inner diameter of the capillary is 50 μm and less [91,92], as long as electrophoresis is carried out in the linear portion of Ohm's Law [93-94].

The principles governing resolution in CE in aqueous BGE's have shown to apply to organic solvents as well as methanol. As previously discussed, ionic mobility decreases with higher ionic strengths. Extension of Stokes' mobility expression to include the effecs of BGE permittivity, viscosity and ionic strength on mobility shows

$$\mu = \mu_o - \left[\frac{82.04}{\sqrt{(\varepsilon T)^3}} \mu_o + \frac{4.275}{\eta \sqrt{\varepsilon T}} \right] \sqrt{I} \qquad (12)$$

that compared to aqueous solvents, the ionic strength induced mobility decrease in organic solvents is approximately 3 and 4 times greater for MeOH and ACN solvents over a 0.01 mol L^{-1} range in ionic strength. For CE enantiomer separations, this means potentially dramatic changes in trends for separation selectivity.

Development of new chiral resolving agents allows for expansion of the number of tools available to the modern day separation scientist. Cyclodextins are among the most versatile chiral resolving agents since they are easily modified to produce different structures capable of different intermolecular interactions with enantiomers. There are currently no SISCD's asymmetrically substituted at all three hydroxy groups. It is the purpose of this dissertation to report the synthesis, characterization and use of the first two such β-CD derivatives for enantiomer separations.

CHAPTER II

SYNTHESIS AND CHARACTERIZATION OF

SINGLE-ISOMER HMAS AND HMS

There are currently no reports on unsymmetrically substituted single-isomer sulfated cyclodextrins in the literature. All species produced for use as chiral resolving agents have been substituted at their C2 and C3 positions and/or at their C2 and C6 positions with identical functionalities. This dissertation describes the preparative- scale synthesis of the first two unsymmetrically substituted SISCD's for use as chiral resolving agents in capillary electrophoretic enantiomer separations: heptakis(2-*O*-methyl-3-*O*-acetyl-6-*O*-sulfo)cyclomaltoheptaose sodium salt (HMAS) and heptakis(2-*O*-methyl-6-*O*-sulfo)cyclomaltoheptaose sodium salt (HMS).

2.1 Materials and Methods

Native β-cyclodextrin was purchased from Cerestar, (Cedar Rapids, IA). Tert-butyldimethylchlorosilane (TBS) was purchased from FMC Lithium Div. (Bessemer City, NC). Triethylsilylchlorosilane (TES) was obtained from Gelest, Inc. (Morrisville, PA). Imidazole (Im) was obtained from Chem Impex (Wood Dale, IL). Dimethylaminopyridine (DMAP), sodium hydride (60% dispersion in mineral oil), iodomethane, sodium fluoride and pyridine complexed sulfur trioxide and all BGE components were purchased from Aldrich Chemical Co. (Milwaukee, WI). Hydrofluoric acid, acetic anhydride and all reaction solvents were obtained from Mallinckrodt

Chemical Co. (St. Louis, MO). Activated, 200-mesh, 4Å- molecular sieves from Fischer Scientific, Inc. (Fairlawn, NJ) were used to dry the solvents. Aluminum backed silica-60 TLC plates from E.M. Science (Gibbstown, NJ) were used to monitor the progress of reactions. A reagent solution composed of 35g α-napthol and 140 mL conc. sulfuric acid in 500mL of an ethanol:water mixture (5.25:1) was used to visualize the cyclodextrin spots. Visualization was accomplished by dipping the TLC plate in the reagent solution and heating it in a 110º C oven for 10 minutes. Imidazolium chloride (ImHCl) produced in the first and second synthetic transformations was isolated and recrystallized from methanol: ethyl acetate until colorless.

An HPLC system consisting of a Beckman 126 solvent module equipped with analytical pump heads, a Rheodyne 7125 injection valve (Rheodyne, Cotati, CA), a Eurosep DDL-31 evaporative light scattering detector (ELSD) (Eurosep Instruments, St. Christophe, France) set to 53º C and 400 gain and a Beckman 406 A/D converter operated under Gold 8.1 chromatography software (Beckman-Coulter, Fullerton, CA) on an IBM PS/2 PC was used to establish the purity of all intermediates. Separations were carried out on 4.6mm i.d. x 250mm analytical columns packed with either 5 μm Luna silica or 5μm Luna C18 stationary phases. All ELSD response factors were assumed to be equal.

The isomeric distribution of the final products was analyzed using a Beckman P/ACE 2100 capillary electrophoresis system equipped with a UV detector operated at 214 nm, a 46cm long, 25μm i.d. bare fused silica capillary (injector to detector length 39 cm) (Polymicro Technologies, Phoenix, AZ), at 20kV separation potential and (-) to (+)

polarity. The BGE used was 30mM β-alanine titrated to pH 3.5 with para-toluenesulfonic acid. The reaction was sampled while in progress, diluted with the BGE and the solution was injected for 1 sec at 1 p.s.i. before application of the separation potential. All analyses were completed at 20º C.

1-D ^{1}H, ^{13}C and DEPT NMR experiments were done on a Varian 500MHz UnityPlus Spectrometer (Varian Assoc., Walnut Creek, CA) equipped with a ^{1}H/^{13}C dual tunable probe using VnmrX 5.3b software running on a SUN workstation. 2-D experiments including double quantum filtered ^{1}H-^{1}H correlation spectroscopy (DQ-COSY) and ^{1}H-^{13}C heteronuclear correlation spectroscopy (HETCOR) were obtained on either the same 500MHz UnityPlus Spectrometer or on a Varian 300 MHz UnityPlus spectrometer equipped with ^{1}H/ ^{19}F/ ^{31}P/ ^{13}C quad probe and Solaris 2.4 software running on a SUN workstation.

High-resolution MALDI-TOF mass spectra were obtained with a Voyager-DE STR Biospectrometry Workstation equipped with delayed extraction capability (Perseptive Biosystems, Framingham, MA) with the following instrument settings: nitrogen laser (λ= 337 nm), reflectron mode, 25 kV acceleration voltage, 70% grid voltage and 180 μs delay time. The mass spectra from 100 laser pulses were averaged to achieve adequate signal-to-noise ratio. All samples were prepared by dissolving 10 mg of 2,4,6-trihydroxyacetophenone (THAP) in 1 mL HPLC grade acetonitrile and 10 mg of the cyclodextrin derivative to be analyzed in 1 mL of either CH_2Cl_2 or water, along with 10 mg of an internal standard, heptakis(2-*O*-methyl)cyclomaltoheptaose. Equal volumes of these solutions were combined and 10 μL applied to a PTFE target stage and allowed

to dry [110].

Crystal structures were obtained on a Bruker SMART 1000 X-ray Diffractometer (Bruker AXS, Madison, WI) from single crystals grown in suitable solvents. Diffraction patterns were solved and refined using the SHELLXTL program suite running on a Pentium III 300 MHz processor PC. Crystal structure and Connelly surface figures were generated using the Insight II molecular modeling software package running on an SGI O_2 workstation.

2.2 Synthesis and Characterization

For silylation, the C6 hydroxy group of β-CD reacts first followed by the C2 hydroxy group and then the C3 hydroxy group. Thus, selective silylation can be achieved, but not without the formation of some undesirably substituted species. The implication is that the reaction products will need to be purified at every stage of the multi-step synthetic scheme on a scale sufficient to produce 50-250g of final products for CZE enantiomer separations.

The synthetic scheme shown in Figure 1 makes use of regioselective protecting group chemistry and orthogonally deprotectable functionalities to produce HMAS and HMS in high yield. The details of the synthetic procedure are outlined in Appendix A.
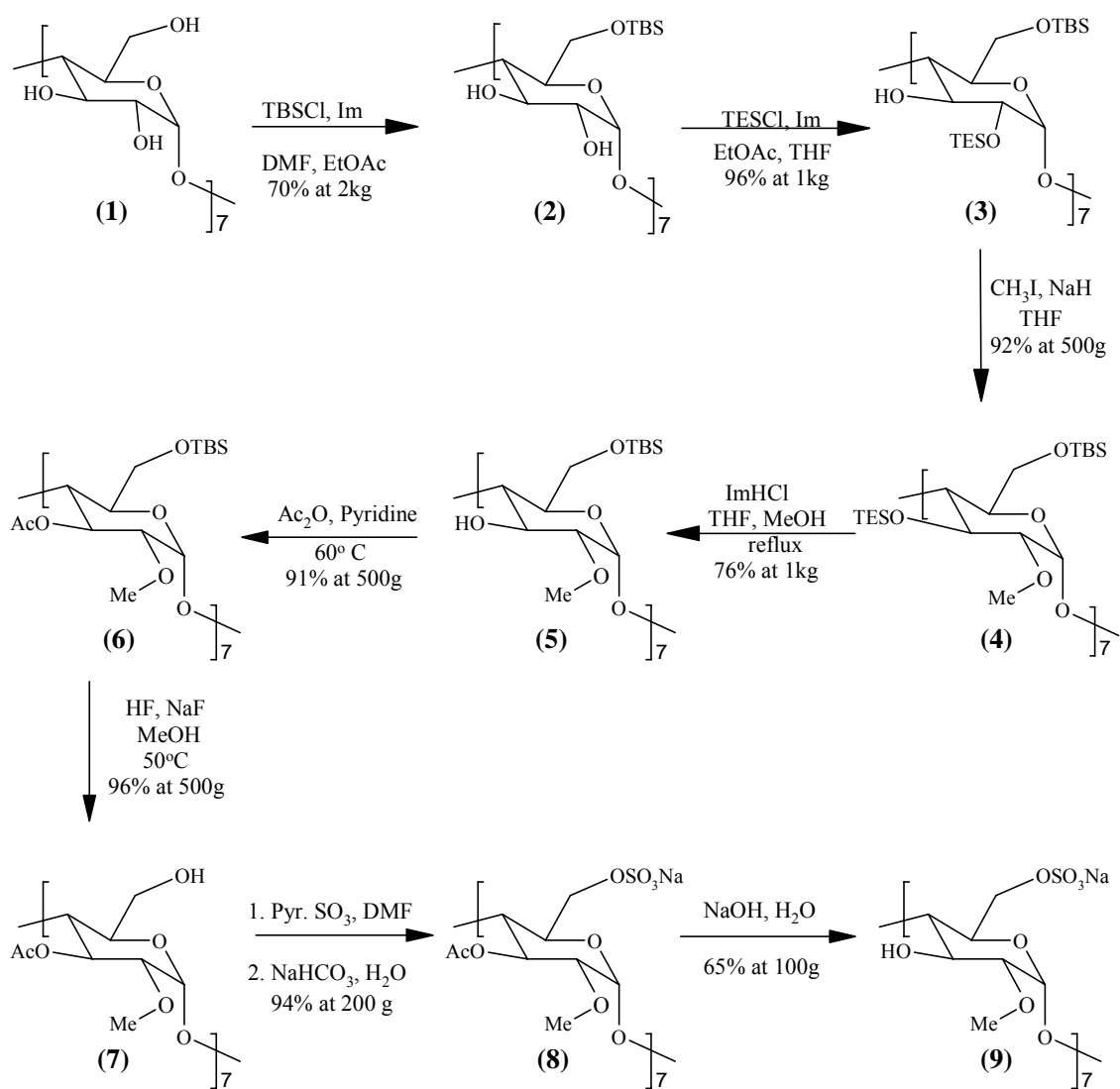
Figure 1. Synthetic scheme for HMAS and HMS.

2.2.1 Heptakis(6-*O*-*t*-butyldimethylsilyl)cyclomaltoheptaose

The primary hydroxy groups at the C6 positions of β-CD were reacted in DMF at room temperature with TBS dissolved in ethyl acetate according to a modified Takeo procedure [44]. Reaction progress was monitored using a 5μm Luna, C18 RP-HPLC column with a 40:60 MeOH:EtOAc isocratic mobile phase at 2 mL/min. The reaction solution was allowed to stir for 10 hrs after completion of TBS addition. The ImHCl precipitate was filtered and the reaction solvent removed under reduced pressure. The crude material was recrystalized four times from a DMF/ acetone/ water ternary solvent mixture and dried in vacuo. This reaction was scaled to 2.0 kg and repeated once more to produce 4.78 kg of white powder with an isomeric purity of 99.5% (70% yield) . Figure 2 is a chromatogram of the crude product overlaid with a chromatogram of the final recrystallized product.

Full ^{1}H and ^{13}C analyses are shown in Figures 3 and 4, respectively. Peak assignments for ^{1}H and ^{13}C NMR spectra are made from 1-dimensional DEPT and 2-dimensional ^{1}H- ^{1}H homonuclear correlation spectroscopy (COSY) and ^{1}H- ^{13}C heteronuclear correlation spectroscopy (HETCOR) experiments. NMR data (CDCl$_3$):^{1}H, δ 5.49 (broad, exchangeable, HO-2 and HO-3), δ 4.89 (d, 7 H, J$_{1,2}$ 3.5 Hz, H-1), δ 4.03 (t, 7H, J$_{3,4}$ 9.0 Hz, H-3), δ 3.90 (d, 7H, J$_{6,6'}$ 10.8 Hz, H-6), δ 3.71 (d, J$_{6',6}$ 10.8 Hz, H-6'6), δ 3.63 (m, 14 H, H-2,5), δ 3.55 (t, 7 H, J$_{4,3}$ 9.0 Hz, H-4), 0.86 (s, 63 H, Si(CH$_3$)$_2$(C(C**H**$_3$)$_3$)), δ 0.04 and δ 0.03 (2×s, 42 H, Si(C**H**$_3$)$_2$(C(CH$_3$)$_3$); ^{13}C δ 102.22 (C-1), δ 81.94 (C4), δ 73.80 (C2), δ 73.64 (C3), δ 72.75 (C5), δ 61.85 (C6), δ 26.13 (Si(CH$_3$)$_2$(C(**C**H$_3$)$_3$), δ 18.49 (Si(CH$_3$)$_2$(**C**(CH$_3$)$_3$), δ - 4.85 (Si(**C**H$_3$)$_2$(C(CH$_3$)$_3$), δ - 4.97
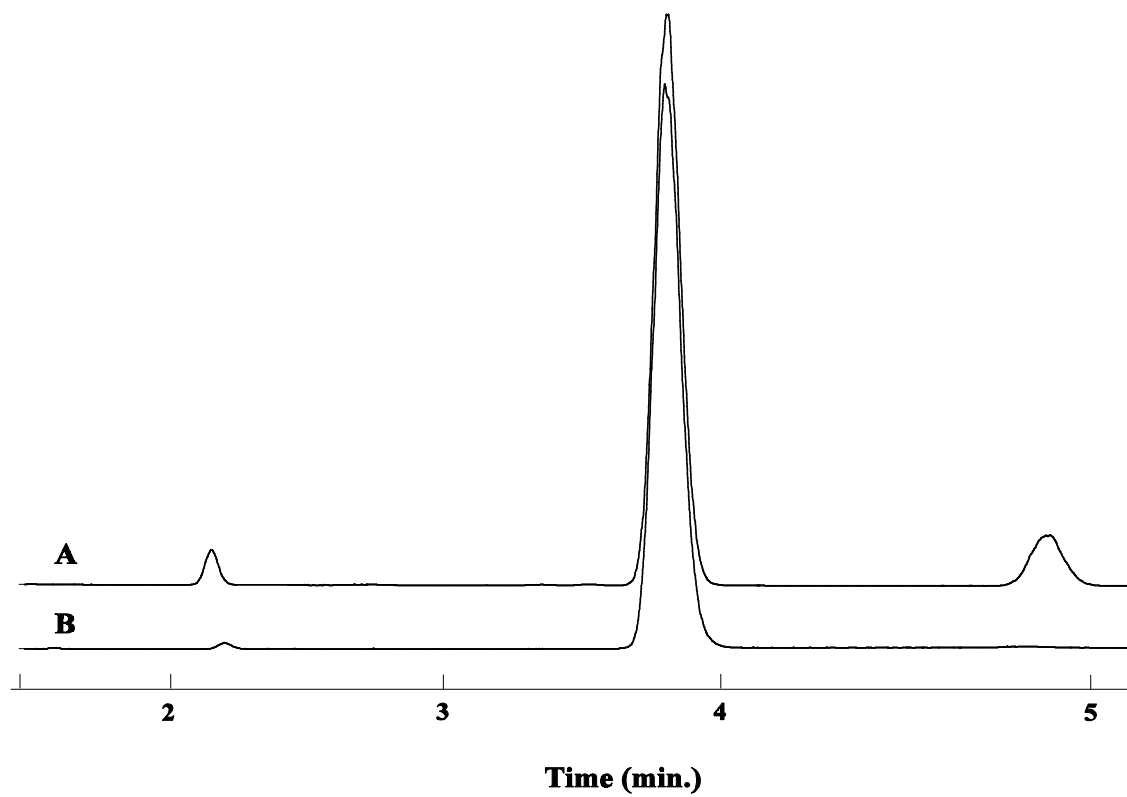
Figure 2. Overlay of A) chromatogram of crude (**2**) and B) chromatogram of
recrystallized (**2**).
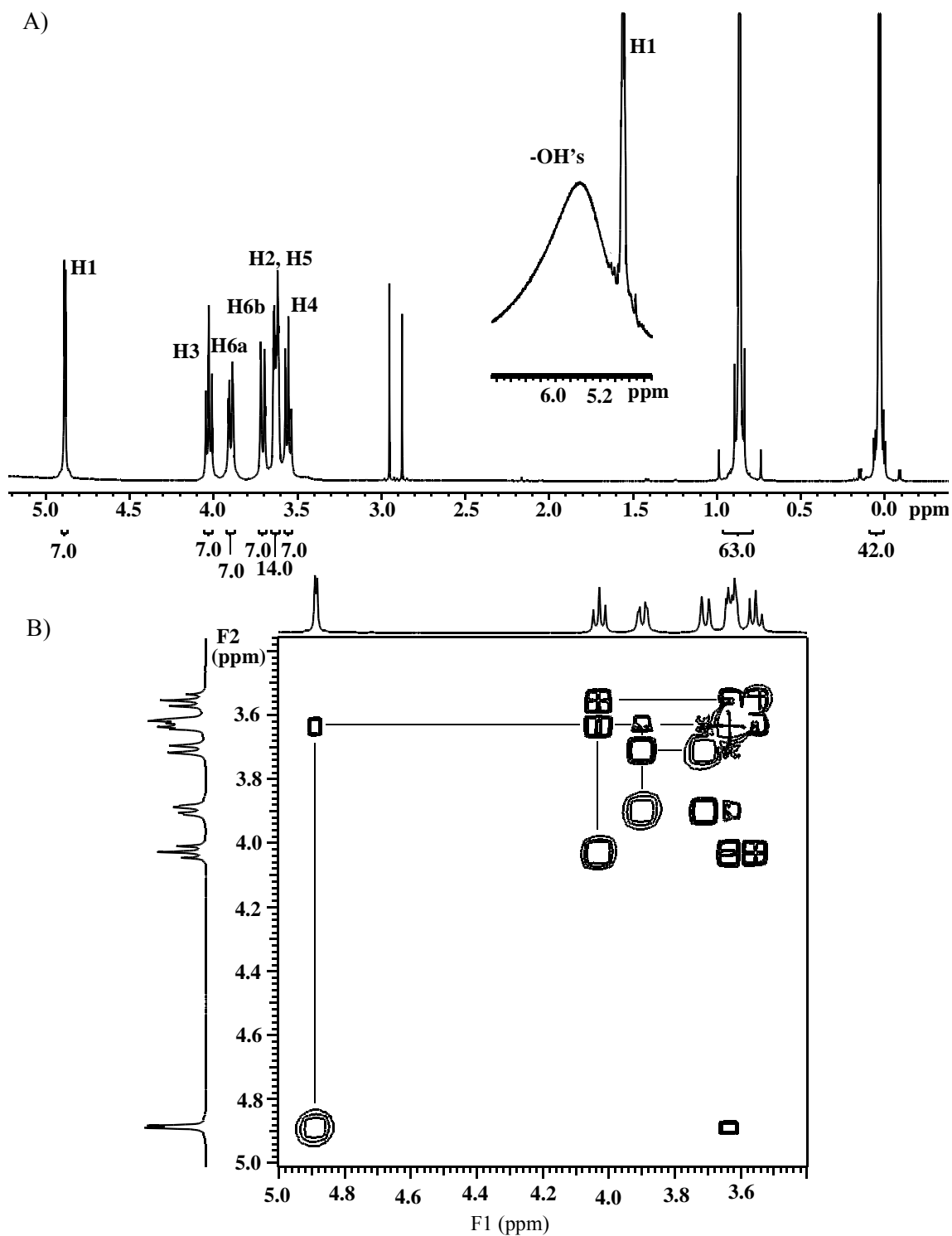
Figure 3. A) ¹H and B) ¹H-¹H COSY spectra of (**2**) in CDCl₃.
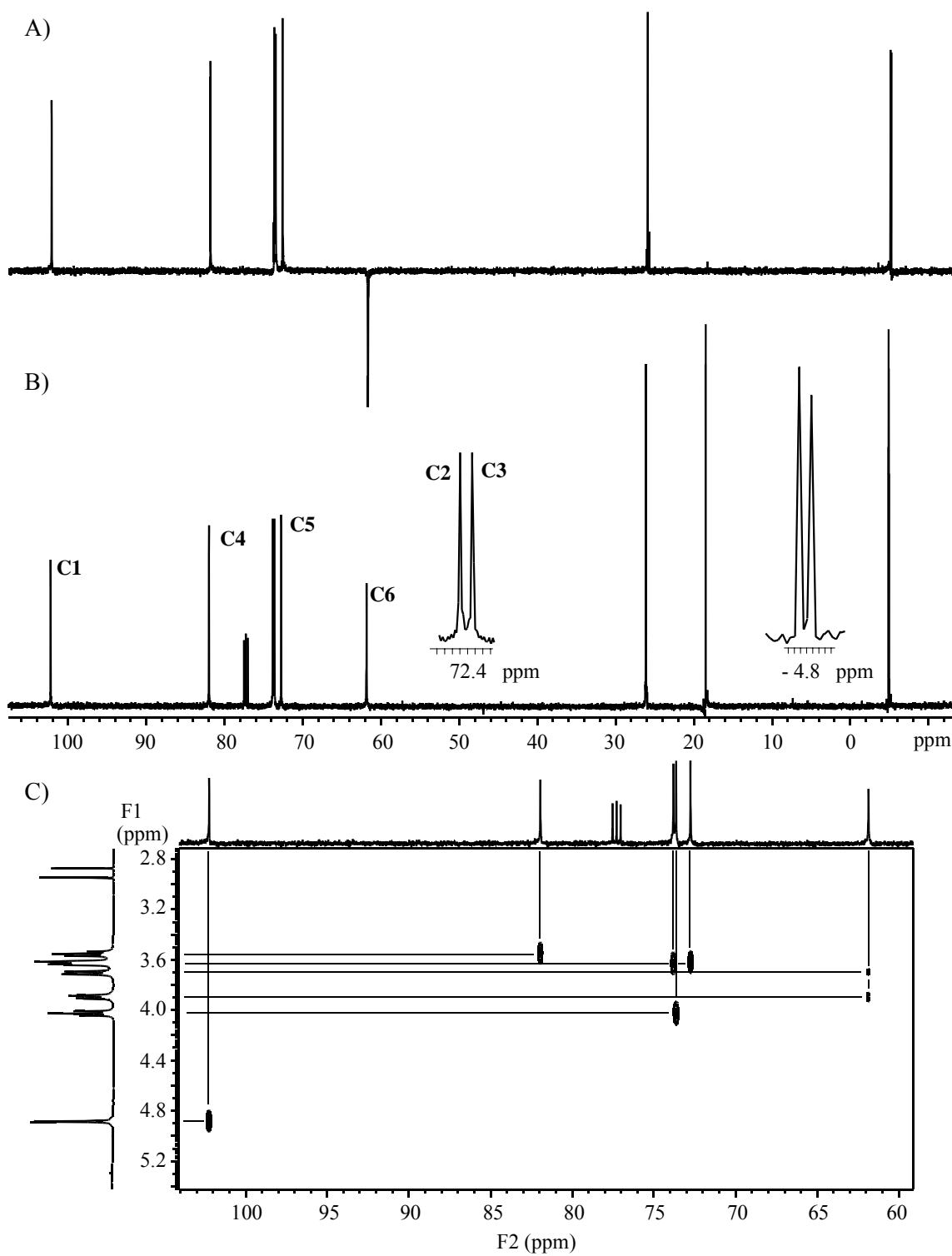
Figure 4. A) DEPT B) ^{13}C and C) ^{1}H- ^{13}C HETCOR spectra of (**2**) in CDCl$_3$.

$(Si(\mathbf{C}H_3)_2(C(CH_3)_3)$. ^{1}H-^{1}H COSY and ^{1}H-^{13}C HETCOR spectra show only the signals corresponding to the CD backbone. DEPT analysis is included to allow easy assignment of silyl-ether carbons. The TBS ether tertiary carbon signal is fully suppressed in the DEPT spectrum and the C6 methylene group is identified as the only negative-going signal. The *t*-butyl methyl signal is upfield of the signal for the diastereotopic methyl group attached directly to silicon. The HETCOR spectrum shows both diastereotopic H6 hydrogens coupled to C6 in the methylene group.

High resolution MALDI-TOF mass spectrometry was used to determine the molecular weight of intermediate (**2**). The MALDI-TOF-MS spectrum of the sodium and potassium adducts of (**2**) is shown in Figure 5. The measured m/z values of 1955.55 and 1971.32 agree well with the value calculated for the monoisotopic sodium and potassium adducts, 1955.96 and 1971. 94, respectively.
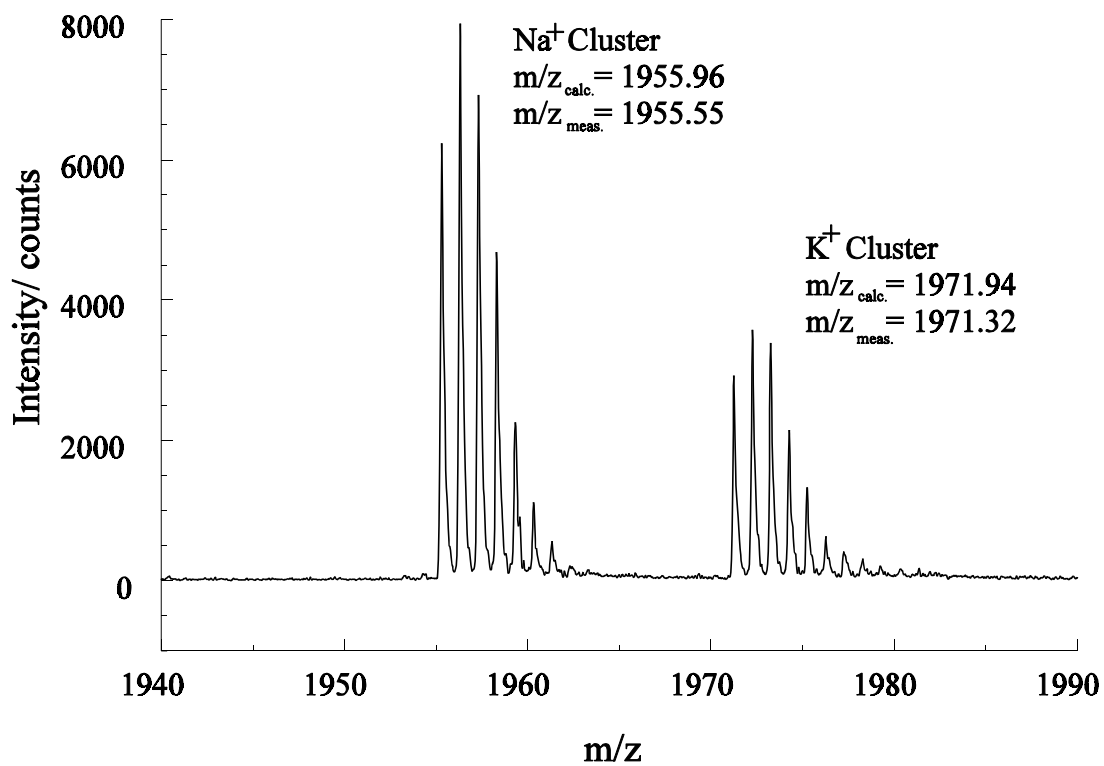
Figure 5. A section of the MALDI-TOF-MS mass spectrum of (**2**).

2.2.2 Heptakis(2-*O*-triethylsilyl-6-*O*-*t*-butyldimethylsilyl)cyclomaltoheptaose

Attempts to use a trimethylsilyl (TMS) ether as a protecting group for the C2

hydroxyl groups failed due to poor regioselectivity over the C3 hydroxyl groups.

Instead, the secondary hydroxy groups at the C2 position were reacted in THF at room

temperature with TES dissolved in ethyl acetate. The reaction progressed with excellent

regioselectivity as can be seen in the chromatogram shown in Figure 6 of a sample taken

from the reaction vessel prior to quenching. The reaction was monitored using a 5μm

Luna, C18 RP-HPLC column and gradient elution at 2 mL/min with a mobile phase that

begins with 40:60 MeOH:EtOAc and after six minutes changes linearly to 100% EtOAC,

in 30 minutes. The very high regioselectivity of TES for the C2 hydroxyl groups is likely

due to steric hindrance at the C3 hydroxyl groups. The reaction solution was allowed to

stir for 10 hrs after completion of TESCl addition. The ImHCl precipitate was filtered

and the reaction solvent removed under reduced pressure. The crude material was

digested twice in acetone and dried in vacuo. This reaction was scaled to 1.0 kg to

produce 1.36 kg of white powder with an isomeric purity of 99.8% (96% yield).

Full ^{1}H and ^{13}C analyses are included in Figures 7 and 8, respectively. Peak

assignments for ^{1}H and ^{13}C NMR spectra are made from 1-dimensional DEPT and 2-

dimensional ^{1}H- ^{1}H COSY and ^{1}H- ^{13}C HETCOR experiments. NMR data (CDCl$_3$): ^{1}H δ

4.81 (d, 7H, $J_{1,2}$ 3.5 Hz, H-1), δ 4.72 (s, 7H, HO-3), δ 3.94 (dd, 7H, $J_{6,6'}$ 11.5 Hz, $J_{6,5}$ 3.1

Hz, H-6), δ 3.82 (t, 7H, $J_{3,2}$= $J_{3,4}$ 9.3 Hz, H-3), δ 3.67 (d, 7H, $J_{6',6}$ 11.5 Hz, H-6'), δ 3.60

(d, 7H, $J_{5,4}$ 11.5 Hz, H-5), δ 3.50 (dd, 7H, $J_{2,3}$ 9.3 Hz, $J_{2,1}$ 3.5 Hz, H-2), δ 3.43 (t, 7H, $J_{4,3}$=

$J_{4,5}$ 9.3 Hz, H-4),δ 0.97 (t, 63H, $J_{8,7}$ 7.9 Hz, Si(CH$_2$C**H**$_3$)$_3$),δ 0.87 (s, 63H,
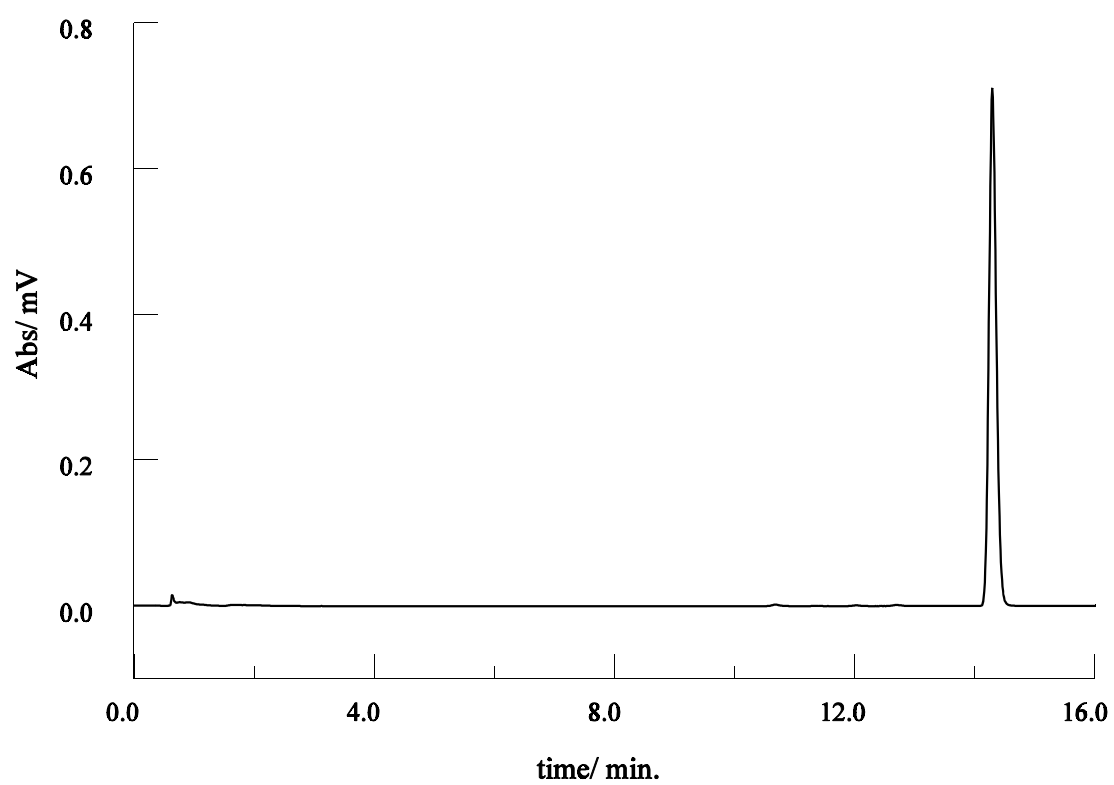
Figure 6. HPLC-ELSD chromatogram of (**3**) obtained for a 1-kg batch prior to quenching of the reaction.
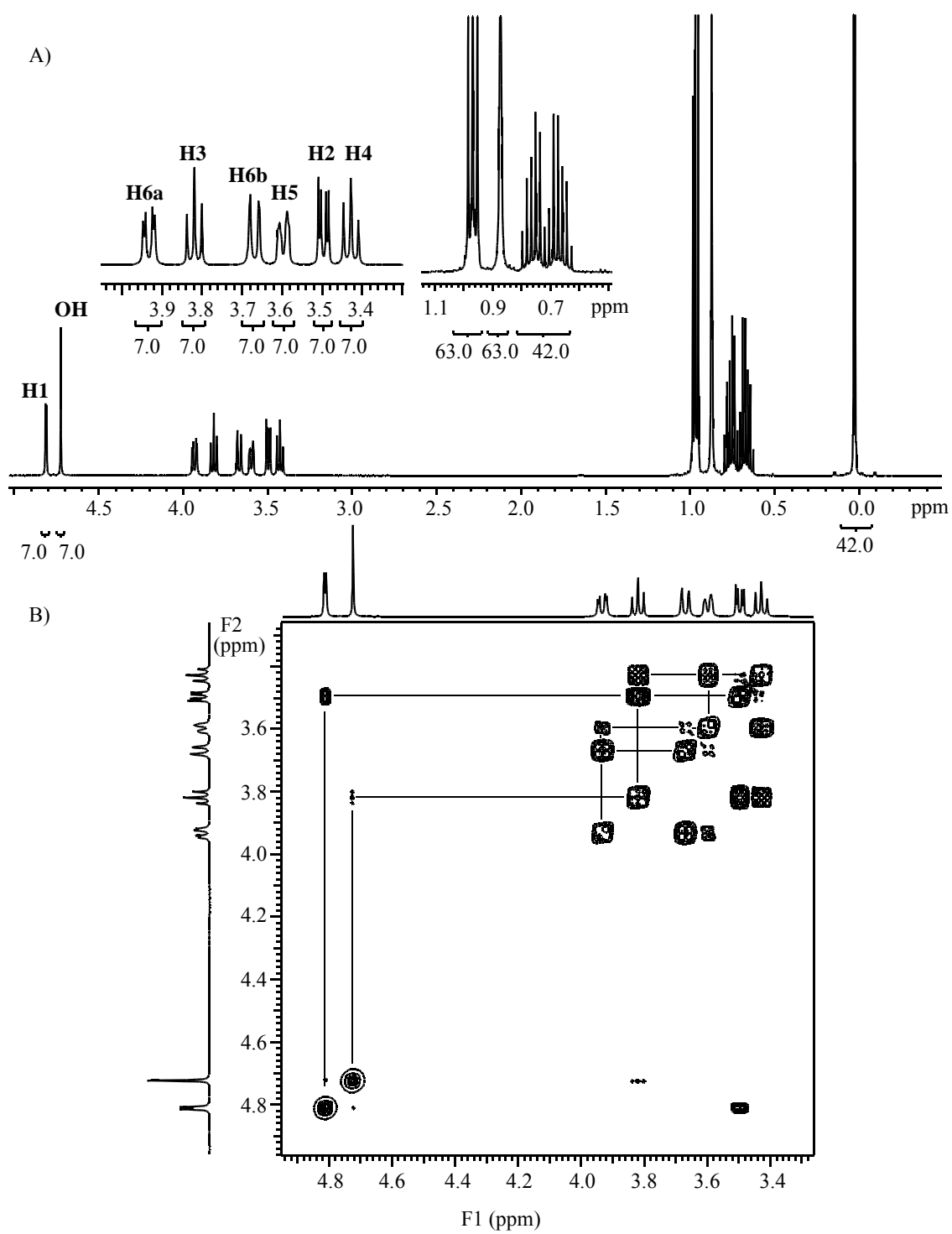
Figure 7. A) ^{1}H and B) ^{1}H-^{1}H COSY spectra of (**3**) in CDCl$_3$.
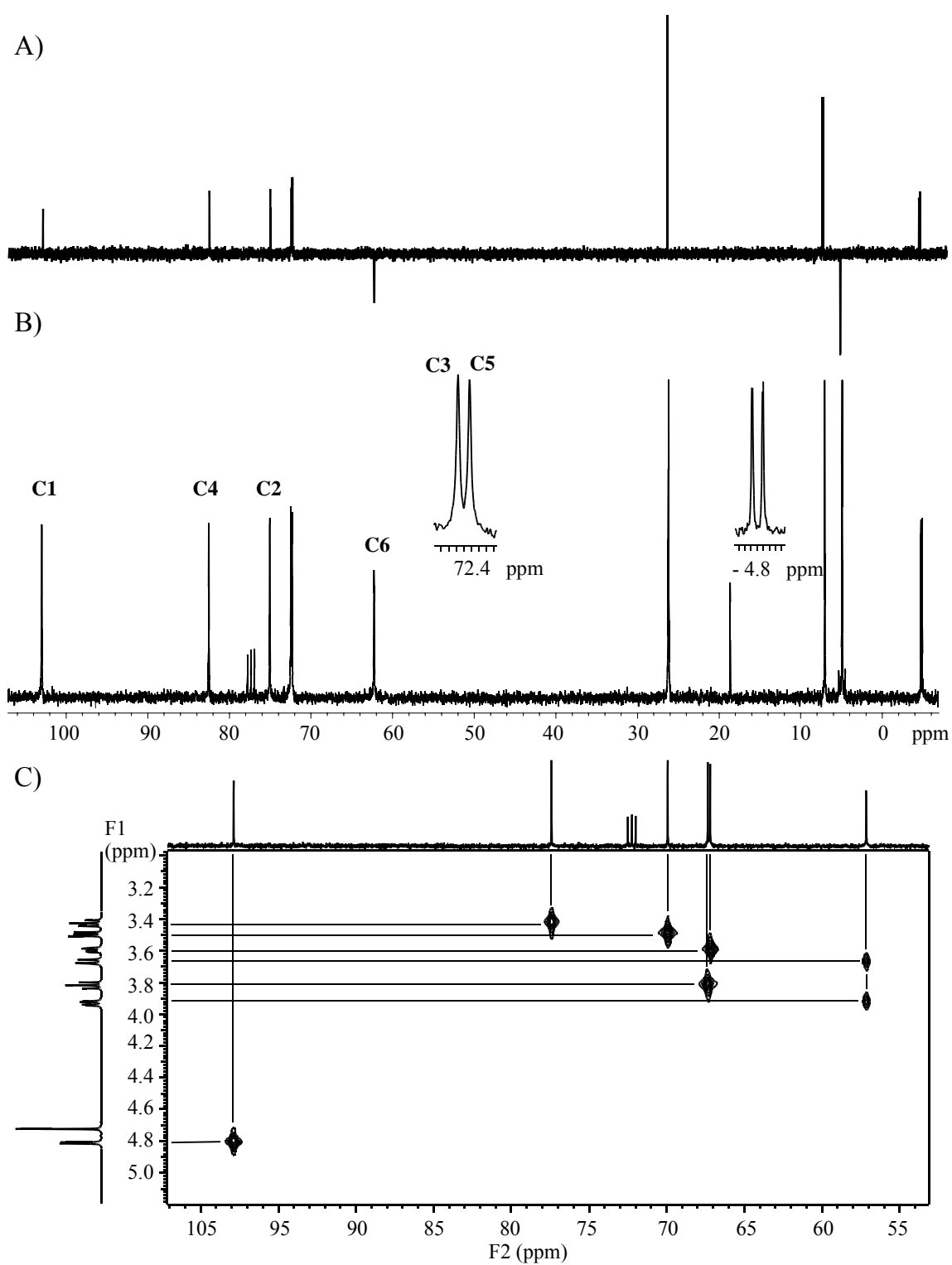
Figure 8. A) DEPT B) ^{13}C and C) ^{1}H- ^{13}C HETCOR spectra of (**3**) in CDCl$_3$.

Si(CH$_3$)$_2$(C(C**H**$_3$)$_3$), δ 0.76 and δ 0.67 (2 × sextet, 42H, J$_{7,7}$ 15.8 Hz, Si(C**H**$_2$CH$_3$)$_3$), δ

0.03 and 0.02 (2 × s, 63H, Si(C**H**$_3$)$_2$(C(CH$_3$)$_3$); ^{13}C δ 102.88 (C-1), δ 82.41 (C4), δ 74.93

(C2), δ 72.35 (C3), δ 72.20 (C5), δ 62.15 (C6), δ 26.09 (Si(CH$_3$)$_2$(C(**C**H$_3$)$_3$), δ 18.51

(Si(CH$_3$)$_2$(**C**(CH$_3$)$_3$), δ 6.93 (Si(CH$_2$**C**H$_3$)$_3$), δ 4.81 (Si(**C**H$_2$CH$_3$)$_3$), δ - 4.84

(Si(**C**H$_3$)$_2$(C(CH$_3$)$_3$), δ - 5.01 (Si(**C**H$_3$)$_2$(C(CH$_3$)$_3$). The ^{1}H-^{1}H COSY and ^{1}H-^{13}C

HETCOR spectra show only the signals corresponding to the CD backbone. The two

sextets in the ^{1}H NMR spectrum are for the diastereotopic TES ether methylene

hydrogens. The expected doublet of quartets for each hydrogen is not observed because

of inadequate resolution. DEPT analysis is included to allow easy assignment of silyl-

ether carbons. The signals for the TES ether methyl and methylene groups are between

the signals for the TBS tertiary and diastereotopic carbon atoms. The negative going

peak corresponds to the methylene group.

A portion of the high resolution MALDI-TOF-MS spectrum of (**3**) is shown in

Figure 9. The measured m/z values of 2754.82 and 2770.79 agree well with the value

calculated for the monoisotopic sodium and potassium adducts, 2754.82 and 2770.79,

respectively.

During development of the TES protection step, acetone was not the first solvent

used for digestion. The first used was anhydrous ethanol which resulted in removal of

the TES groups as suggested by the RP-HPLC-ELSD chromatogram shown in Figure 10.

Here, seven peaks are visible where the latest eluting peak is the fully TES substituted

derivative. The earlier eluting peaks are successively deprotected species having had one

or more TES groups removed. At the time of this experiment, the reaction conditions

still included DMF as a part of the reaction solvent. Aqueous extraction was required to

remove the dissolved ImHCl. It was shown that the small amount of ImHCl remaining

after extraction and slightly wet conditions was responsible for the silyl loss.
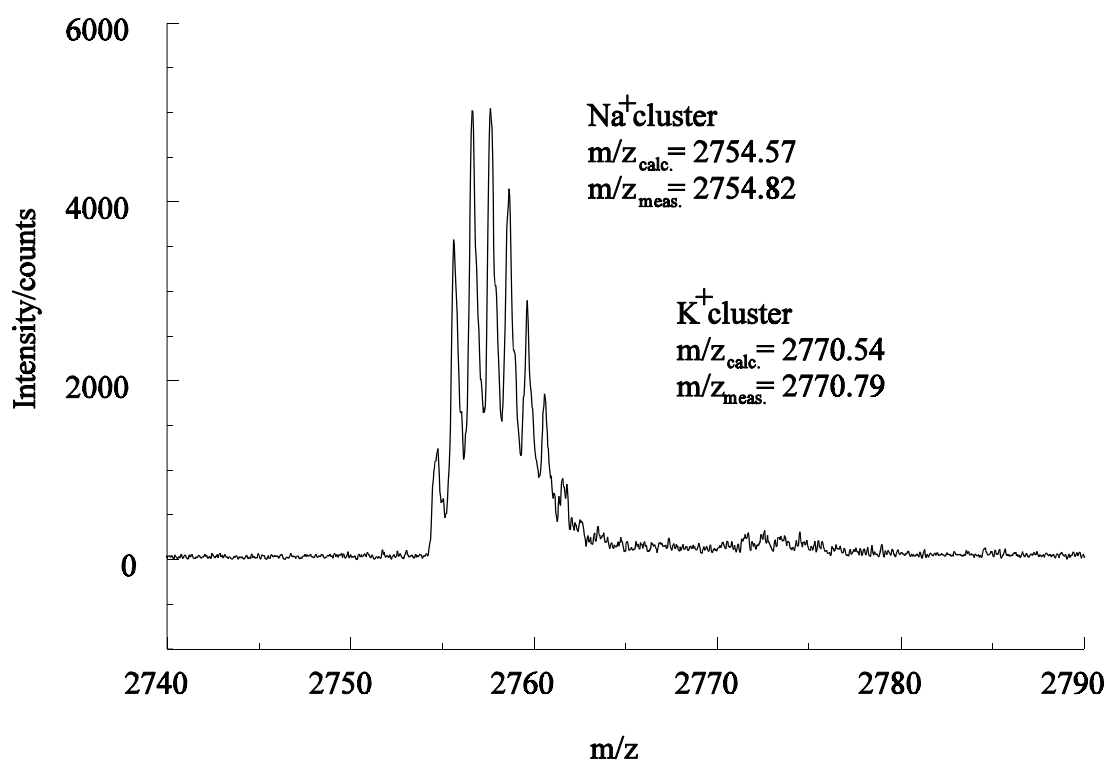
Figure 9. A section of the MALDI-TOF-MS mass spectrum of (**3**).
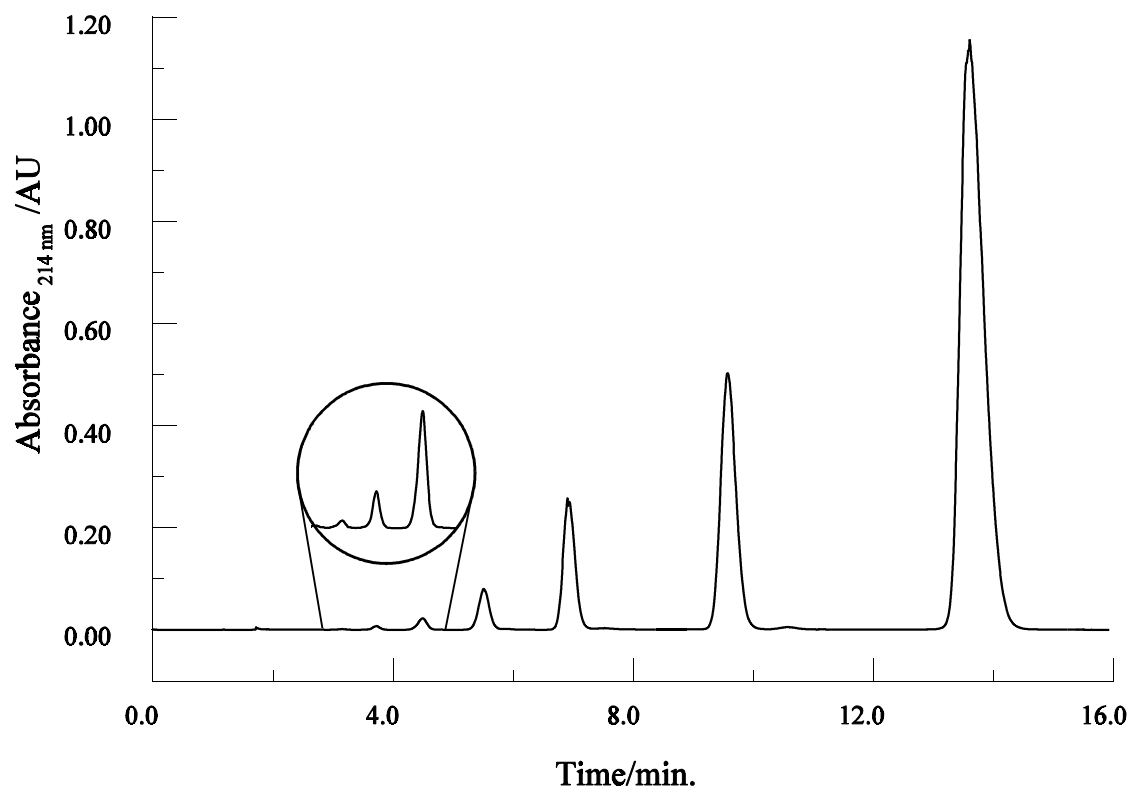
Figure 10. RP-HPLC chromatogram of partially deprotected (**3**) obtained from ethanol digestion in the presence of ImHCl and water contaminants.

2.2.3 Heptakis(2-*O*-methyl-3-*O*-triethylsilyl-6-*O*-*t*-butyldimethylsilyl)cyclomalto-heptaose

Methylation of (**3**) was accomplished in THF at room temperature using iodomethane in the presence of sodium hydride, in 4 hrs, to obtain (**4**) at 97% conversion. This reaction was conducted on the 500 g scale and repeated twice. Reaction progress was monitored using a 5μm Luna, C18 RP-HPLC column with a 30:70 MeOH:EtOAc isocratic mobile phase at 2 mL/min. Upon completion, the reaction was quenched with MeOH. After stirring for an additional half-hour, hexanes were added and sodium iodide was extracted with water. The hexanes were removed under reduced pressure and the crude recrystallized four times from acetone and dried in vacuo to yield 563g (92% yield) of (**4**) as a white powder at a 99.8% isomeric purity. Shown in Figure 11 is an overlay of the RP-HPLC chromatograms for the recrystallized reaction product before (trace A) and after (trace B) recrystallization from acetone.

Full ^{1}H and ^{13}C analyses are included in Figures 12 and 13, respectively. Peak assignments for ^{1}H and ^{13}C NMR spectra are made from 1-dimensional DEPT and 2-dimensional ^{1}H- ^{1}H COSY and ^{1}H- ^{13}C HETCOR experiments. NMR data (CDCl$_3$): ^{1}H δ 5.27 (d, 7H, $J_{1,2}$ 3.5 Hz, H-1), δ 4.22 (d, 7H, $J_{6,6'}$ 12.0 Hz, H-6), δ 4.02 (t, 7H, $J_{3,2}$ = $J_{3,4}$ 8.0 Hz, H-3), δ 3.81 (t, 7H, $J_{4,3}$ = $J_{4,5}$ 8.0 Hz, H-4), δ 3.66 (m, 14H, H-5,6'), δ 3.36 (s, 21H, Methyl ether), δ 2.99 (dd, 7H, $J_{2,1}$ 3.5 Hz, $J_{2,3}$ 8.0 Hz, H-2), δ 0.96 (t, 63H, $J_{9,8}$ 7.7 Hz, Si(CH$_2$**CH**$_3$)$_3$), δ 0.89 (s, 63H, Si(CH$_3$)$_2$(C(**CH**$_3$)$_3$), δ 0.68 (doublet of quartets, $J_{8,8}$ 3.0 Hz, Si(**CH**$_2$CH$_3$)$_3$), δ 0.034 and 0.030 (2 × s, 63H, Si(**CH**$_3$)$_2$(C(CH$_3$)$_3$); ^{13}C δ 96.55 (C-1), δ 81.75 (C2), δ 78.49 (C4), δ 73.36 (C3), δ 71.98 (C5), δ 62.95 (C6), δ 57.11 (**CH**$_3$O),
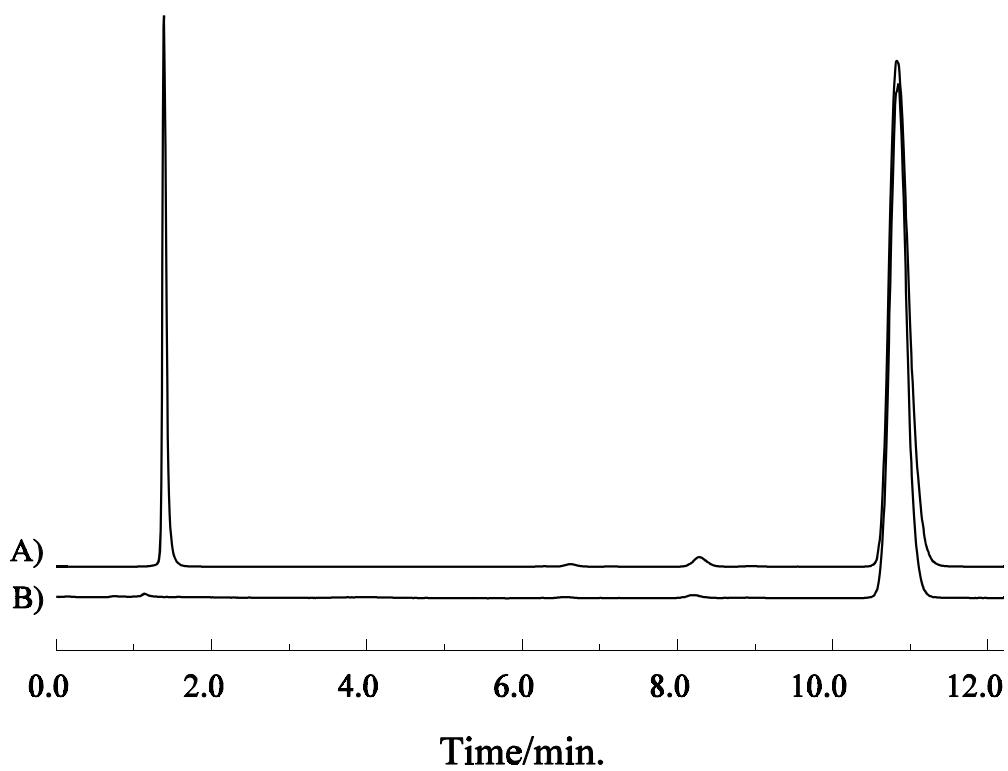
Figure 11. HPLC-ELSD chromatogram of (**4**) A) before and B) after recrystallization.
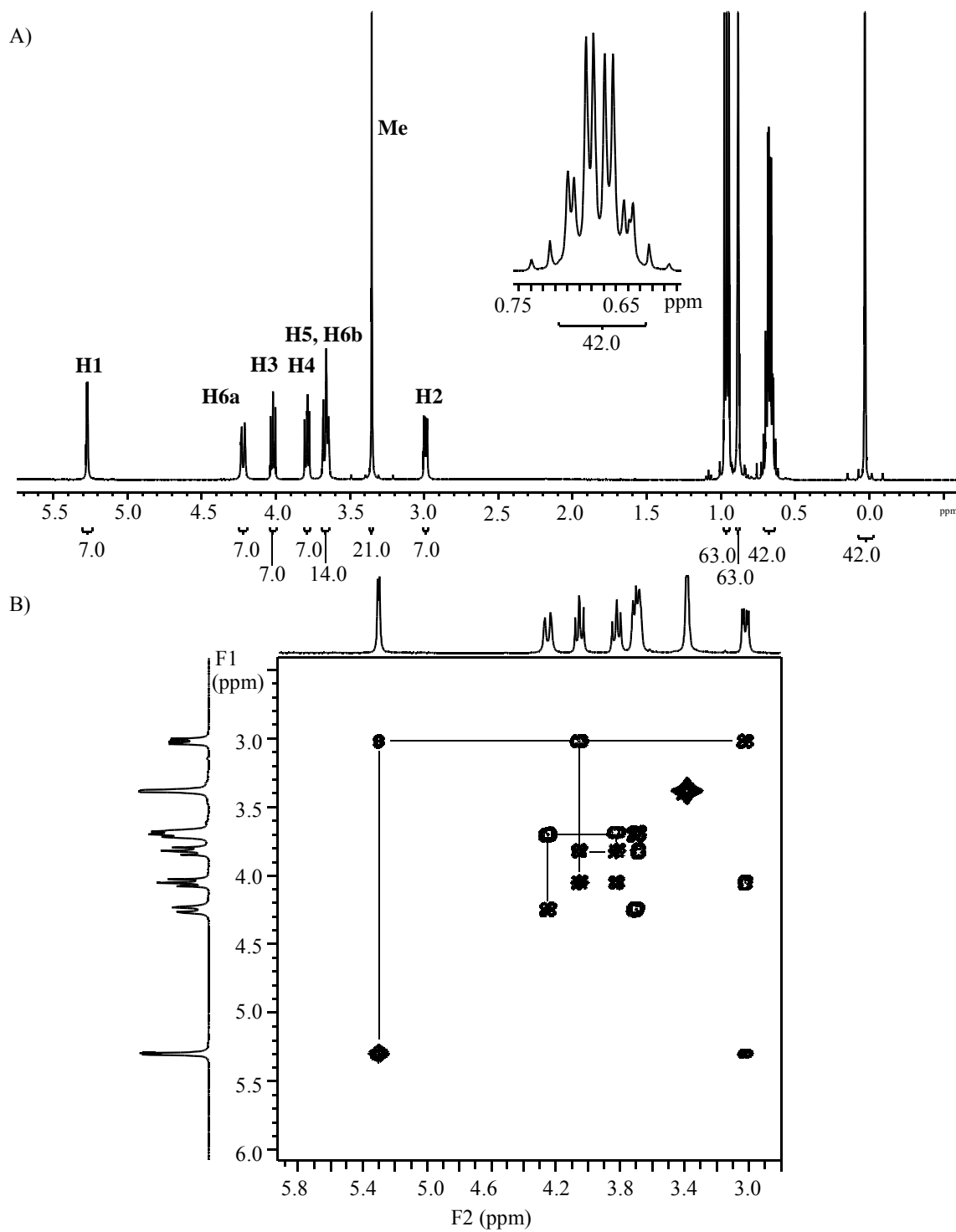
Figure 12. A) ^{1}H and B) ^{1}H-^{1}H COSY spectra of (**4**) in CDCl$_3$.

Figure 13. A) DEPT B) ^{13}C and C) ^{1}H- ^{13}C HETCOR spectra of (**4**) in CDCl$_3$.
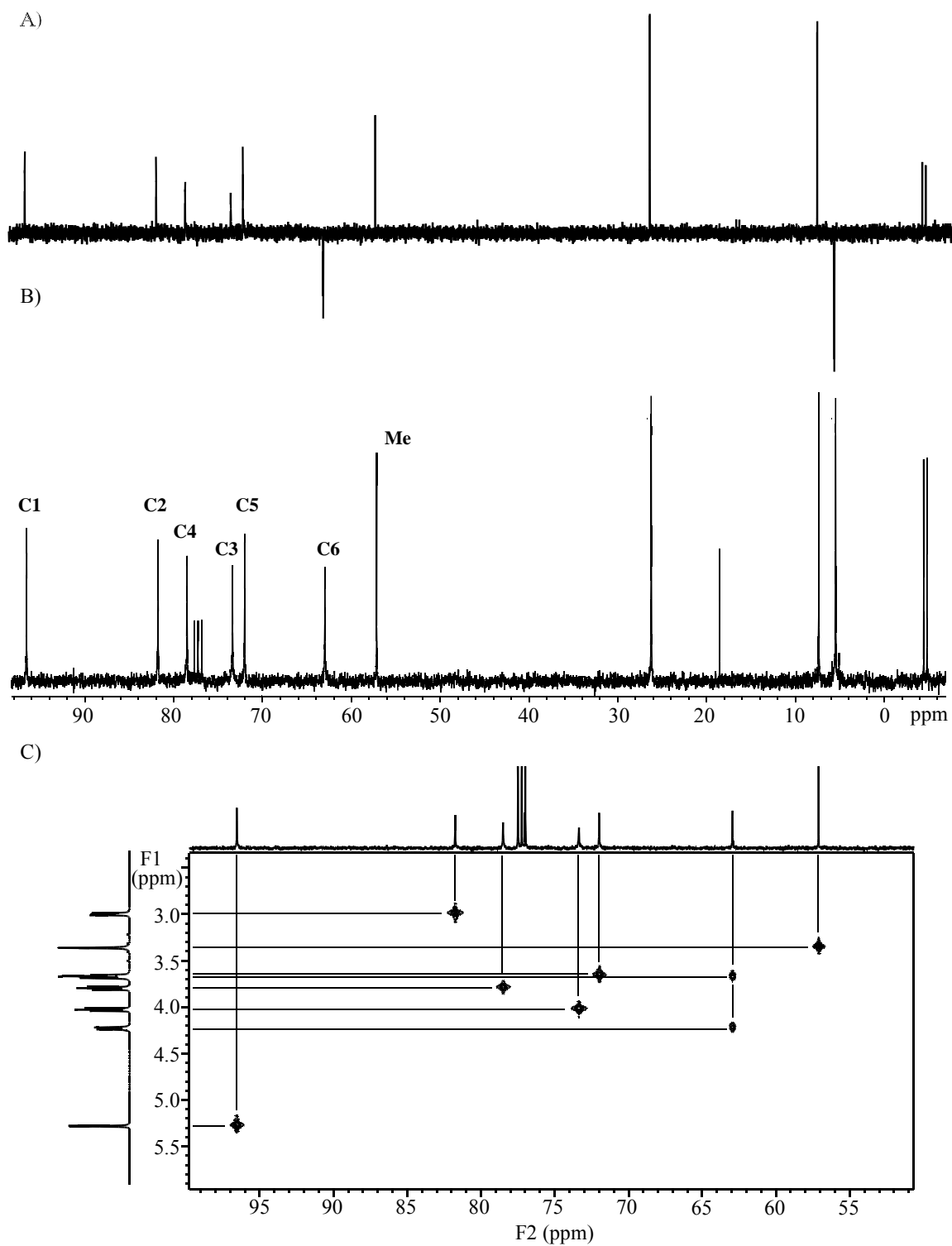
δ 26.23 (Si(CH$_3$)$_2$(C(**CH**$_3$)$_3$), δ 18.54 (Si(CH$_3$)$_2$(**C**(CH$_3$)$_3$), δ 7.37 (Si(CH$_2$**CH**$_3$)$_3$), δ 5.47 (Si(**CH$_2$**CH$_3$)$_3$), δ - 4.45 and - 4.83 (Si(**CH$_3$**)$_2$(C(CH$_3$)$_3$).

^{1}H-^{1}H COSY and ^{1}H-^{13}C HETCOR spectra show only the signals corresponding to the CD backbone. The signal for the TES ether diastereotopic protons has collapsed to two nearly overlapping quartets. The J-coupling constant for the two almost magnetically equivalent diastereotopic protons is much smaller after than before migration of the TES group from the C2 hydroxy to the C3 hydroxy. Silyl migration is also indicated in the ^{13}C- NMR spectrum where the signal for the C2 nucleus is shifted downfield (less shielded) after substitution with the methyl group.

High resolution MALDI-TOF mass spectrometry was used to determine the molecular weight of intermediate (**4**). The MALDI-TOF-MS spectrum of the sodium and potassium adducts of (**4**) is shown in Figure 14. The measured m/z values of 2852.70 and 2868.67 agree well with the value calculated for the monoisotopic sodium and potassium adducts, 2852.68 and 2868.65, respectively.
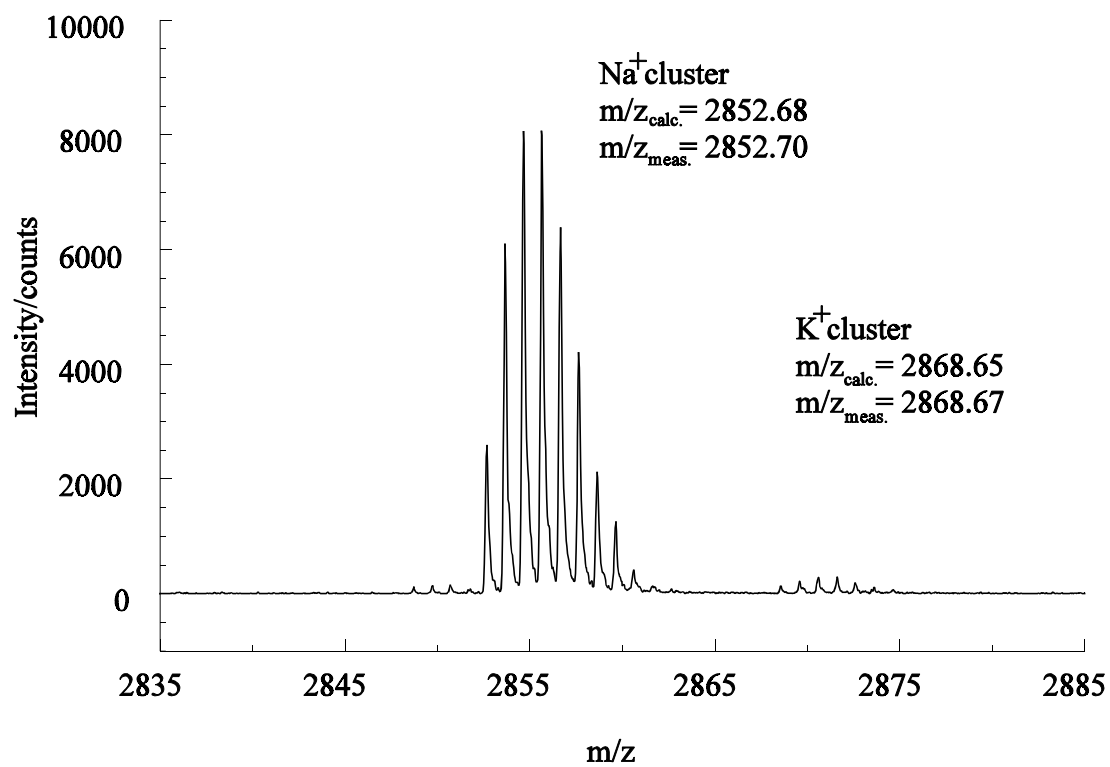
Figure 14. A section of the MALDI-TOF-MS mass spectrum of (**4**).

2.2.4 Heptakis(2-*O*-methyl-6-*O*-*t*-butyldimethyl)cyclomaltoheptaose

Selective deprotection of (**4**) was accomplished by stirring with ImHCl in a 35:65 MeOH: THF solution, under reflux for 6 hrs, to give (**5**) with 96% conversion. This reaction was conducted at the 1-kg scale and repeated once. Reaction progress was monitored using a 5μm Luna, C18 RP-HPLC column and gradient elution at a flow rate of 2 mL/min with a mobile phase that begins with 35:65 MeOH:EtOAc and after nine minutes changes linearly to 90% EtOAC, in 6 minutes. Once judged complete, the reaction solvent was removed under reduced pressure and the crude redissolved in EtOAc. Next, ImHCl was filtered and EtOAc removed under reduced pressure. The crude product was extracted with 2×100-mL water and recrystallized twice from 50:50 MeOH:EtOAc and dried in vacuo to yield 546 g (76% yield) of (**5**) as a white powder at 99.6% isomeric purity (m.p. 257.0- 257.5 ° C). Shown in Figure 15 is an overlay of the RP-HPLC chromatograms of the product after recrystallization and the recrystallization mother liquor.

Full ^{1}H and ^{13}C analyses are included in Figures 16 and 17, respectively. Peak assignments for ^{1}H and ^{13}C NMR spectra were made from 1-dimensional DEPT and 2-dimensional ^{1}H- ^{1}H double-quantum filtered COSY and ^{1}H- ^{13}C HETCOR experiments. NMR data (CDCl$_3$): ^{1}H δ 5.07 (exchangeable, HO-3), δ 4.96 (d, 7H, $J_{1,2}$ 3.7 Hz, H-1), δ 3.95 (t, 7H, $J_{3,2} = J_{3,4}$ 9.5 Hz, H-3), δ 3.93 (d, 7H, $J_{6,6'}$ 9.0 Hz, $J_{6,5}$ 2.6 Hz, H-6), δ 3.67 (d, 7H, $J_{6',6}$ 9.0 Hz, H-6'), δ 3.65 (s, 21H, C**H**$_3$O-), δ 3.57 (d, 7H, $J_{5,4}$ 9.5 Hz, H-5), δ 3.52 (t, 7H, $J_{4,2} = J_{4,3}$ 9.5 Hz, H-4), δ 3.18 (dd, 7H, $J_{2,3}$ 9.5, $J_{2,1}$ 3.5 Hz, H-2), δ 0.89 (s, 63H, Si(CH$_3$)$_2$(C(C**H**$_3$)$_3$), δ 0.048 and δ 0.039 (2× s, 42H, Si(C**H**$_3$)$_2$(C(CH$_3$)$_3$); ^{13}C δ 100.83 (C-
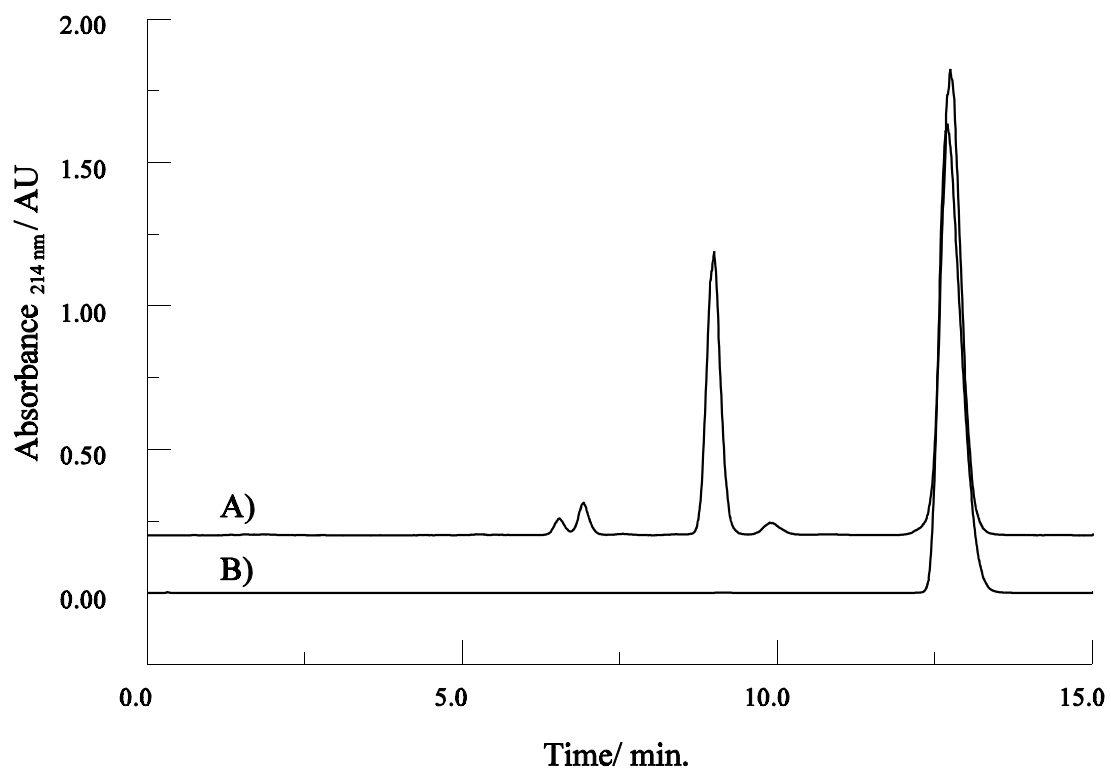
Figure 15. HPLC-ELSD chromatogram of (**5**) A) recrystallization mother liquor and B) after recrystallization.
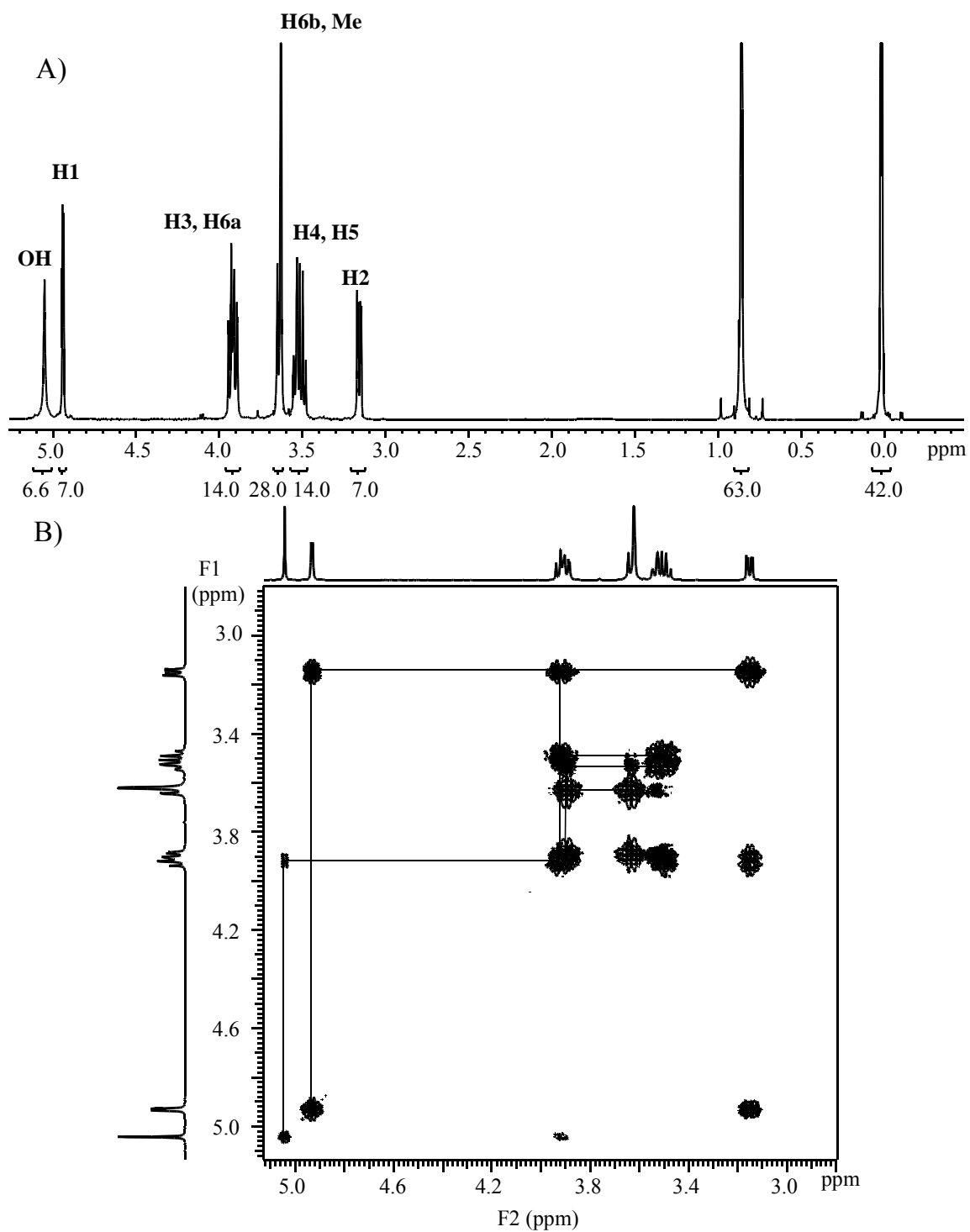
Figure 16. A) ^{1}H and B) ^{1}H-^{1}H double-quantum filtered COSY spectra of (**5**) in CDCl$_3$.
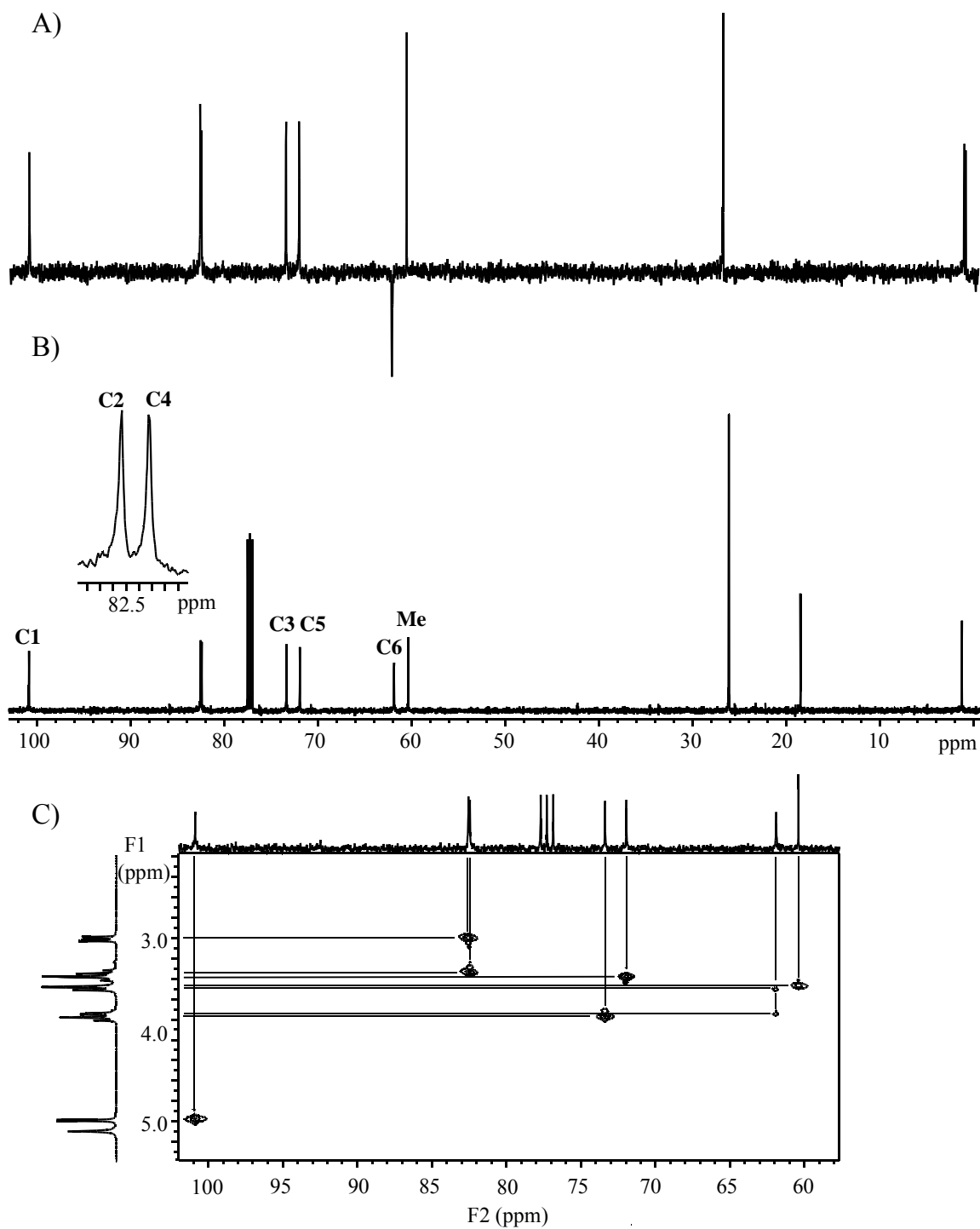
Figure 17. A) DEPT B) ^{13}C and C) ^{1}H- ^{13}C HETCOR spectra of (**5**) in CDCl$_3$.

1), δ 82.52 (C2), δ 82.41 (C4), δ 73.35 (C3), δ 71.92 (C5), 61.87 (C6), δ 60.35

(Si(**CH**$_3$)$_2$(C(**CH**$_3$)$_3$)). ^{1}H-^{1}H double-quantum filtered COSY and ^{1}H-^{13}C HETCOR spectra

show only the signals corresponding to the CD backbone. The ^{1}H and ^{13}C NMR spectra

indicate that the TES group has been selectively removed without removal of the TBS

protecting group. The COSY spectrum indicates that the exchangeable proton is coupled

to the proton at the C3 position, as expected.

A portion of the high resolution MALDI-TOF-MS spectrum of (**5**) is shown in

Figure 18. The measured m/z values of 2053.26 and 2069.05 agree well with the value

calculated for the monoisotopic sodium and potassium adducts, 2054.07 and 2070.05,

respectively.

Conditions reported in the literature for selective removal of TES in the presence

of TBS failed to produced the selectively deprotected derivative with high conversion

rate. Tested conditions included use of AcOH in pyridine, several dilute concentrations

of HF and NaF in MeOH and several dilute concentrations of HCl in THF. Conditions

using AcOH were ineffective, resulting in no deprotection. Conditions using HF/NaF

and those using HCl showed no selectively between TES and TBS deprotection. It was at

this time that efforts were put toward development of TES deprotection in the presence

of ImHCl. Initial experiments showed that a protic solvent was required and for this

MeOH was chosen.. The reaction is thought to follow the acid catalyzed mechanism

shown in Figure 19. The proposed mechanism is simply the reverse of the protection

mechanism except that the chloride anion is substituted for methoxide. The scheme was

supported by GC-MS analysis of the reaction mixture where triethylmethoxysilane was

identified as a major constituent.

Figure 20 is a plot of the change in the log of the area ratio of (**3**) to an internal

standard versus the concentration of ImHCl as measured by RP-HPLC-ELSD for five

individual deprotection reactions, each successively higher in ImHCl concentration. The

linear relationship was used to project the ImHCl concentration required to accomplish

the reaction in twelve hours. Reaction conditions were then altered to include a

MeOH/THF co-solvent so that the multiple of the concentrations of ImHCl, (**3**) and

MeOH could be set to a maximum. This allowed reaction completion in six hours.

Finally, anhydrous conditions were found to afford (**4**) with highest conversion.
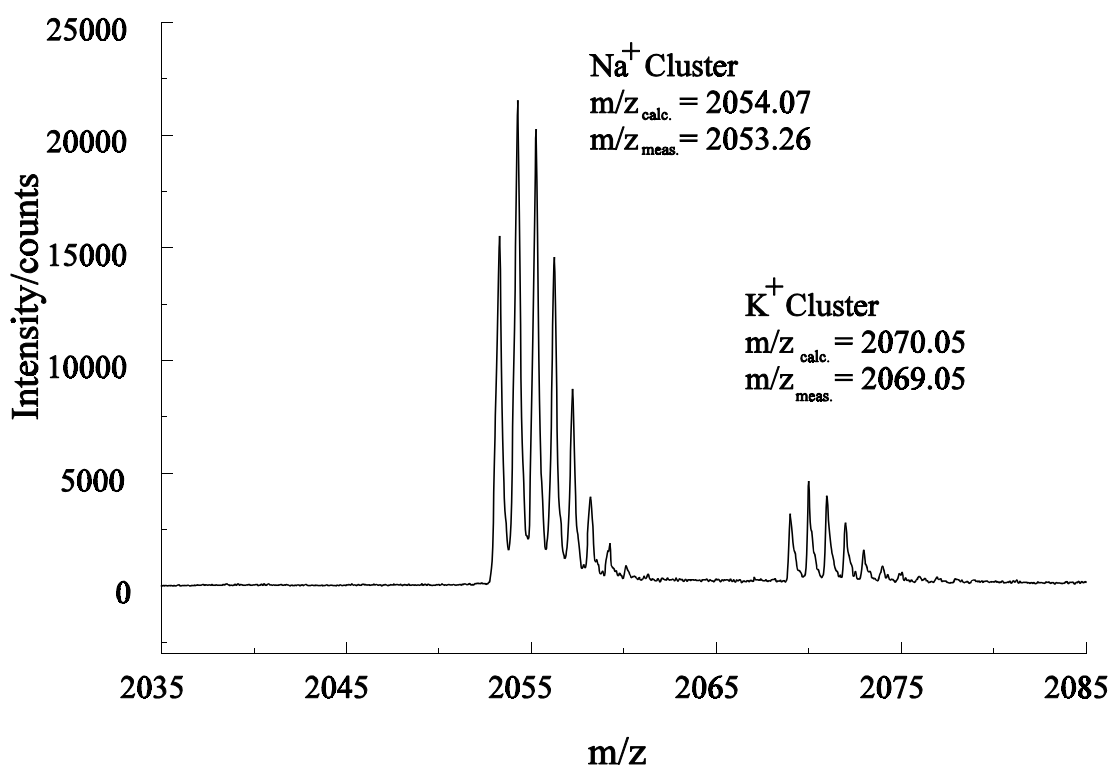
Figure 18. A section of the MALDI-TOF-MS mass spectrum of (**5**).
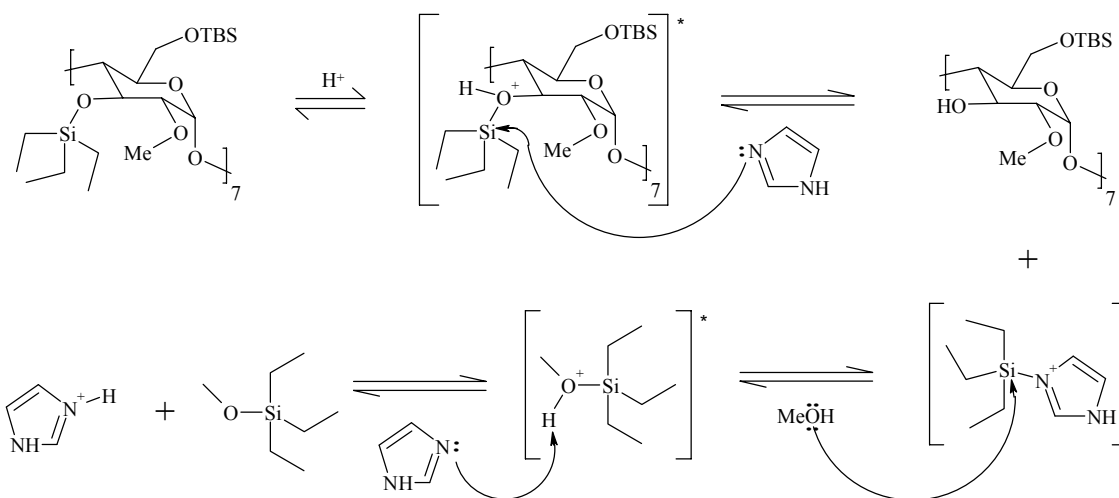
Figure 19. Possible deprotection mechanism.
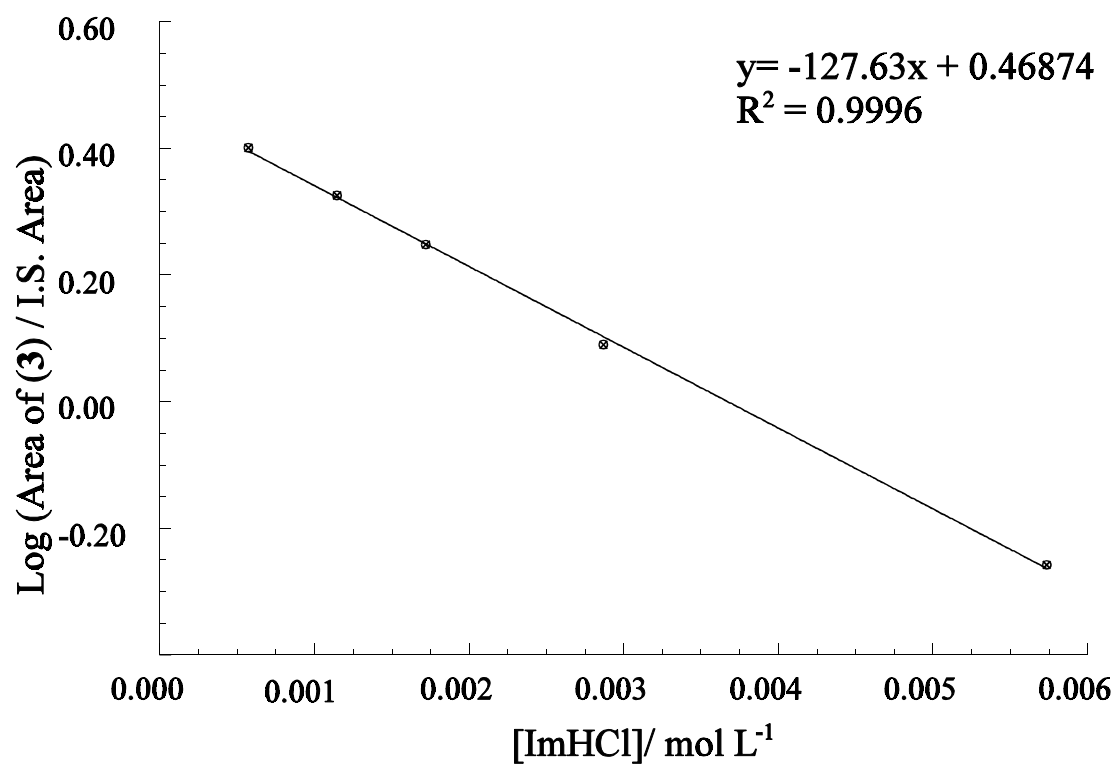
Figure 20. Progress of desilylation as a function of ImHCl concentration.

2.2.5 Heptakis(2-*O*-methyl-3-*O*-acetyl-6-*O*-*t*-butyldimethylsilyl)cyclomaltoheptaose

Acetylation of (**5**) was carried out in pyridine at 50º C for 32 hrs, in the presence of excess acetic anhydride. This reaction was scaled to 0.5 kg. Reaction progress was monitored using two separate sets of chromatographic conditions. A 5μm Luna, C18 RP-HPLC column and a 2 mL/min, 55:45 EtOAc:MeOH isocratic mobile phase was used to quantify the amount of desilylated side-products relative to the amount of all other species. A 5μm Luna, NP-HPLC silica column and gradient elution at a flow rate of 2 mL/min using a mobile phase that begins at 95:5 $CHCl_3$:MeOH and changes to 100% MeOH in 7 min. was used to quantify the amount of under-acetylated species relative to the amount of all other species. The proportion of the amount of target to all other species was calculated from the values obtained by the two different methods. Upon completion, the reaction solvent and acetic acid by-product were removed under vacuum. The crude solid was redissolved in hexanes and purified via counter-current extraction with DMF. The target was concentrated in the hexanes phase while all other species were concentrated in the DMF phase. The hexanes were removed under reduced pressure and the product dried in vacuo to yield 522 g (91% yield) of (**6**) as a white powder at 99.4% isomeric purity. Figure 21 shows the RP-HPLC chromatogram of the hexanes extract obtained from the counter-current extraction process.

Full ^{1}H and ^{13}C analyses are included in Figures 22 and 23, respectively. Peak assignments for ^{1}H and ^{13}C NMR spectra were made from 1-dimensional DEPT and 2-dimensional ^{1}H-^{1}H COSY and ^{1}H-^{13}C HETCOR experiments. NMR data ($CHCl_3$): ^{1}H δ 5.12 (t, 7H, $J_{3,2} = J_{3,4}$ 9.3 Hz, H-3), δ 5.07 (d, 7H, $J_{1,2}$ 3.5 Hz, H-1), δ 4.13 (dd, 7H, $J_{6,6'}$
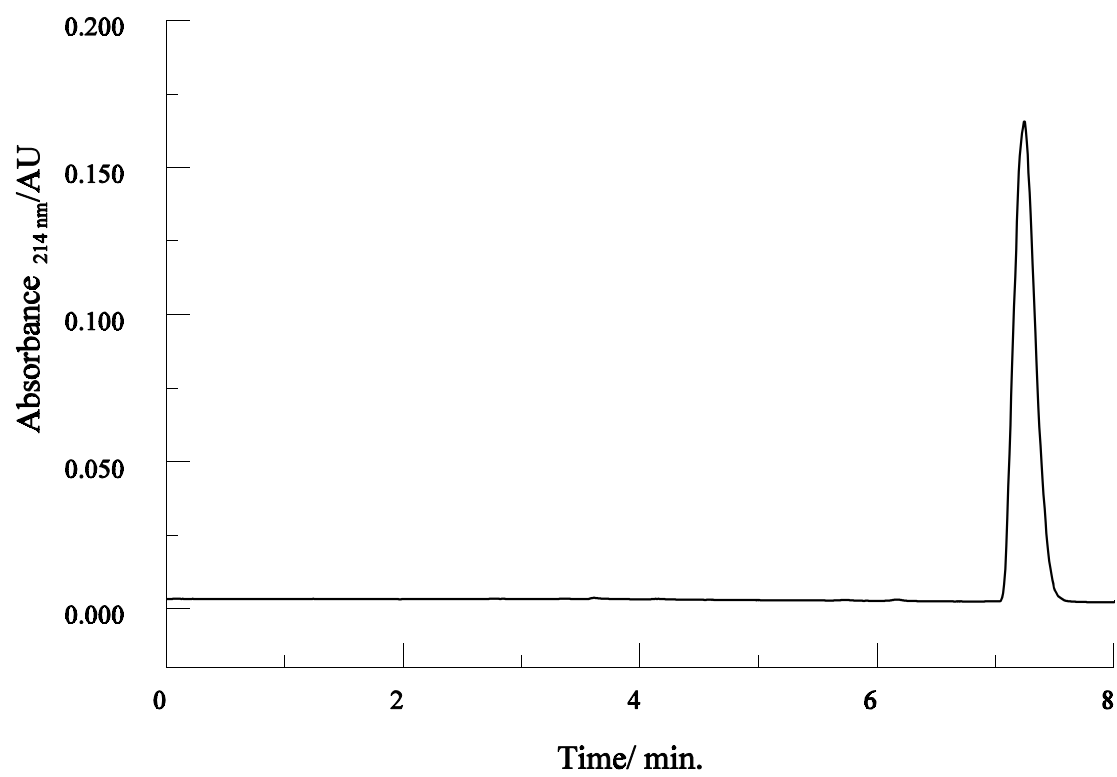
Figure 21. HPLC-ELSD chromatogram of (**6**) after counter-current extraction.
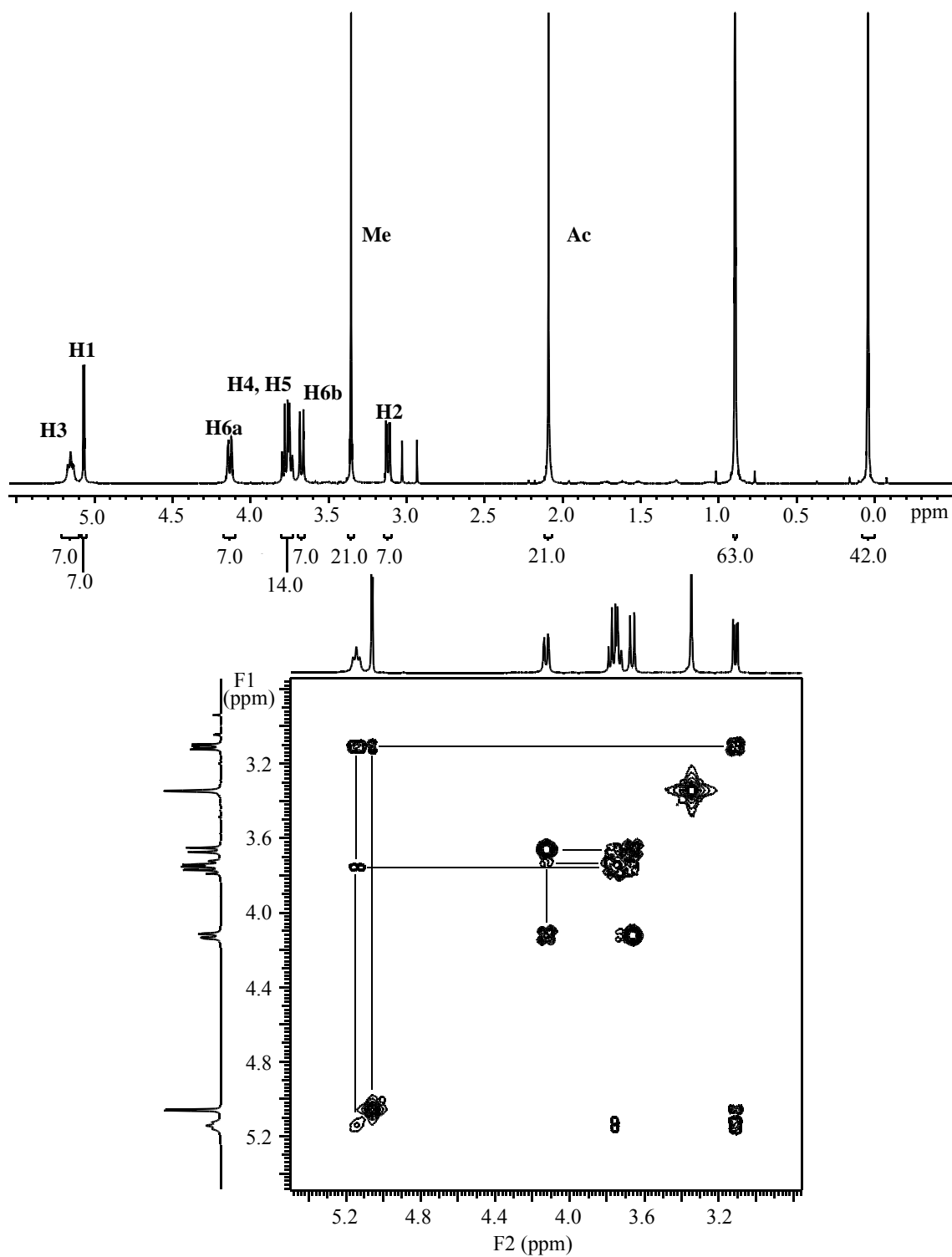
Figure 22. A) ¹H and B) ¹H-¹H COSY spectra of (**6**) in CDCl₃.
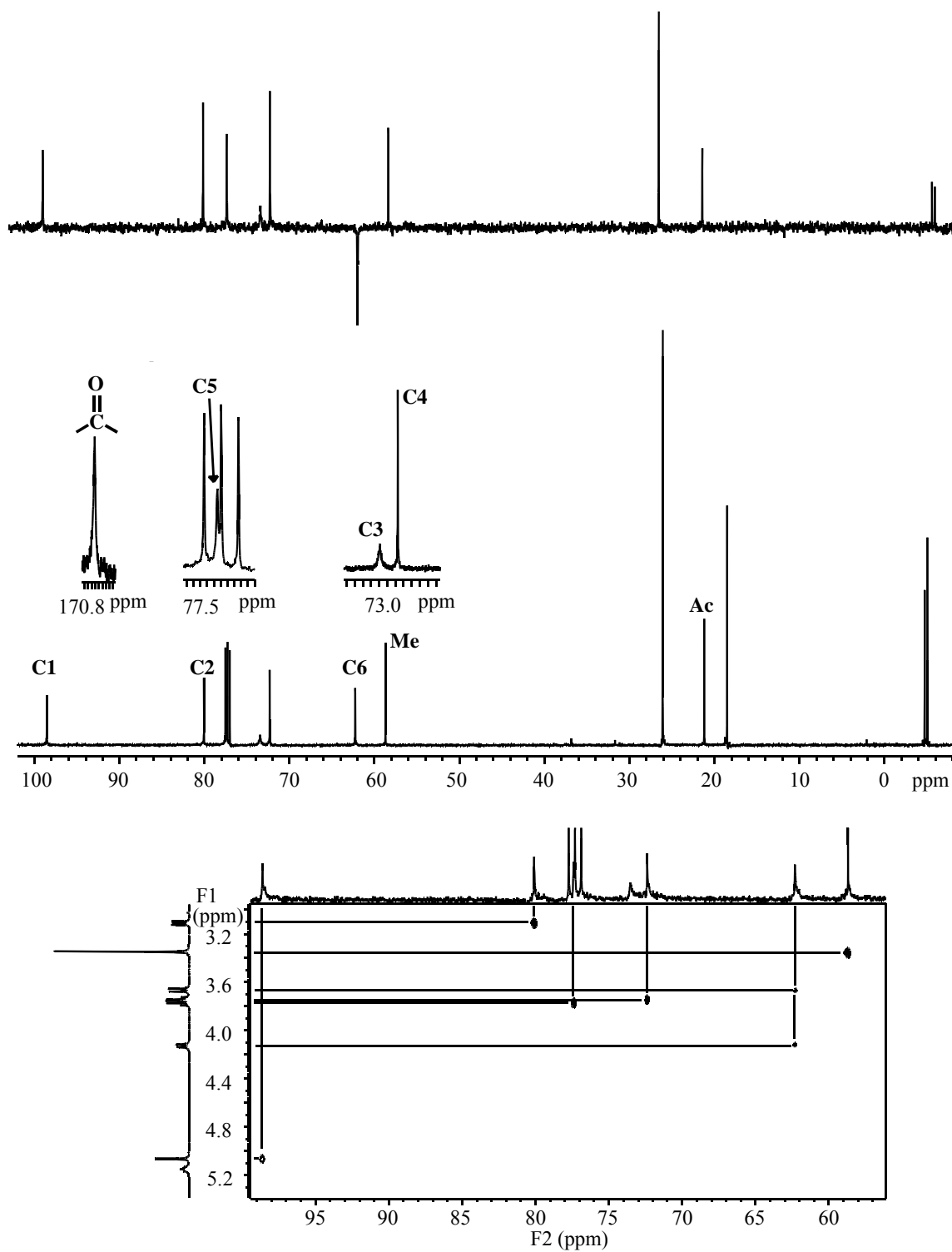
Figure 23. A) DEPT B) ^{13}C and C) ^{1}H- ^{13}C HETCOR spectra of (**6**) in CDCl$_3$.

11.0 Hz, $J_{6,5}$ 2.0 Hz, H-6), δ 3.78 (t, 7H, $J_{4,5} = J_{4,3}$ 9.3 Hz, H-4), δ 3.74, (d, 7H, $J_{5,4}$ 9.3 Hz, H-5), δ 3.67 (d, 7H, $J_{6',6}$ 11.0 Hz, H-6'), δ 3.36 (s, 21H, **CH**$_3$O-), δ 3.12 (dd, 7H, $J_{2,3}$ 9.3 Hz, $J_{2,3}$ 9.3 Hz, $J_{2,1}$ 3.5 Hz, H-2), δ 2.09 (s, 21H, **CH**$_3$CO-), δ 0.90 (s, 63H, Si(CH$_3$)$_2$(C(**CH**$_3$)$_3$), δ 0.046 and 0.044 (2 × s, 42H, Si(**CH**$_3$)$_2$(C(CH$_3$)$_3$); ^{13}C δ 170.31 (CH$_3$**C**O-), δ 98.55 (C-1), δ 80.07 (C2), δ 77.36 (C5), δ 73.45 (C3), δ 72.35 (C4), δ 62.26 (C6), δ 58.70 (**CH**$_3$O-), δ 26.10 (Si(CH$_3$)$_2$(C(**CH**$_3$)$_3$), δ 21.20 (**CH**$_3$CO-), δ 18.50 (Si(CH$_3$)$_2$(**C**(CH$_3$)$_3$), δ- 4.73 and - 5.06 (Si(**CH**$_3$)$_2$(C(CH$_3$)$_3$).

^{1}H-^{1}H COSY and ^{1}H-^{13}C HETCOR spectra show only the signals corresponding to the CD backbone. Upfield shift of the H-3 signal in the proton NMR confirms acetylation at the C3 hydroxy group. The ^{13}C NMR shows a broad weak signal for the C3 carbon. A likely explanation is that conformational change about the C3 carbons is slow on the NMR time scale. The same spectral feature was not observed in deuteroacetone (CD$_6$CO). NMR analysis was conducted in CDCl$_3$ because better spectral resolution was observed in the ^{1}H spectrum.

A portion of the high resolution MALDI-TOF-MS spectrum of (**6**) is shown in Figure 24. The measured m/z values of 2348.26 and 2364.26 agree well with the value calculated for the monoisotopic sodium and potassium adducts, 2348.14 and 2364.13, respectively. X-ray crysallographic data were collected from a single crystal of (**6**) grown from EtOAc. Shown in Figure 25 are the stick representation and the Connelly solvent surface of (**6**). Clearly, the substitution pattern is as expected. The Connelly solvent surface shows that the cavity diameter of (**6**) in the crystal is approximately 8-12Å.

Figure 24. A section of the MALDI-TOF-MS mass spectrum of (**6**).
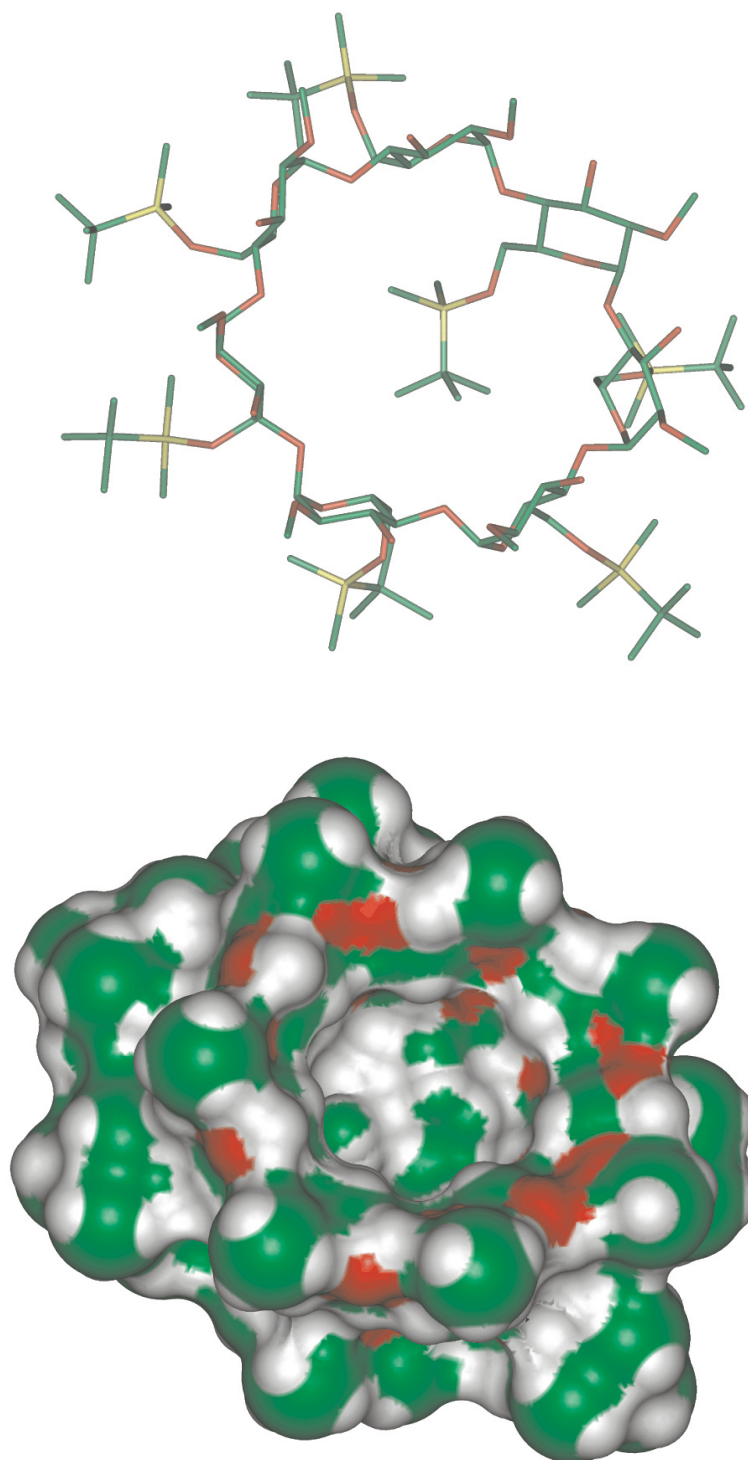
Figure 25. X-ray crystal structure of (**6**) in stick (top) and Connelly solvent surface (bottom) representations.

2.2.6 Heptakis(2-O-methyl-3-*O*-acetyl)cyclomaltoheptaose

Deprotection of (**6**) was done using hydrofluoric acid and sodium fluoride in

MeOH at 50º C in 72 hrs. The reaction was monitored using a 5μm Luna, C18 RP-HPLC

column and gradient elution at a flow rate of 2 mL/min with a mobile phase that begins

at 95:5 H_2O:THF and changes in twelve minutes to 25:75 H_2O:THF for five minutes.

Once desilylation was complete, the reaction solvent was removed under reduced

pressure and the product redissolved in CH_2Cl_2. Sodium fluoride was filtered and the

solvent volume reduced. The crude product was then four times digested in 1.5 L diethyl

ether to yield 314 g (96% yield) of (**7**) as a white powder at 99.4% isomeric purity.

Shown in Figure 26 is the RP-HPLC chromatogram (**7**) after digestion in diethyl ether.

Full ^{1}H and ^{13}C analyses are included in Figures 27 and 28, respectively. Peak

assignments for ^{1}H and ^{13}C NMR spectra were made from 1-dimensional DEPT and 2-

dimensional ^{1}H- ^{1}H COSY and ^{1}H- ^{13}C HETCOR experiments. NMR data (D_2O): ^{1}H δ

5.11 (t, 7H, $J_{3,4}$ 10.0, H-3), δ 5.06 (d, 7H, $J_{1,2}$ 3.5 Hz, H-1), δ 3.83 (dd, 14H, $J_{6,6'}$ 12.5 Hz,

$J_{6,5}$ 3.5 Hz, H-6), δ 3.78 (m, H-5,6'), δ 3.67 (t, 7H, $J_{4,3}$10.0 Hz, H-4), δ 3.30 (m, 21H, H-2,

CH$_3$O-), δ 2.0 (s, 21H, **CH**$_3$CO-); ^{13}C δ 173.22 (CH$_3$**C**O-), δ 98.26 (C-1), δ 78.92 (C2), δ

77.39 (C4), δ 73.06 (C3), δ 71.91 (C5), δ 60.38 (C6), δ 58.67 (**CH**$_3$O-), δ 20.85

(**CH**$_3$CO). ^{1}H-^{1}H COSY and ^{1}H-^{13}C HETCOR spectra show only the signals

corresponding to the CD backbone.

A portion of the high resolution MALDI-TOF-MS spectrum of (**7**) is shown in

Figure 29. The measured m/z values of 2348.26 and 2364.26 agree well with the value

calculated for the monoisotopic sodium and potassium adducts, 2348.14 and 2364.13,
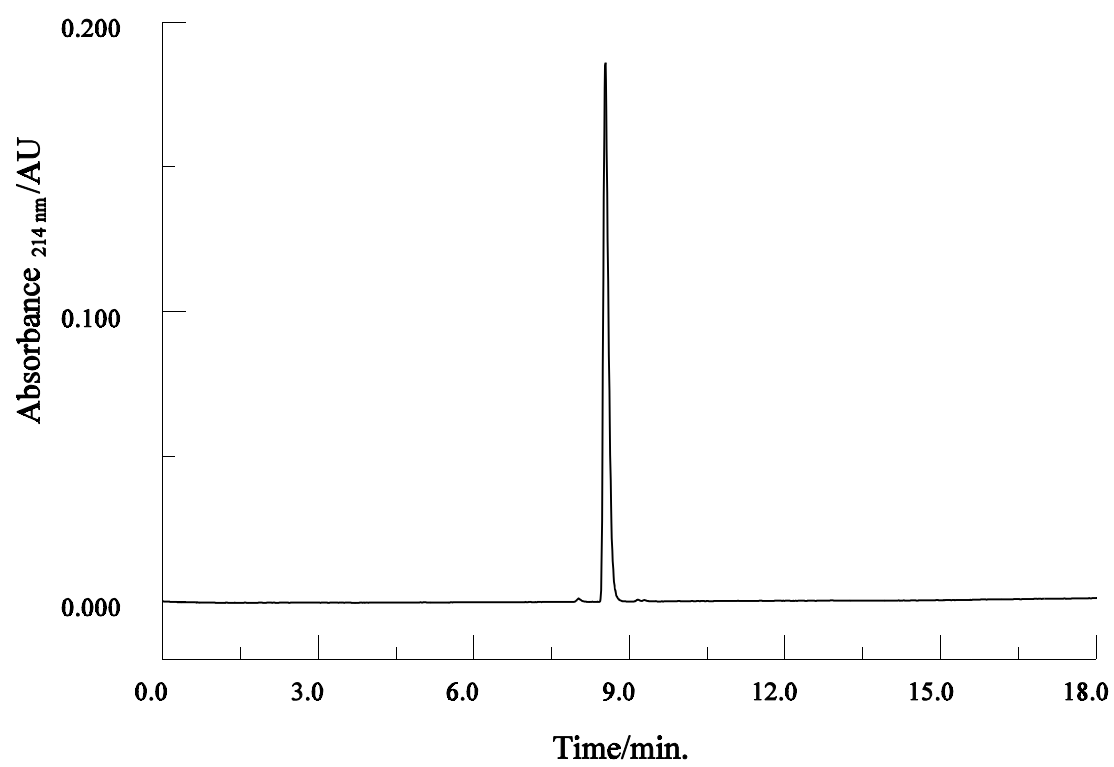
Figure 26. HPLC-ELSD chromatogram of (**7**) after diethyl ether digestion.
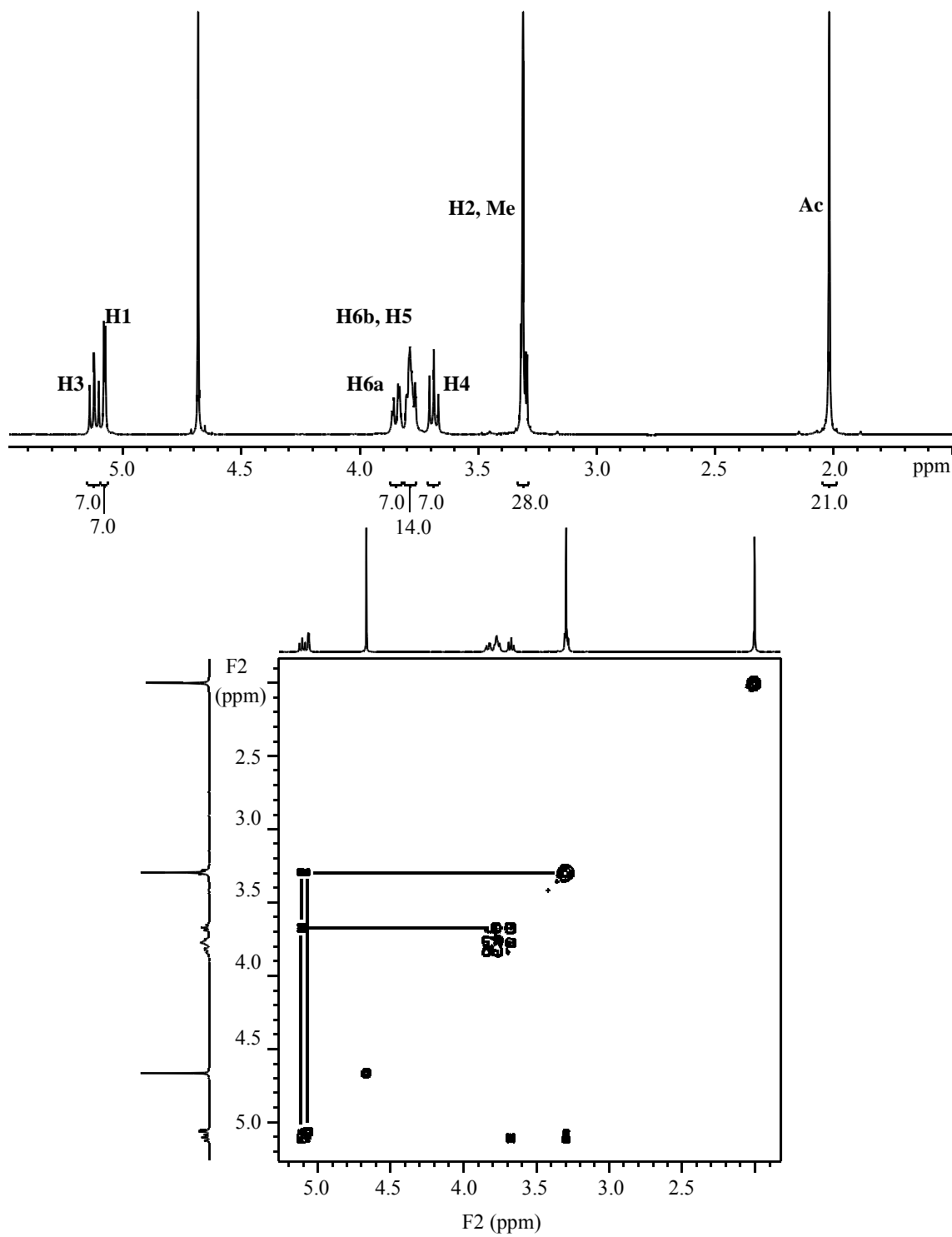
Figure 27. A) ^{1}H and B) ^{1}H-^{1}H COSY spectra of (**7**) in D$_2$O.
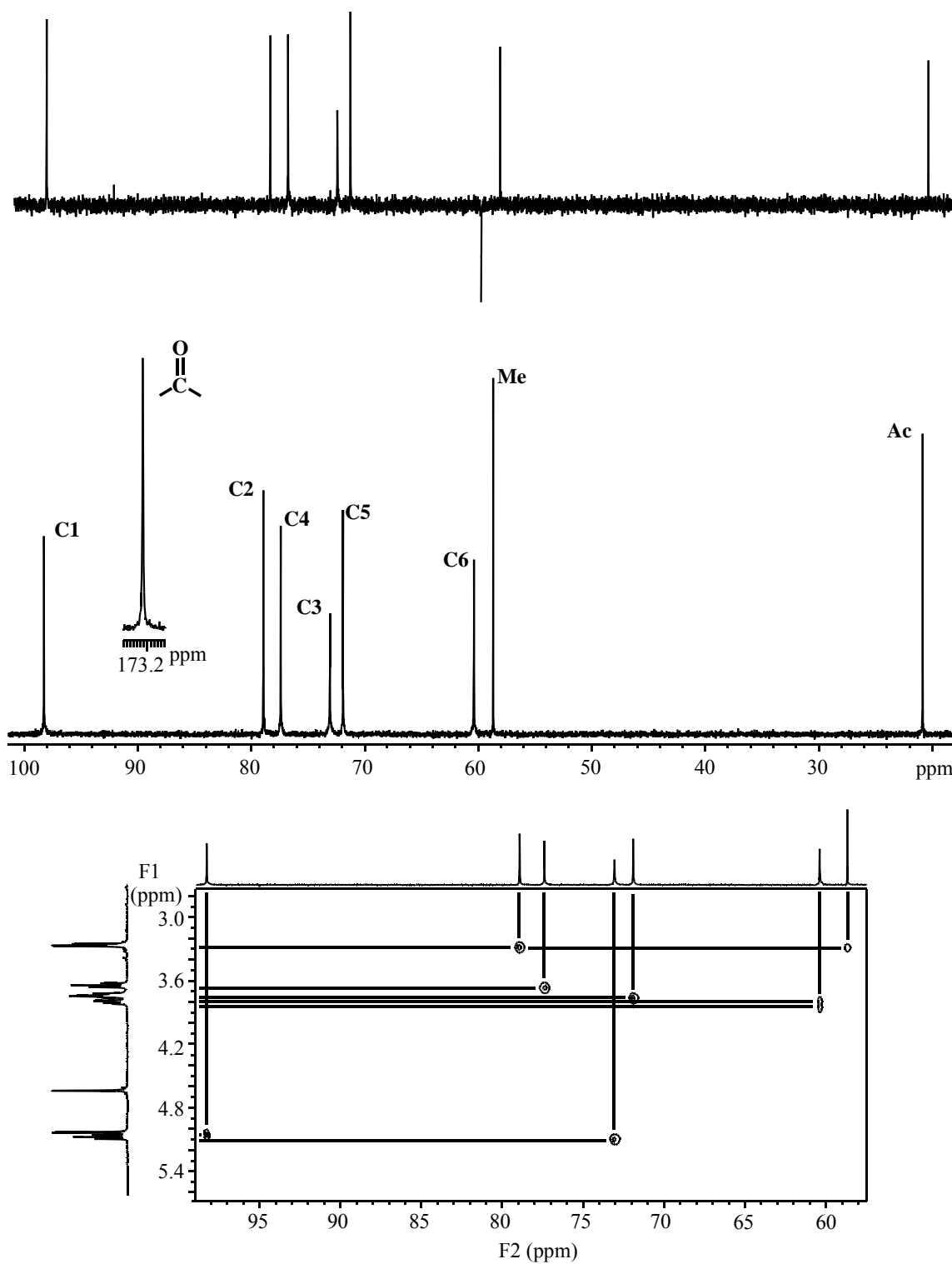
Figure 28. A) DEPT B) ^{13}C and C) ^{1}H- ^{13}C HETCOR spectra of (**7**) in D$_2$O.

from EtOAc. Shown in Figure 30 are the stick representation and the Connelly solvent

surface of (**7**). Clearly, the substitution pattern is as expected, and the Connelly solvent

surface shows a cavity diameter of approximately 8-12Å for (**7**).
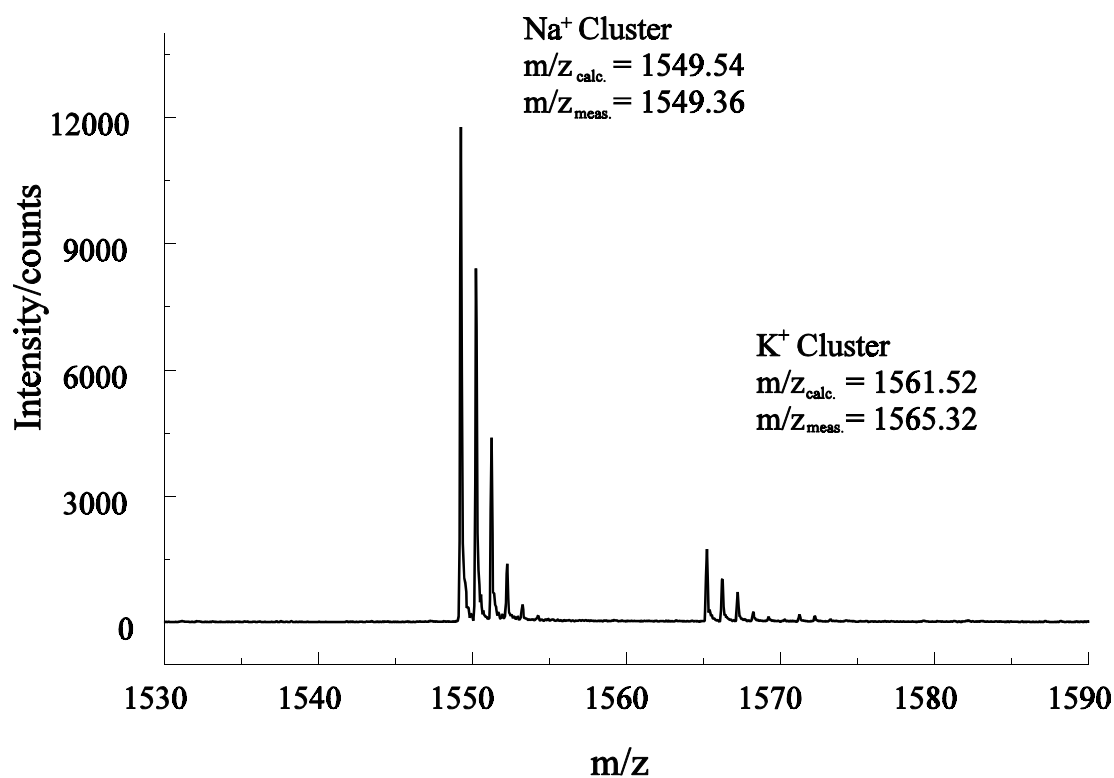
Figure 29. A section of the MALDI-TOF-MS mass spectrum of (**7**).
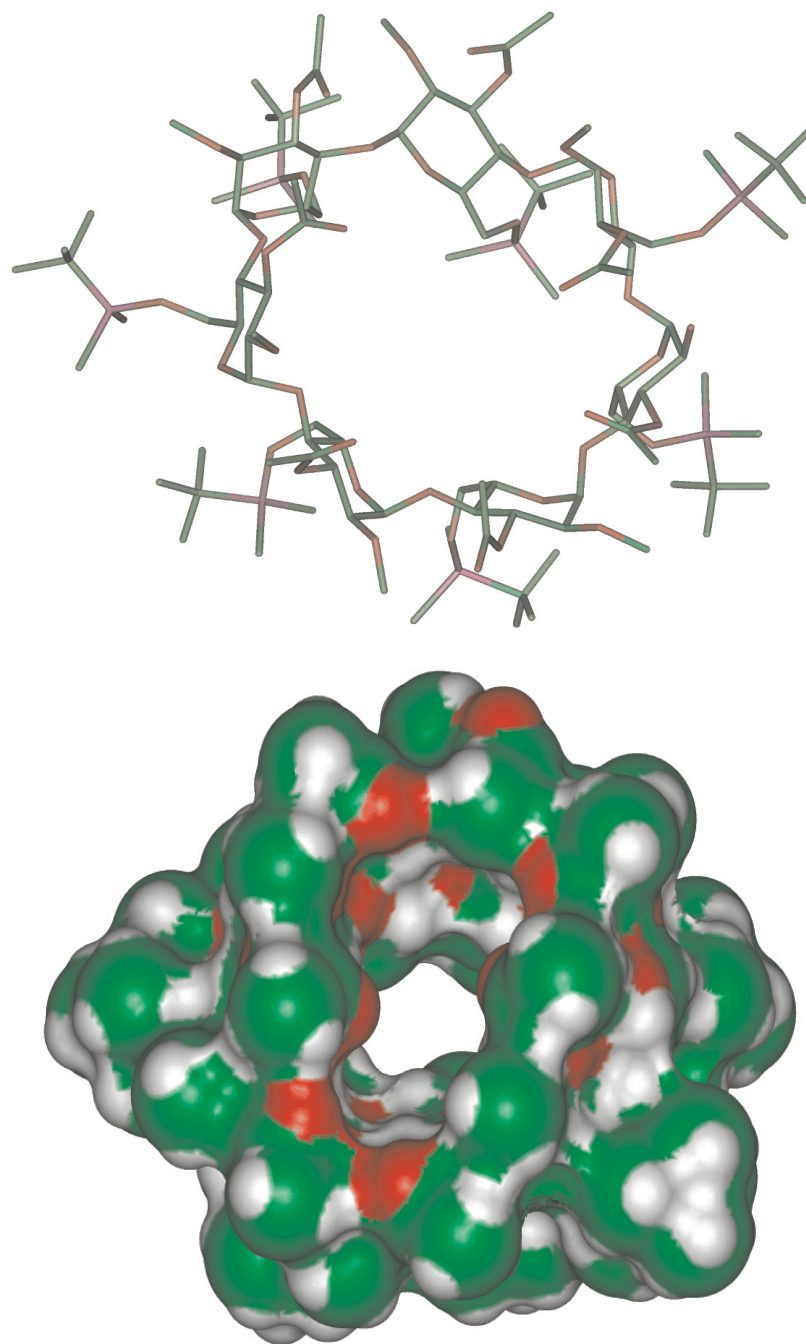
Figure 30. X-ray crystal structure of (7) in stick (top) and Connelly solvent surface (bottom) representations.

2.2.7 Heptakis(2-*O*-methyl-3-*O*-acetyl-*6*-O-sulfo)cyclomatoheptaose

Sulfation of (**7**) was conducted in DMF at room temperature with an excess of pyridine complexed sulfur trioxide. Reaction completion was monitored using indirect-UV CE with a BGE consisting of 30 mM β-alanine titrated to pH 3.5 with para-toluenesulfonic acid. Polarity was set (-) to (+), across a 46 cm long, 25 μm I.D. capillary (39 cm to detector) with 20 kV potential and detection at 214 nm. After 1 hr stirring, the reaction was quenched with sodium bicarbonate and sodium sulfate filtered. DMF was removed under reduced pressure, the crude material dissolved in a minimum volume of MeOH and precipitated by pouring it into diethylether. This was repeated four to six times or until all DMF traces were removed as indicated by proton NMR. The remaining sodium sulfate was removed by dissolving the product at concentration of 50 mM in MeOH and filtering. MeOH was removed under reduced pressure and the product was redissolved in water which was removed under reduced pressure. This procedure was scaled to 200 g. The product was dried in vacuo to give 276 g (94% yield) of (**8**) as a white powder that was >97% isomerically pure. The indirect-UV CE trace of (**8**) is shown in Figure 31.

Full ^{1}H and ^{13}C analyses are included in Figures 32 and 33, respectively. Peak assignments for ^{1}H and ^{13}C NMR spectra were made from 1-dimensional DEPT and 2-dimensional ^{1}H-^{1}H COSY and ^{1}H-^{13}C HETCOR experiments. NMR data (D_2O): ^{1}H δ 5.17 (d, 7H, $J_{1,2}$ 3.5 Hz, H-1), δ 5.14 (t, 7H, $J_{3,4} = J_{4,5}$ 9.4 Hz, H-3), δ 4.42 (d, 7H, $J_{6,6'}$ 11.0 Hz, H-6), δ 4.19 (d, 7H, $J_{6',6}$ 11.0 Hz, H-6'), δ 3.98 (d, 7H, $J_{5,4}$ 9.4 Hz, H-5), δ 7H, $J_{4,3} = J_{4,5}$ 9.4 Hz, H-4), δ 3.34 (m, 28H, H-2, **CH**$_3$O-), δ 2.04 (s, 21H, **CH**$_3$CO-); ^{13}C δ

Figure 31. Indirect UV-detection CE of HMAS. Conditions: 30 mM β-alanine titrated to pH 3.5 with para-toluenesulfonic acid. Polarity was set (-) to (+), L_d/ L_t = 39.6/ 46.4 cm, 20 kV, (+) to (-) polarity.
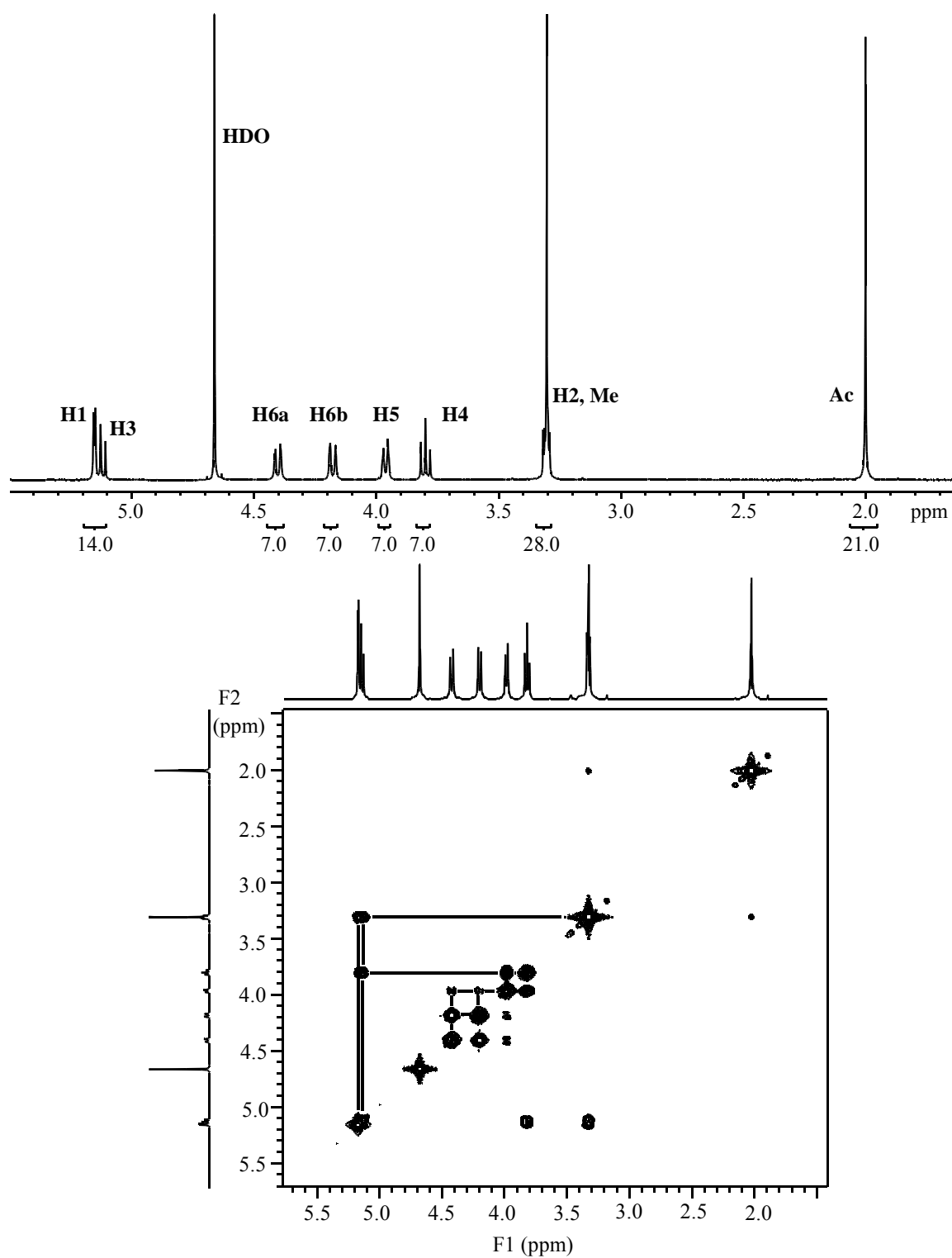
Figure 32. A) ^{1}H and B) ^{1}H-^{1}H COSY spectra of (**8**) in D$_2$O.
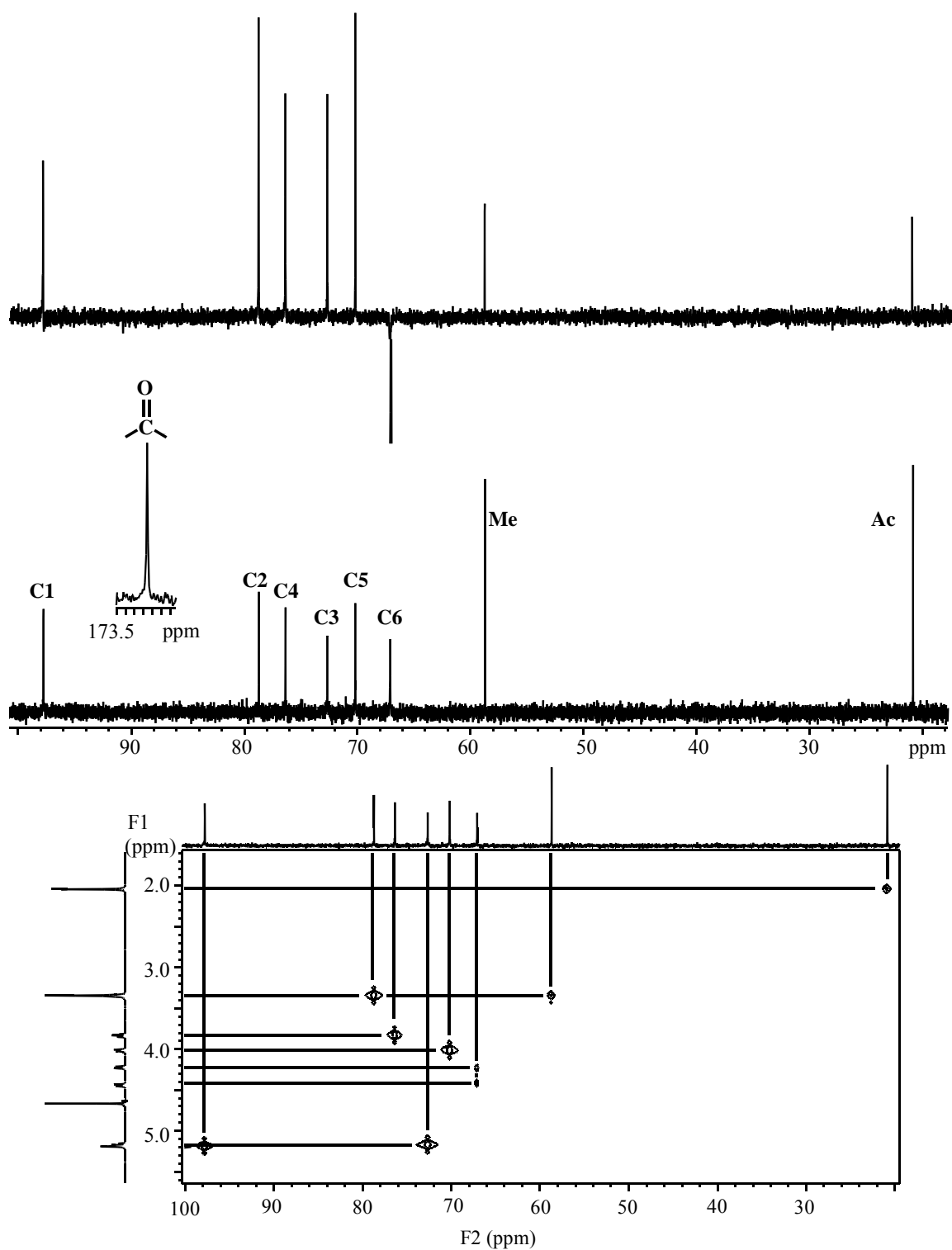
Figure 33. A) DEPT B) ^{13}C and C) ^{1}H- ^{13}C HETCOR spectra of (**8**) in D$_2$O.

173.28, δ 97.78 (C-1), δ 78.72 (C2), δ 76.35 (C4), δ 72.66 (C3), δ 70.19 (C5), δ 67.10

(C6), δ 58.69 (**CH**$_3$O-), δ 20.85 (**CH**$_3$CO-). ^{1}H-^{1}H COSY and ^{1}H-^{13}C HETCOR spectra

show only the signals corresponding to the CD backbone. Selective deprotection of the

C6 hydroxy group occurred without concurrent deacetylation as is evident in the proton

spectrum integration values.

A portion of the high resolution MALDI-TOF-MS spectrum of (**8**) is shown in

Figure 34. The measured m/z value of 2263.11agrees well with the value calculated for

the monoisotopic sodium adduct, 2263.58. No potassium adduct was observed.

Ionization of a potassium adduct was likely suppressed due to the abundance of sodium

in the sodium salt of the final product.
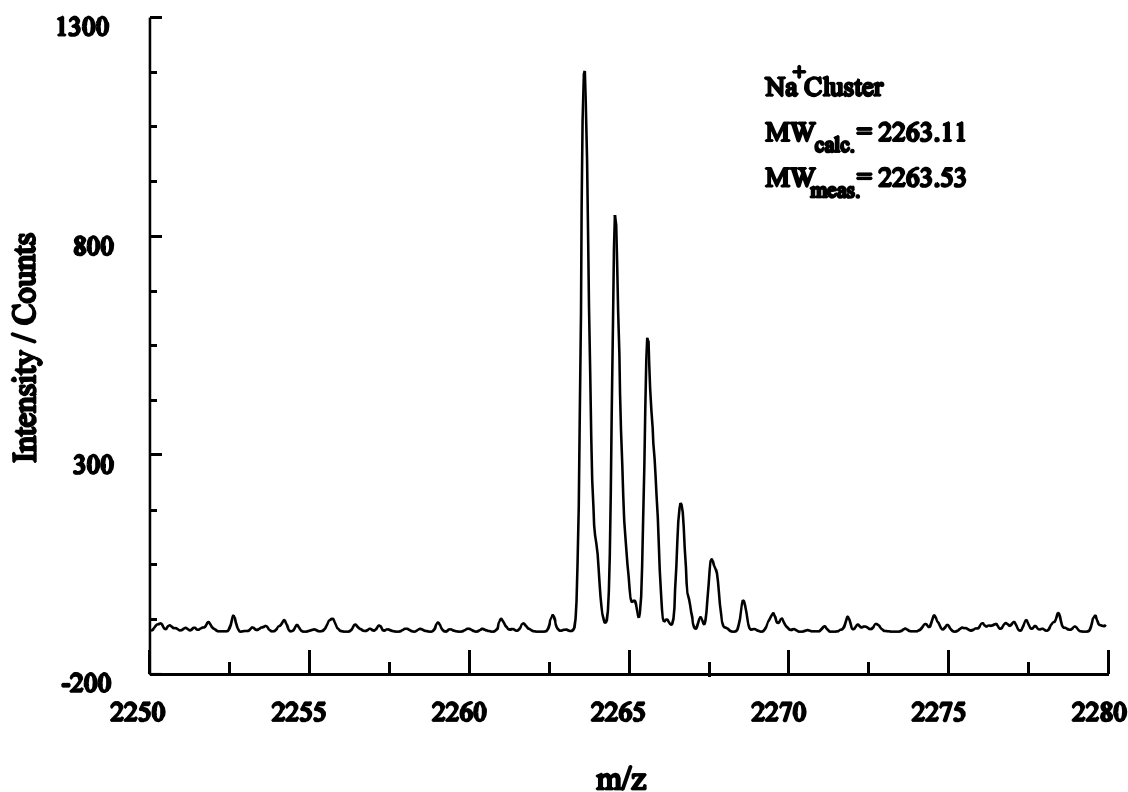
Figure 34. A section of the MALDI-TOF-MS mass spectrum of (**8**).

2.2.8 Heptakis(2-*O*-methyl-3-hydroxy-6-*O*-sulfo)cyclomaltoheptaose

Deacetylation of (**8**) was carried out under basic aqueous conditions. Completion

of the reaction was monitored using indirect-UV CE with a BGE consisting of 30 mM β-

alanine titrated to pH 3.5 with para-toluenesulfonic acid. Polarity was set (-) to (+),

across a 46 cm long, 25 μm I.D. capillary (39 cm to detector) with 20 kV potential and

detection at 214 nm. After 3 hr stirring, the volume of the reaction mixture was reduced

under reduced pressure to produce a viscous solution. The crude product was

precipitated by pouring it into anhydrous isopropanol (IPA). This was repeated six times

to complete removal of acetate as indicated by indirect-UV CE analysis using a BGE that

was 30-mM in THAM titrated to pH 8.1 with para-toluenesulfonic acid. Other conditions

were as in Section 2.2.7. Shown in Figure 35 is the indirect-UV CE trace of (**9**) after

precipitation from water/IPA. This reaction was scaled to 100 g. The product was dried

in vacuo to give 60 g (65% yield) of (**9**) as a white powder that was >97% isomerically

pure.

Full ^{1}H and ^{13}C analyses are included in Figures 36 and 37, respectively. ^{1}H-^{1}H

COSY and ^{1}H-^{13}C HETCOR spectra show only the signals corresponding to the CD

backbone. Peak assignments for ^{1}H and ^{13}C NMR spectra were made from 1-dimensional

DEPT and 2-dimensional ^{1}H- ^{1}H COSY and ^{1}H- ^{13}C HETCOR experiments. NMR data

(D_2O): ^{1}H δ 5.53 (d, 7H, $J_{1,2}$ 3.5, H-1), δ 4.41 (d, 7H, $J_{6,6'}$ 10.5 Hz, H-6), δ 4.30 (d, 7H,

$J_{6',6}$ 10.5 Hz, H-6'), δ 4.17 (d, 7H, $J_{5,4}$ 10.0 Hz, H-5), δ 4.05 (t, 7H, $J_{3,2}$ = $J_{3,4}$ 10.0 Hz, H-

3), δ 3.81 (t, 7H, $J_{4,3}$ = $J_{4,5}$ 10.0 Hz, H-4), δ 3.58 (s, 21H, C**H**$_3$O-), δ 3.37 (dd, 7H, $J_{2,1}$ 3.5

Hz, $J_{2,3}$ 10.0 Hz, H-2); ^{13}C δ 97.03 (C-1), δ 81.17 (C2), δ 77.54 (C4), δ 71.99 (C3), δ
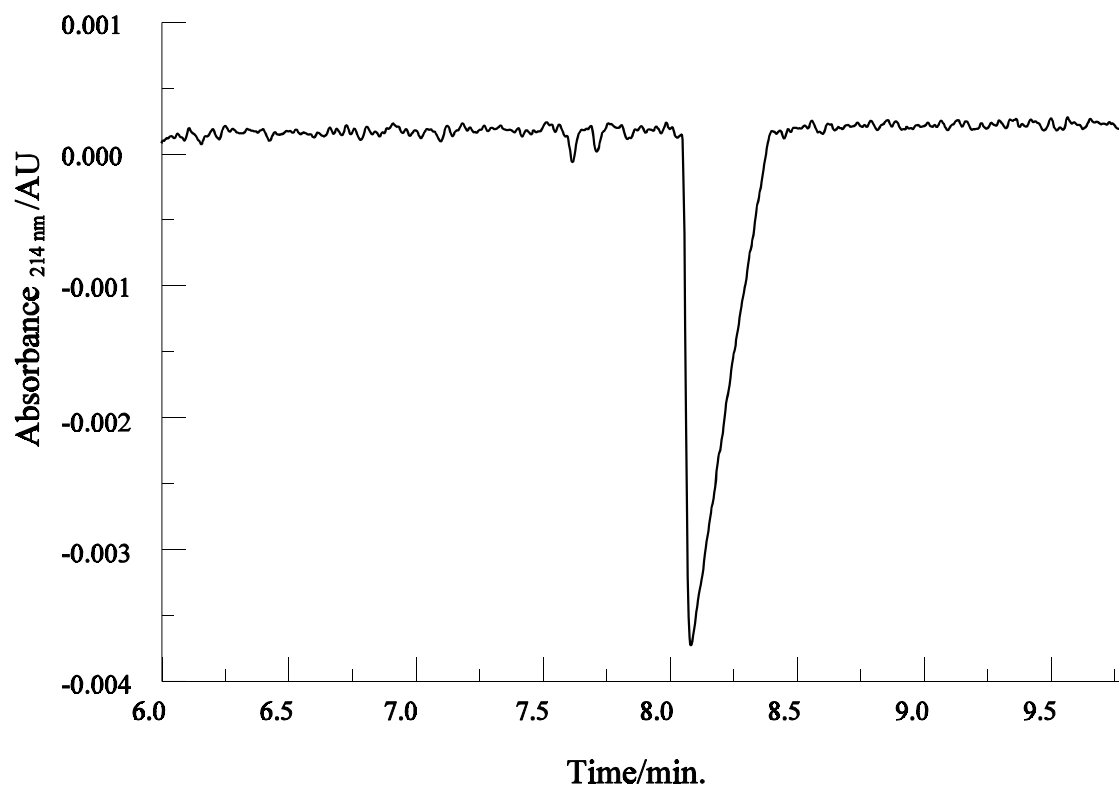
Figure 35. Indirect UV-detection CE of HMAS. Conditions: 30 mM β-alanine titrated to pH 3.5 with para-toluenesulfonic acid. Polarity was set (-) to (+), $L_d/L_t = 39.6/46.4$ cm, 20 kV, (+) to (-) polarity.
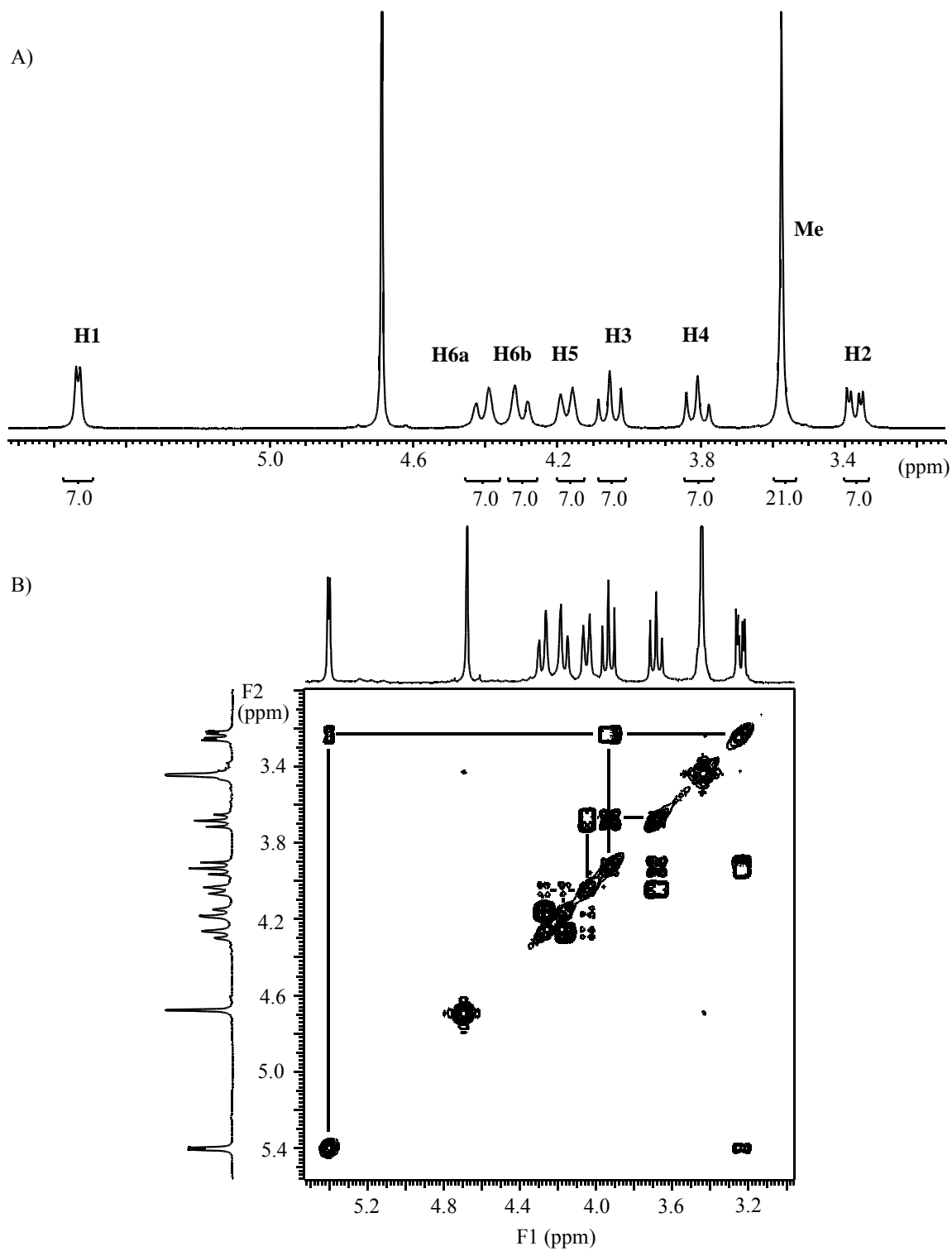
Figure 36. A) ^{1}H and B) ^{1}H-^{1}H COSY spectra of (**9**) in D$_2$O.
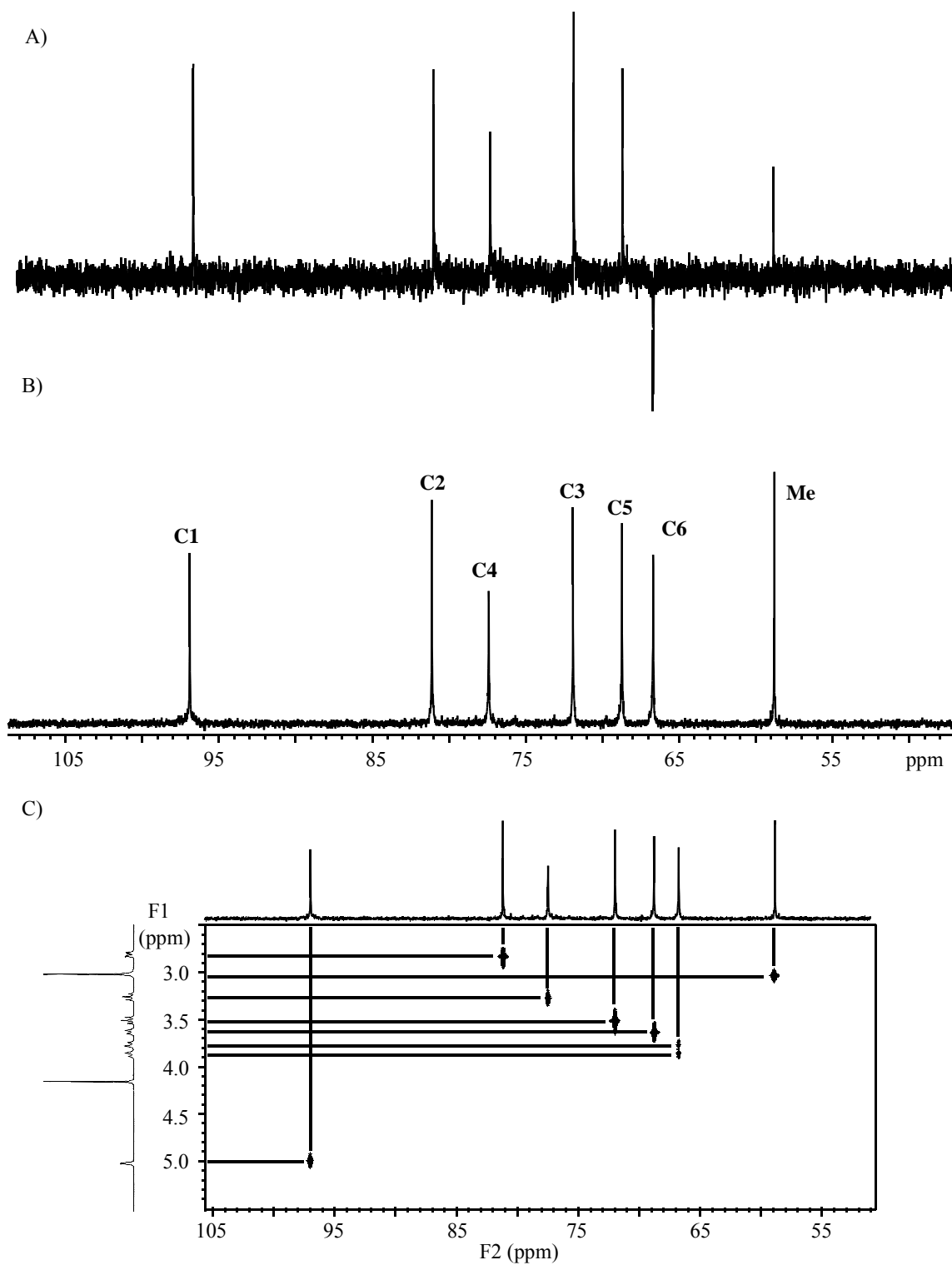
Figure 37. A) DEPT B) ^{13}C and C) ^{1}H- ^{13}C HETCOR spectra of (**9**) in D$_2$O.

68.78 (C5), δ 66.78 (C6), δ 58.94 ($\mathbf{C}H_3O$-). ^{1}H-^{1}H COSY and ^{1}H-^{13}C HETCOR spectra show only the signals corresponding to the CD backbone.

A portion of the high resolution MALDI-TOF-MS spectrum of (**9**) is shown in Figure 38. The measured m/z value of 1969.29 agrees well with the value calculated for the monoisotopic sodium adduct, 1969.04. Little potassium adduct was observed. Ionization of a potassium adduct was likely suppressed due to the abundance of sodium in the sodium salt of the final product.
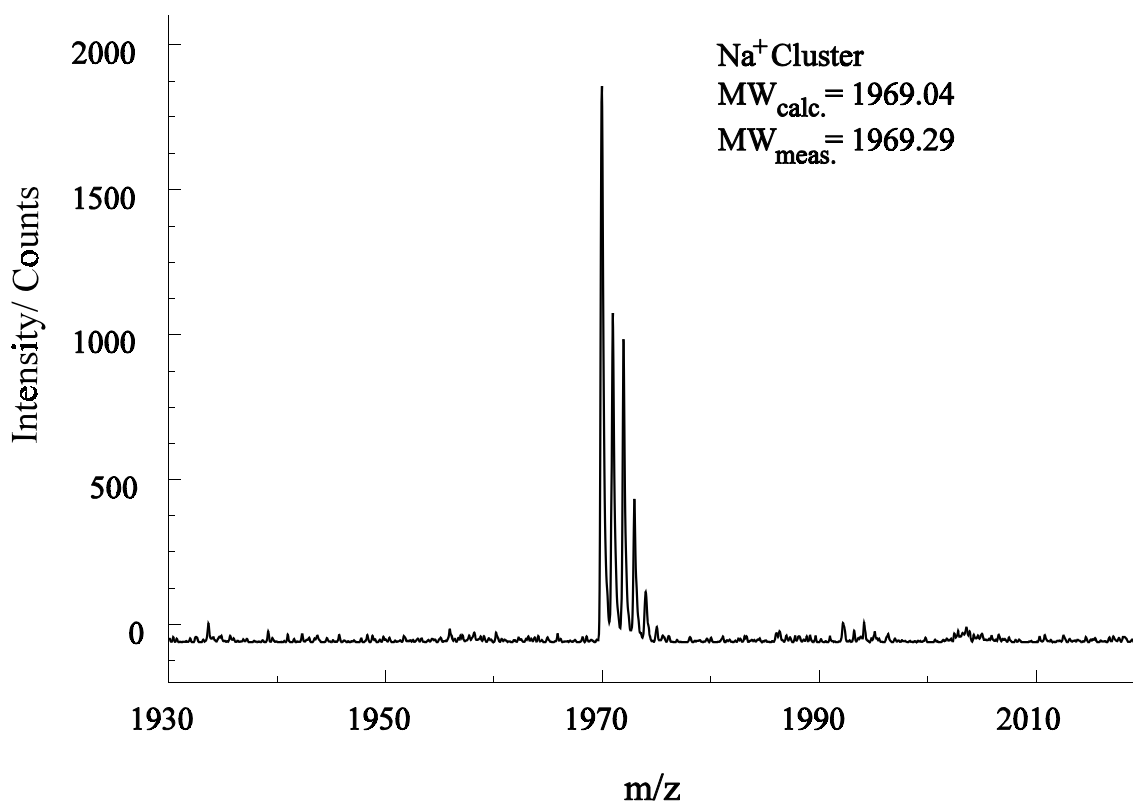
Figure 38. A section of the MALDI-TOF-MS mass spectrum of (**9**).

2.4 Summary

The large-scale synthesis of the sodium salts of HMAS and HMS for use as chiral resolving agents in capillary electrophoretic separation of enantiomers has been accomplished via an eight-step synthetic methodology. Development of new, highly selective deprotection reaction conditions made possible these new derivatives in a minimum number of synthetic steps. The overall yields for HMAS and HMS were 39% and 25%, respectively. The final products, along with each intermediate, have been been extensively characterized by analytical methods including HPLC-ELSD, indirect-UV detection CE, MALDI-TOF MS, 1D and 2D NMR and X-ray diffraction crystallography to show that, indeed, the single-isomer SISCD's were produced.

CHAPTER III

ENANTIOMER SEPARATIONS

3.1 Use of HMAS and HMS as Chiral Resolving Agents

The structures of the twenty four, structurally diverse, weakly basic

pharmaceuticals selected to evaluate the utility of HMAS and HMS as chiral resolving

agents for use in CE enantiomer separations are shown in Figure 39. Separation

selectivity (α) was determined as a function of concentration of the chiral resolving agent

in two BGE's, including an aqueous low pH BGE and a methanolic low pH BGE, each

with variable HMAS or HMS concentrations. All twenty four weakly basic compounds

have been shown to have cationic effective mobilities under the selected conditions in

the absence of SISCD. The effective mobilities (μ^{eff}) and the normalized electroosmotic

mobilities (β) were calculated per Equations 1 and 8 (see Chapter I), respectively. Peak

resolution was calculated from peak half-height widths (w^h) as $Rs=[2(t_2-$

$t_1)]/[1.699(w^h_2+w^h_1)]$. Migration time values used were taken at the point of infinite

dilution for peaks suffering electromigration dispersion (EMD). Effective mobilities and

separation selectivities were plotted as a function of the resolving agent concentration to

evaluate the best chiral resolving agent and concentration for the highest available

separation selectivity. Whenever possible, qualitative comparisons were made between

the separations achieved in aqueous and non-aqueous BGE's as well as to separations

achieved using other SISCD's bi-functionalized at the C-2 and C-3 hydroxyl groups.
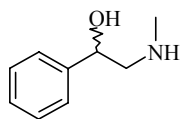
B04: Halostachine
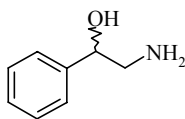
B06: Phenylethanolamine
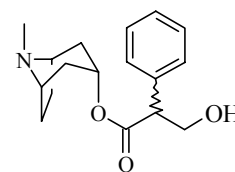
B09: Atropine
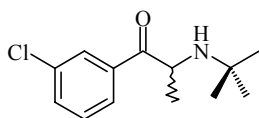
B11: Bupropion
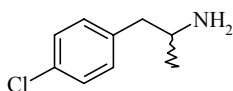
B13: 4-Chloroamphetamine
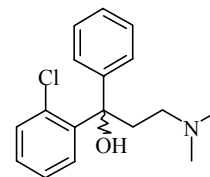
B14: Chlophedianol
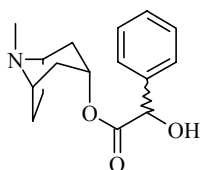
B19: Homatropine
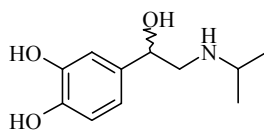
B21: Isoproterenol
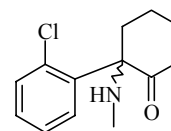
B22: Ketamine
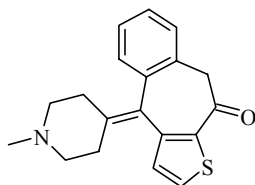
B23: Ketotifen
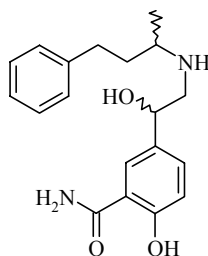
B24: Labetolol
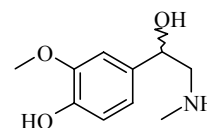
B26: Metanephrine

Figure 39. Names and structures of weakly basic analytes.
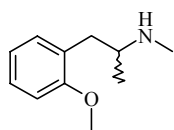
B28: Methoxyphenamine
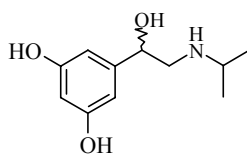
B30: Metaproterenol
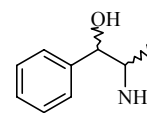
B34: Norephedrine
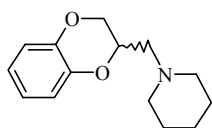
B38: Piperoxan
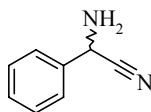
B39: Phenylglycinonitrile
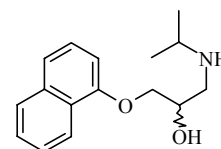
B42: Propranolol
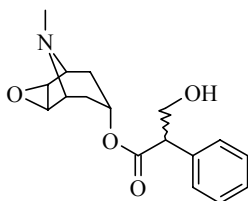
B46: Scopolamine
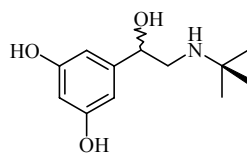
B47: Terbutaline
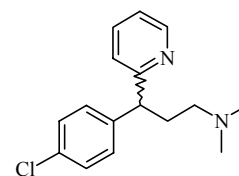
B56: Chlorpheniramine
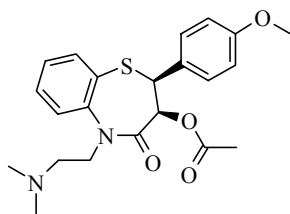
B57: Diltiazem
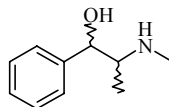
B60: Ephedrine
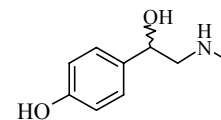
B61: Synephrine

Figure 39. Continued.

3.2 Materials and Methods

All chiral analytes listed in Figure 39 were obtained from either Sigma (St. Louis, MO), Aldrich Chemical Co. (Milwaukee, WI), Wiley Organics (Coshocton, OH) or Research Diagnostics (Rockdale, MD). Dimethylsulfoxide (DMSO) and HPLC grade methanol were purchased from EM Science (Gibbstown, NJ). Aqueous solutions were prepared from deionized water obtained from an in-house Milli-Q unit (Millipore, Milford, MA). All solutions were filtered prior to use with a 0.45 μm Nalgene nylon membrane filter (VWR, South Plainfield, NJ). Naphthalenesulfonic acid (NSA), phosphoric acid and lithium hydroxide were purchased from Aldrich Chemical Co. HMAS and HMS were prepared as described in Chapter II.

Capillary electrophoretic measurements were made using either a P/ACE 2050 or P/ACE 2100 CE instrument with its UV detector set to 214 nm. A 26.4 cm total length (19.6 cm to detector), 27 μm i.d., naked fused-silica capillary was used for both the aqueous and for the nonaqueous CE measurements. The aqueous BGE was buffered at low pH with 25 mM H_3PO_4 (pKa_1 2.1), titrated to pH 2.5 with LiOH. An acidic methanolic buffer was prepared from 25 mM H_3PO_4 and 12.5 mM NaOH for use in nonaqueous measurements. The stock buffers were used to prepare the 0-30 mM SISCD BGE's for CE enantiomer separations. The enantiomers were dissolved in the BGE and co-injected for 1 s by 1 psi nitrogen with either the EOF marker or the anionic mobility marker from a solution approximately 0.5 mM in both the analyte and the marker. Ohm's plots were measured from 0-30 mM SISCD at 2.5, 5, 10, 20 and 30 mM SISCD concentrations in each BGE. Effective mobility measurements were carried out within

the linear region of Ohm's law. The effective mobilities of the enantiomers were measured against either a dimethylsulfoxide (DMSO) neutral marker which possesses no intrinsic charge and thus has zero effective mobility at the pH of the BGE's or NSA which is a monovalent anion at the pH of the BGE's. The effective mobility of NSA in the various SISCD containing BGE's was measured relative to DMSO using the three-band PreMCE method [95].

3.3 Low pH Aqueous Separations Using HMAS as Chiral Selector

Effective mobilities for moderate molecular weight (200 < MW < 500), singly-charged, weakly basic compounds usually lie in the $+10 \times 10^{-5}$ $cm^2V^{-1}s^{-1}$ to $+25 \times 10^{-5}$ $cm^2V^{-1}s^{-1}$ range. Consequently, use of low pH BGE's, where μ^{eo} values are around $+10 \times 10^{-5}$ $cm^2V^{-1}s^{-1}$ to $+25 \times 10^{-5}$ $cm^2V^{-1}s^{-1}$ in naked fused silica capillaries, is conducive to good resolution because more favorable β values are obtained than in high pH BGE's where typical μ^{eo} values are higher than $+50 \times 10$ $cm^2V^{-1}s^{-1}$ [68]. Previous work has shown that, in the molecular weight range specified, complexation of weak bases with SISCD's commonly leads to anionic effective mobilities as high as -25 mobility units ($\times 10^{-5}$ $cm^2V^{-1}s^{-1}$) and occasionally as high as -33 mobility units. This means that it is possible to adjust the concentration of SISCD's to bring about an effective mobility for weakly basic enantiomers that is nearly equal in magnitude but opposite in direction to the electroosmotic flow mobility and thus, take advantage of even the lowest separation selectivity to achieve resolution [68]. For these reasons, evaluation of the potential of a new SISCD to be used as a chiral resolving agent almost always begins with the

separation of weakly basic enantiomers in low pH BGE's.

Table 1 lists the effective mobilities of the less mobile enantiomers, μ, the separation selectivities, α, the peak resolution, Rs, the normalized EOF mobility values, β, and the injector-to-detector potential drop, U, obtained in the low pH aqueous BGE for the weakly basic enantiomers. An entry of N/A implies that a value could not be calculated because of overlap with a non-comigrating system peak or overlap with the neutral marker or anionic mobility marker. The applied potential was 20 kV at 2.5 mM HMAS-containing BGE and decreased with increasing HMAS concentration to 10 kV at 30 mM HMAS-containing BGE. Over the 2.5 to 30 mM HMAS concentration range, the μ^{EOF} values were 16 to 31 mobility units and were higher at greater HMAS concentration. Higher μ^{EOF} values at greater HMAS concentrations likely indicate that HMAS absorbs to the wall of the capillary since this would result in an increase in the zeta potential at the fused silica capillary wall. No studies were conducted to quantify the contribution to resolution resulting from chromatographic retention of the analytes.

There was at least some separation selectivity for the enantiomers of 19 of the 24 analytes in the aqueous BGE using HMAS as chiral resolving agent. Of these, 15 were baseline resolved (i.e., Rs > 1.5) under the conditions used. For five analytes there was no resolution including atropine, homatropine, chlorpheniramine, scopolamine and diltiazem. Two of these, atropine and homatropine, were only weakly complexing at all HMAS concentrations. Chlorpheniramine has a chiral center sterically crowded by two aromatic rings, scopolamine is a doubly bridged heterocycle and diltiazem has no chiral center rather, a chiral plane provided by the large, seven membered thiazepine ring. All

Table 1. Separations data in pH 2.5 aqueous HMAS BGE's (μ, in $10^{-5}cm^2/Vs$ units).

[HMAS]	0 mM*	2.5 mM			
U (kV)	14.8	14.8			
Analyte	μ	μ	α	β	Rs
B04	21.5	-14.9	0.78	-1.6	3.5
B06	22.1	-18.9	0.69	-1.4	10.4
B09	16.5	5.5	1.00	4.4	0.0
B11	16.0	-8.7	0.74	-2.7	3.3
B13	21.4	-24.6	0.99	-0.66	<0.5
B14	16.0	4.3	1.22	5.4	1.2
B19	17.0	5.1	1.00	4.6	0.0
B21	15.7	-27.3	0.88	-0.59	3.9
B22	18.2	11.4	1.06	2.0	0.7
B23	15.4	-6.7	0.81	-3.4	3.1
B26	18.7	-7.1	1.00	-3.2	0.0
B28	20.1	-14.0	-0.44	-1.6	14.0
B30	17.3	-30.9	0.96	-0.55	2.8
B34	21.4	-15.6	0.76	-1.6	5.8
B38	19.8	-31.1	0.87	-0.5	5.0
B39	23.5	2.5	3.79	9.5	7.2
B42	16.5	-2.6	0.89	-0.6	5.9
B46	16.0	6.4	1.00	3.6	0.0
B47	16.1	-25.8	0.95	-0.64	2.0
B56	16.2	-20.9	1.00	-1.2	0.0
B57	10.4	5.3	1.00	0.0	45
B60	18.4	-12.2	0.58	-1.9	3.6
B61	20.8	-23.1	0.85	-1.3	5.6

Table 1. Continued.

[HMAS]	5 mM				10 mM			
U (kV)	13.4				11.1			
Analyte	μ	α	β	Rs	μ	α	β	Rs
B04	-19.9	0.83	-1.3	3.4	-19.8	0.87	-1.8	2.9
B06	-21.3	0.80	-1.2	6.5	-20.8	0.83	-1.6	4.9
B09	3.8	1.00	6.6	0.0	1.6	1.00	20	0.0
B11	-10.4	0.79	-2.4	3.3	-12.5	0.85	-2.4	4.0
B13	-24.7	0.99	-1.4	<0.5	-22.5	0.99	-1.6	<0.5
B14	2.1	1.52	11.8	0.6	N/A			
B19	4.0	1.00	6.2	0.0	2.5	1.00	12	0.0
B21	-27.7	0.9	-1.2	6.9	-23.1	0.94	-1.4	4.9
B22	8.8	1.09	2.8	0.8	7.1	1.13	4.1	0.8
B23	-9.2	0.84	-2.8	4.4	-10.3	0.87	-2.8	4.4
B26	-9.3	0.98	-3.3	<0.5	-10.0	0.97	-2.9	0.6
B28	-16.3	-0.22	-1.5	12.1	-15.2	-0.04	-2.0	17
B30	-30.3	0.97	-0.68	3.2	-25.2	0.99	-1.2	2.7
B34	-17.4	0.83	-1.5	5.7	-17.3	0.86	-1.6	5.8
B38	-30.2	0.89	-0.8	9.6	-26.4	0.91	-1.2	12
B39	-3.4	-1.22	-7.3	10.4	-5.5	-0.38	-5.0	13
B42	-2.7	0.92	-0.76	9.2	-23.0	0.93	-1.2	13
B46	2.5	1.00	11.0	0.0	N/A			
B47	-26.5	0.96	-0.78	3.9	-22.5	0.97	-1.3	4.1
B56	-20.1	1.00	-1.4	0.0	-17.0	1.00	-1.6	0.0
B57	-2.6	1.00	-9.2	0.0	-4.5	1.00	-6.2	0.0
B60	-16.3	0.72	-1.6	4.7	-15.5	0.77	-1.8	6.1
B61	-24.5	0.90	-1.2	10.4	-22.0	0.92	-1.3	15

Table 1. Continued.

[HMAS]	20 mM				30 mM			
U (kV)	8.9				7.4			
Analyt	μ	α	β	Rs	μ	α	β	Rs
B04	-19.6	0.88	-1.8	3.7	-16.3	0.89	-1.8	3.7
B06	-19.6	0.83	-1.5	5.7	-16.5	0.84	-1.7	6.4
B09	N/A				N/A			
B11	-12.6	0.85	-1.7	10.3	-11.6	0.86	-2.6	5.2
B13	-19.9	0.99	-1.6	0.6	-17.1	0.99	-1.7	0.5
B14	-1.1	0.66	-19	1.6	-1.9	0.87	-15	0.6
B19	1.1	1.00	20	0.0	0.70	1.00	41	0.0
B21	-20.9	0.94	-1.5	7.8	-18.5	0.95	-1.6	5.0
B22	6.0	1.18	3.6	2.3	4.5	1.21	6.9	1.7
B23	-10.9	0.92	-2.0	3.8	-11.1	0.93	-2.7	3.7
B26	-10.4	0.97	-2.0	1.4	-8.8	0.96	-3.3	1.3
B28	-13.8	0.03	-2.2	27	-11.6	0.06	-2.5	37
B30	-22.7	0.98	-1.3	3.8	-20.1	0.98	-1.5	2.7
B34	-16.7	0.87	-1.3	8.3	-13.9	0.87	-2.0	6.4
B38	-22.6	0.92	-1.3	11.4	-19.9	0.91	-1.5	11
B39	-7.0	-0.07	-2.5	22	-6.1	-0.02	-4.6	22
B42	-20.9	0.93	-1.4	5.3	-18.2	0.94	-1.6	8.7
B46	N/A				-1.2	1.00	-24	0.0
B47	-20.2	0.98	-1.4	5.3	-11.8	0.98	-1.6	2.4
B56	-14.3	1.00	-2.2	0.0	-11.9	1.00	-2.3	0.0
B57	-6.0	1.00	-5.2	0.0	-6.5	1.00	-4.2	0.0
B60	-14.2	0.79	-2.6	5.2	-12.9	0.80	-2.2	4.7
B61	-19.6	0.93	-1.7	4.8	-17.4	0.93	-1.6	4.1

* From Ref. [39].

are strongly complexing hence, lack of separation selectivity is likely due to the very strong interaction with HMAS. The four remaining unresolved analytes showed some separation selectivity but require more favorable β-values than provided by the separation conditions used.

According to ref. [51], SISCD mediated separations of weakly basic compounds generally fall into three categories: weakly binding, moderately strongly binding and strongly binding. Categorization of the separations in this way provides some insight into the separation selectivity patterns observed as well as allowing qualitative comparison of the utility of the various available SISCD's for a given enantiomer separation. The effective mobilities of weakly binding bases do not become anionic over the SISCD concentration range used. The mobility (left panel) and separation selectivity (right panel) curves for ketamine, B22, the only baseline resolved, weakly binding base, is shown in the top panel of Figure 40. The effective mobility is initially cationic at approximately 25 mobility units. As the HMAS concentration is increased, the effective mobility approaches zero due to an increase in the mole fraction of the HMAS-analyte complex and to ionic strength-related depression of the effective mobilities of both the free and the complexed forms of the weak base. The separation selectivity curve gradually increases without approaching a limiting value over the tested HMAS concentration range.

The effective mobilities of moderately strongly binding bases are, like the weakly binding bases, initially cationic but become anionic at some intermediate SISCD concentration. The middle panel of Figure 40 shows the effective mobility (left panel)
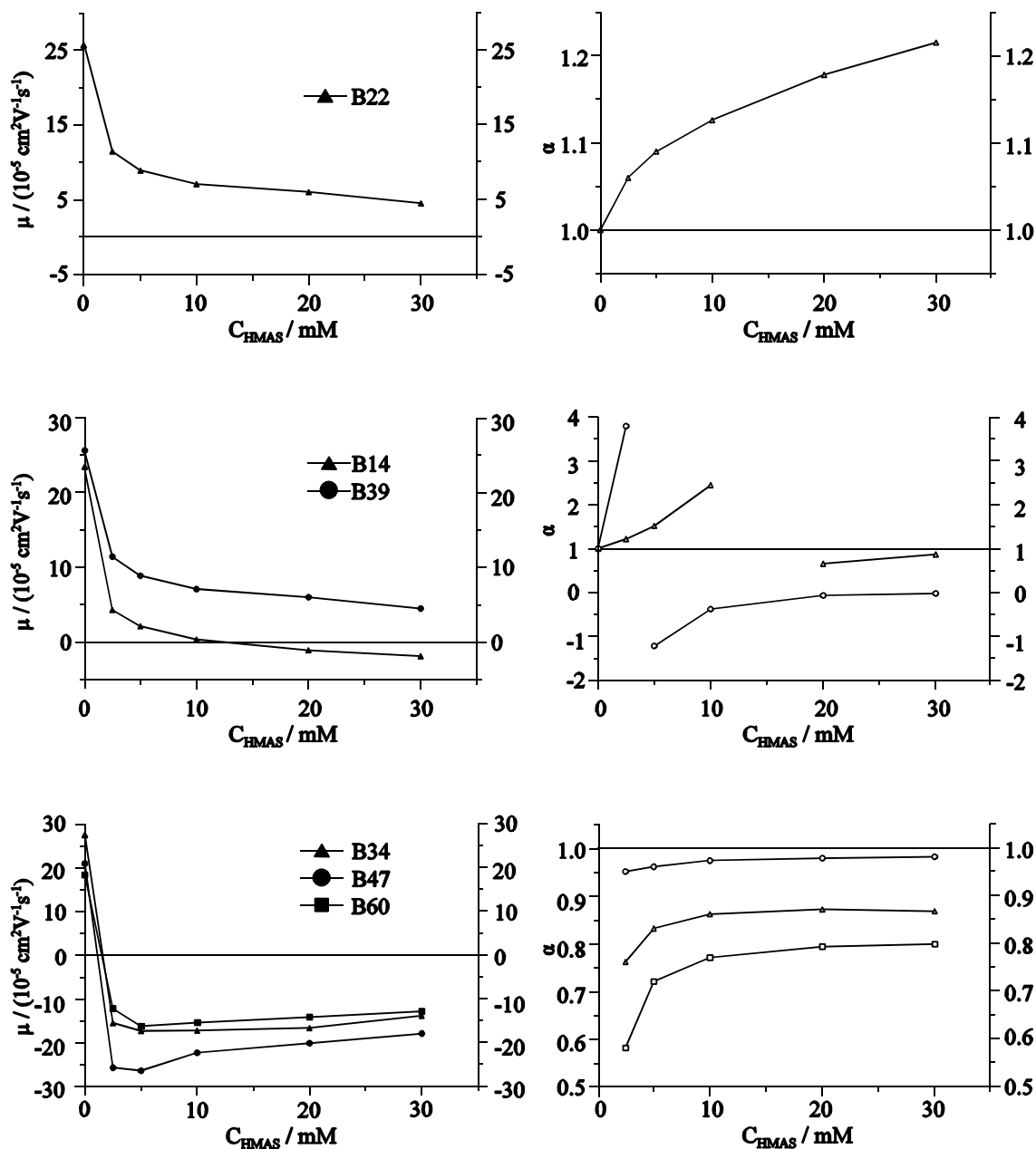
Figure 40. Effective mobilities (left panel) and separation selectivities (right panel) of weakly binding (top panel), moderately strongly binding (middle panel) and strongly binding (bottom panel) weakly basic analytes. Zero concentration effective mobility values as reported in Ref. [39].

and the separation selectivity (right panel) for the two moderately strongly binding weak bases, chlophedianol, B14, and phenylglycinonitrile, B39. In both cases, the effective mobilities of the enantiomers are cationic at zero and low HMAS concentrations but at an intermediate HMAS concentration become anionic. At HMAS concentrations where the effective mobilities of both enantiomers are cationic, the separation selectivity is positive and approaches an infinite value as the effective mobility of the faster migrating enantiomer approaches zero. At higher HMAS concentrations, the separation selectivity value is negative but becomes positive again and approaches unity as the HMAS concentration is increased and the effective mobilities of both enantiomers remain anionic.

Strongly binding bases include those whose effective mobilities have become anionic already at very low SISCD concentrations. The bottom panel of Figure 40 shows the mobility curves (left panel) and separation selectivity curves (right panel) for three representative strongly binding weak bases, norephedrine, B34, terbutaline, B47, and ephedrine, B60. Their effective mobilities are all anionic at HMAS concentrations as low as 2.5 mM and remain anionic over the entire HMAS concentration range used. Their effective mobilities approach zero at higher HMAS concentrations due to the effects of higher ionic strength. The separation selectivities for all three analytes are positive, and approach a limiting value of $\alpha < 1$ with increasing HMAS concentrations. The $\alpha > 1$ portions of the separation selectivity curves were not observed since they occur at HMAS concentrations lower than 2.5 mM.

Representative electropherograms obtained for the pH 2.5 separations of some of
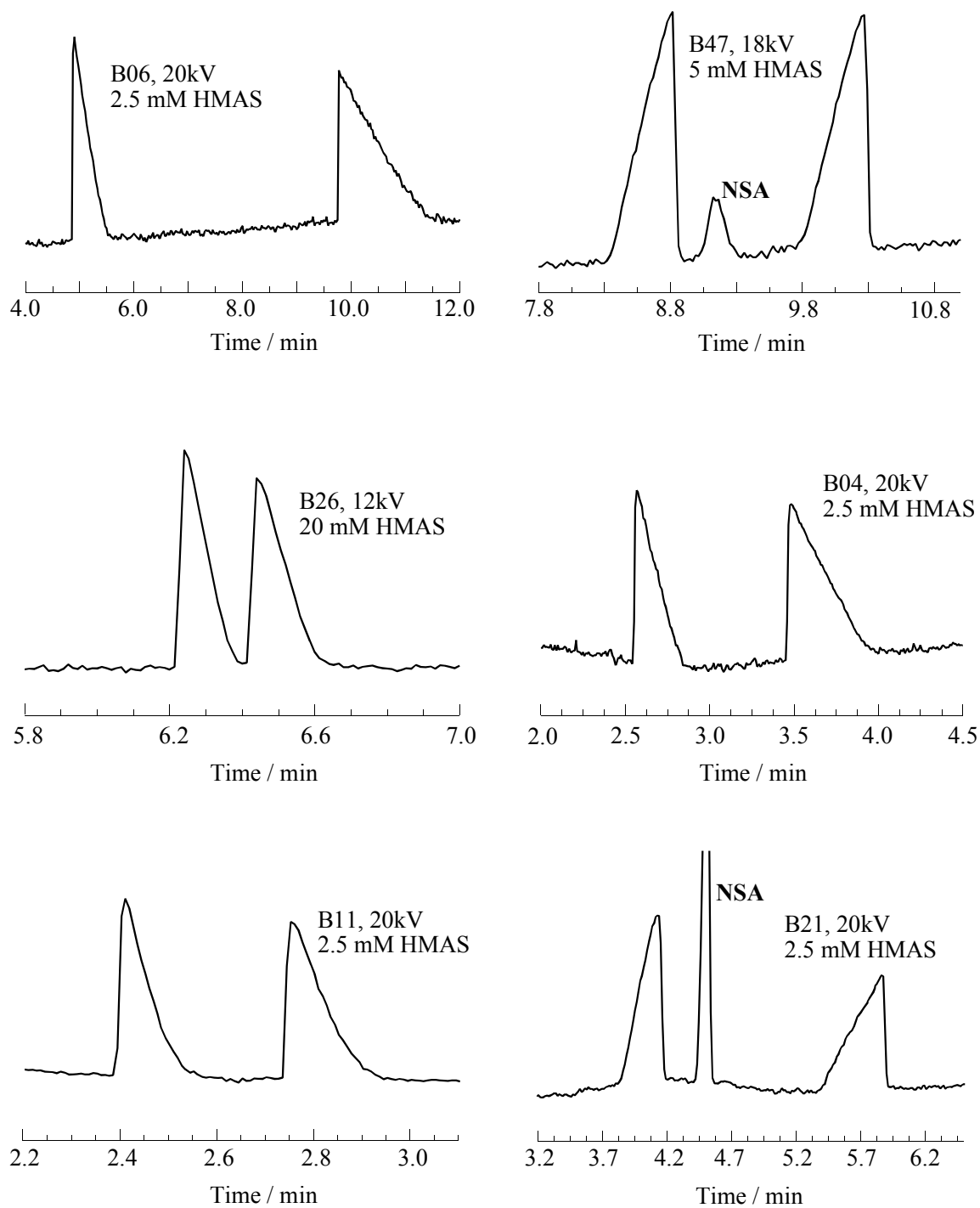
Figure 41. Typical electropherograms of weak base analytes in pH 2.5 BGE with HMAS.
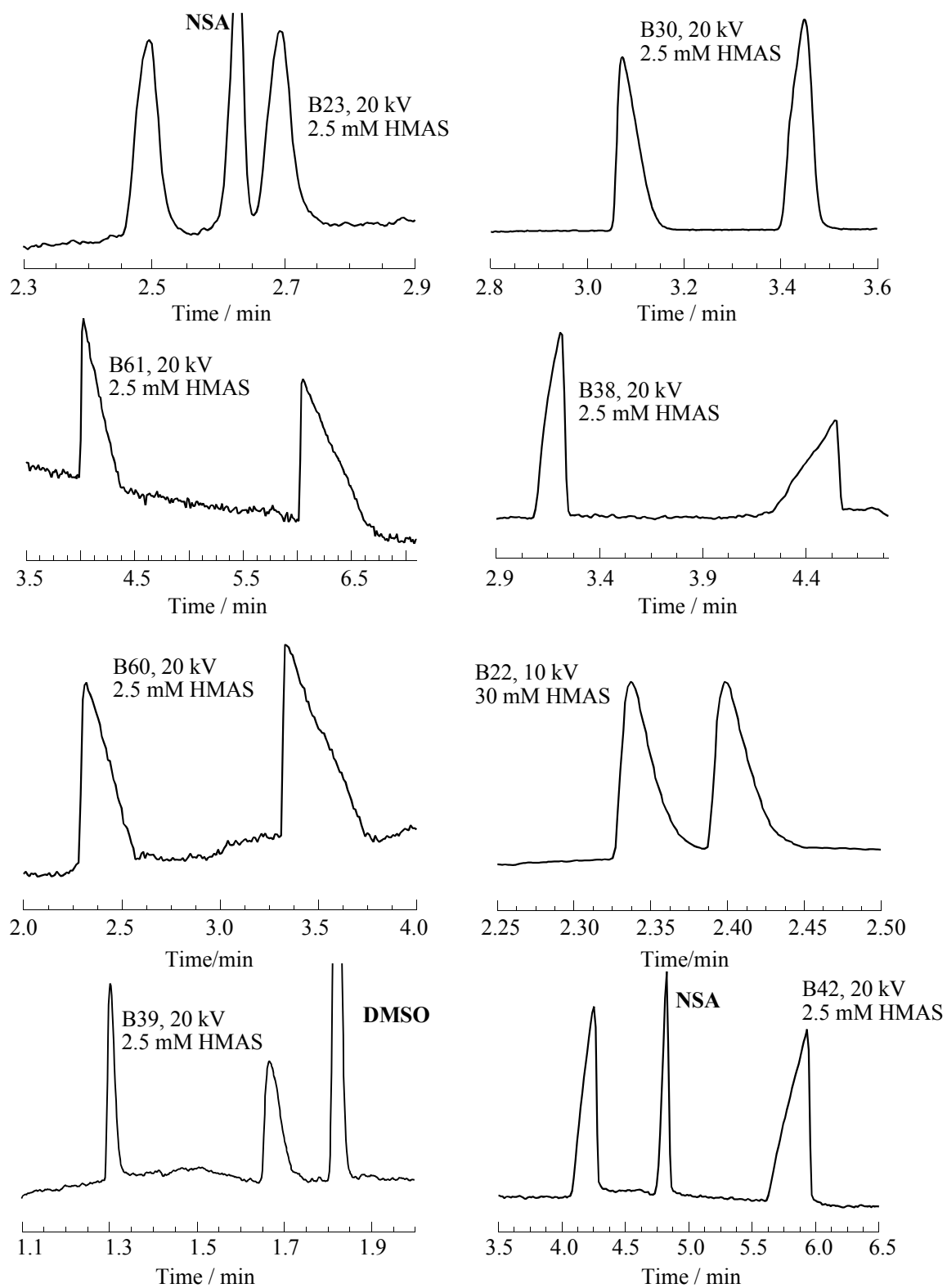
Figure 41. Continued.

the weak base enantiomers are shown in Figure 41. Each electropherogram includes the analyte identifier (see Figure 30), the applied potential (in kV) and the HMAS concentration used for the separation. Some include the zero mobility marker, denoted DMSO, or the anionic mobility marker, denoted NSA. Baseline resolution was achieved in all cases in short run times with the shortest run time at two minutes for phenyglycinonitrile, B39, and the longest for the strongly binding phenylethanolamine, B06, at twelve minutes. Average run times were three to six minutes.

3.3.1 Effects of Weak Base Structure on Separation Selectivity in Aqueous CE Separations Using HMAS

An enantiomer's binding strength is highly dependent on its structure and the structure of the chiral resolving agent. Small structural changes in the analytes can lead to dramatic changes in the separations. As an example, Figure 42 shows the effective mobility (top panel) and the separation selectivity (bottom panel) curves for several structurally related weak bases including B47, B30, B21, B26 and B60. Each is a strongly binding weak base with effective mobilities varying from -9 mobility units for B26 to -31 mobility units for B30 at 5mM HMAS. In order of increasing binding strength, they are B30 > B47 >B21 > B60 > B26. It appears that the binding strength is most dependent on the size and type of the substituents about the aromatic ring. The most strongly binding enantiomers are the ortho- and meta- catecholamines due to strong intermolecular interactions with HMAS. The least strongly binding are metanephrine, B26, with one methylated phenol group and ephedrine, B60, with no phenol groups.
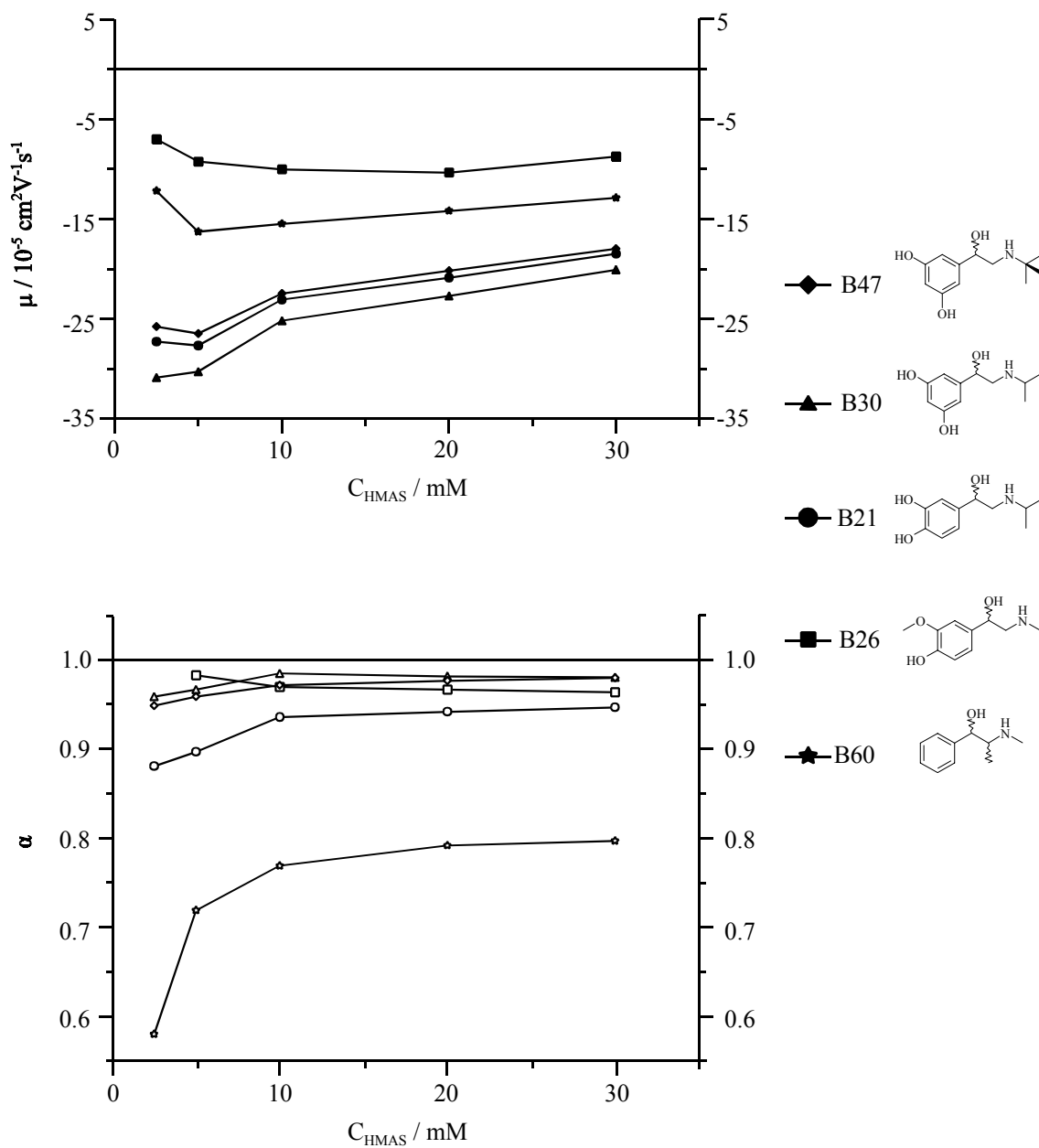
Figure 42. Effects of analyte structure on effective mobilities and separation selectivities for weak bases B21, B26, B30, B47 and B60 obtained in pH 2.5 BGE using HMAS.

Interestingly, the two weak bases with the least bulky aromatic substituents are also the two with separation selectivities furthest from unity. Isoproterenol, B21, with its ortho-phenol groups and ephedrine, B60, exhibit better separation selectivities than bulkier terbutaline, B47, and metaproterenol, B30, each with phenolic group in meta- position and metanephrine, B26, which possesses a methylated phenol group. These observations, while valid, provide little insight into the enantiorecognition mechanism without reinforcement from1-D ROESY NMR experiments [34,35,37].

3.4 Acidic Methanolic Separations Using HMAS as Chiral Selector

Non-aqueous CE (NACE) allows for separation of analytes with low water solubility. Some NACE solvents have low viscosity and low conductivity, which permits the use of higher potentials and lead to faster separations. Commonly used NACE solvents include DMSO, N-methylformamide (NMF), N,N-dimethylformamide (DMF) and propylene carbonate (PC) as well as methanol (MeOH) and acetonitrile (ACN). Some, such as DMSO, NMF, DMF, and PC have high UV cut-off values relative to the others. The solubility of most SISCD's, including HMAS, is greater in methanol than ACN, therefore methanol is the solvent of choice for SISCD enantiomer separations in NACE BGE's.

Study of the use of HMAS as a chiral resolving agent in an acidic methanol BGE was carried out using the same set of 24 weakly basic enantiomers as used in the acidic aqueous BGE (see Figure 39). Table 2 lists the effective mobilities of the less mobile enantiomer (μ), the separation selectivity (α), the corresponding normalized

Table 2. Separations data in acidic methanol HMAS BGE's (μ, in $10^{-5}cm^2/Vs$ units).

[HMAS]	0 mM*	2.5 mM			
U (kV)	19.3	19.3			
Analyte	μ	μ	α	β	Rs
B04	23.0	14.3	0.72	-10	1.0
B06	23.0	-17.0	0.76	-7.2	1.6
B09	21.2	-5.1	1.00	-2.8	0.0
B11	26.2	3.3	1.96	3.7	9.4
B13	24.5	-3.5	0.87	-4.2	1.9
B14	16.5	-3.0	1.00	-4.1	0.0
B19	14.0	-6.0	1.00	-2.4	0.0
B21	22.1	0.61	2.07	20.7	2.3
B22	25.6	9.7	1.03	0.6	1.5
B23	7.6	-8.5	0.98	-1.5	1.0
B26	19.3	-3.7	0.90	-3.4	1.3
B28	27.8	3.0	1.00	4.7	0.0
B30	18.3	-0.58	-0.47	-22	3.5
B34	23.4	1.9	1.00	7.8	0.0
B38	19.3	-6.3	0.91	-2.0	2.4
B39	26.5	0.58	1.37	25	0.7
B42	20.1	-4.6	0.95	-2.7	1.4
B46	16.1	-6.4	1.00	-2.3	0.0
B47	17.8	1.9	1.14	6.7	0.7
B56	14.4	-5.5	1.00	-2.7	0.0
B57	15.8	-1.9	1.00	-5.0	0.0
B60	26.3	1.1	1.30	14	0.8
B61	25.4	-2.1	0.92	-5.8	0.8

Table 2. Continued.

[HMAS]	5 mM				10 mM			
U (kV)	19.3				19.3			
Analyte	μ	α	β	Rs	μ	α	β	Rs
B04	-17.7	0.78	-8.0	1.2	-2.8	0.89	-2.7	2.7
B06	-25.2	0.89	0.86	-4.5	-2.7	0.91	-2.8	1.3
B09	-5.5	1.00	-2.1	0.0	-4.3	0.99	-1.5	0.6
B11	2.2	2.63	7.34	5.4	1.7	2.68	4.5	7.9
B13	-3.3	0.89	-4.1	7.3	-3.0	0.90	-2.2	4.1
B14	-3.3	1.00	-2.4	0.0	-2.5	0.96	-2.7	1.1
B19	-5.7	1.00	-2.3	0.0	-5.3	1.00	-1.6	0.0
B21		N/A			0.30	-0.52	-22	3.9
B22	8.3	1.08	1.4	<0.5	7.8	1.11	0.87	0.9
B23	-7.5	0.98	-1.6	1.1	-5.9	0.98	-1.4	1.13
B26	-4.4	0.93	-2.5	1.9	-3.7	0.94	-2.0	2.5
B28	1.9	1.00	6.6	0.0	1.5	1.00	5.1	0.0
B30	-1.6	0.60	-6.5	3.6	-1.1	0.82	-6.8	1.9
B34	1.2	1.00	8.5	0.0	0.81	1.00	10.3	0.0
B38	-6.3	0.95	-1.7	2.3	-4.8	0.97	-1.8	1.2
B39	0.15	2.67	71	1.4	0.16	3.0	46	1.9
B42	-5.3	0.98	-2.0	0.6	-3.4	0.97	-1.8	1.2
B46	-6.3	1.00	-1.9	0.0	-5.1	1.00	-1.5	0.0
B47	-0.67	1.36	15	0.7	0.50	1.48	17	1.2
B56	-5.5	1.00	-1.9	0.0	-4.4	1.00	-1.7	0.0
B57	-5.2	1.00	-2.1	0.0	-4.0	1.00	-2.0	0.0
B60	-0.66	0.61	-15	0.9	-0.44	0.30	-18	2.3
B61	-3.3	0.93	1.03	1.0	-2.7	0.96	-3.1	1.0

Table 2. Continued.

[HMAS]	20 mM				30 mM			
U (kV)	19.3				19.3			
Analyte	μ	α	β	Rs	μ	α	β	Rs
B04	-2.0	0.87	-2.4	3.2	-1.6	0.84	-2.3	4.3
B06	-2.0	0.91	-2.5	2.2	-1.9	0.89	-2.0	3.9
B09	-3.0	1.00	-1.6	<0.5	-1.9	1.00	-1.8	0.0
B11	1.2	2.65	3.9	17	0.79	2.63	4.4	11
B13	-2.0	0.89	-2.4	1.9	-1.2	0.89	-2.8	2.0
B14	-1.8	0.97	-2.6	0.7	-1.4	0.97	-2.4	1.1
B19	-3.3	0.99	-1.3	1.2	-2.4	0.99	-1.4	0.9
B21	N/A				-0.13	-0.75	-27	2.7
B22	6.8	1.13	0.70	3.0	-0.60	1.16	0.55	4.2
B23	N/A				N/A			
B26	-2.2	0.91	-2.1	4.9	-1.6	0.88	-2.1	6.4
B28	2.0	1.00	2.4	0.0	2.3	1.04	1.3	0.6
B30	0.36	0.77	-14	1.2	-0.29	0.48	-9.9	1.9
B34	0.52	1.00	10	0.0	-0.50	1.00	7.9	0.0
B38	-3.0	0.92	-1.5	4.6	-0.20	0.65	-14	1.7
B39	0.36	2.17	12	4.6	0.53	1.78	6.9	5.4
B42	-2.0	0.96	-2.3	1.4	-1.5	0.96	-2.7	0.7
B46	-3.4	1.00	-1.3	0.0	-2.5	1.00	-1.4	0.0
B47	0.68	1.19	6.9	2.0	0.77	1.12	4.5	1.6
B56	-2.8	1.00	-1.5	0.0	-2.4	1.00	-1.5	0.0
B57	-2.8	1.00	-1.6	0.0	-2.0	1.00	-1.7	0.0
B60	N/A				0.17	2.15	20	4.0
B61	-2.1	0.95	-2.1	1.9	-1.7	0.94	-2.1	2.8

* From Ref. [47].

electroosmotic flow mobility (β), the peak resolution and the injector-to-detector

potential drop (U) values for the NACE separations. An entry of N/A implies that a value

could not be calculated because of overlap with a non-comigrating system peak or

overlap with the neutral marker or anionic mobility marker.

All separations were carried out within the linear region of Ohm's law with

applied potentials at 26 kV in all of the HMAS- containing BGE's. Over the 2.5 to 30

mM HMAS concentration range, the μ^{EOF} were as low as 9 mobility units in the 2.5 mM

HMAS- containing BGE's and as high as 41 mobility units in the 30 mM HMAS-

containing BGE's. Again, the higher μ^{EOF} values at greater HMAS concentration likely

indicate that HMAS adheres to the fused silica capillary wall resulting in a greater zeta

potential and higher μ^{EOF} values. No studies were conducted to quantify the contribution

to resolution resulting from chromatographic retention of the analytes.

The enantiomers of 18 of the 24 analytes showed at least some separation

selectivity in the methanolic BGE using HMAS as chiral resolving agent. Of these, 15

were baseline resolved (i.e., Rs > 1.5) under the conditions used. The six analytes for

which no resolution was achieved included the same five analytes that showed no

separation selectivity in aqueous BGE's plus norephedrine, B34. Norephedrine is only

weakly binding in the methanolic BGE's, unlike in the aqueous BGE's where it is

strongly binding.

Mobility (left panel) and separation selectivity (right panel) curves for some of

the weak base enantiomers are shown in the top panel of Figure 43. As in the aqueous

BGE's, migration behaviors of the weak bases studied fell into one of three mobility
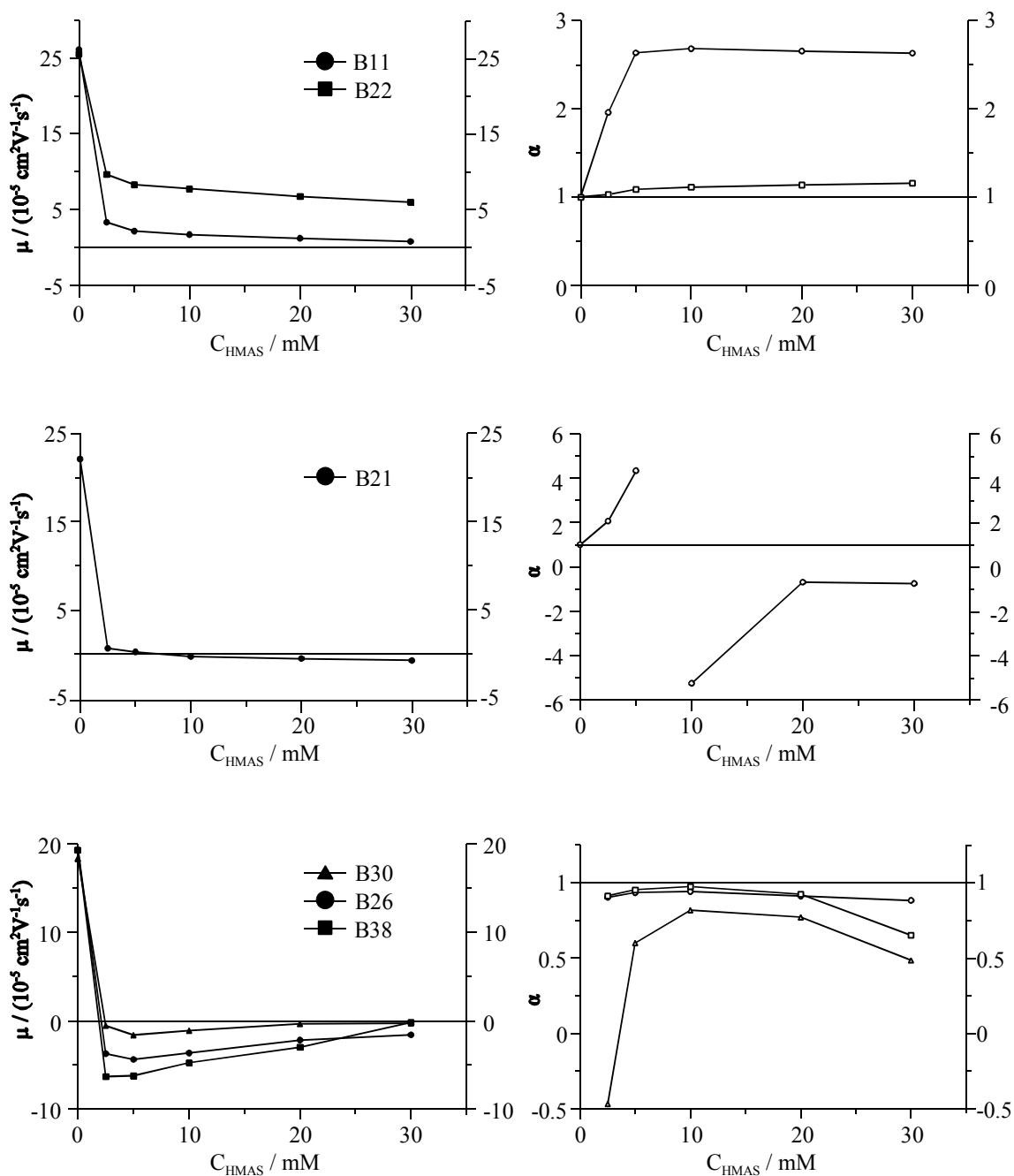
Figure 43. Effective mobilities (left panel) and separation selectivities (right panel) of weakly binding (top panel), moderately strongly binding (middle panel) and strongly binding (bottom panel) weakly basic analytes. Zero concentration effective mobility values as reported in Ref. [47].

patterns. The weak bases whose effective mobilities remained cationic throughout the HMAS concentration range are weakly binding (top panel) and have their effective mobilities depressed toward zero by the increasing complexation and the increasing ionic strength. There is no discontinuity in the separation selectivity pattern similar to the aqueous CE separations weak base enantiomers.

Isoproterenol, B21, is strongly binding in the aqueous BGE's (see Figure 42) but is the only moderately strongly binding weak base in the methanolic BGE's. Moderately strongly binding bases (middle panel) are cationic until, at some intermediate HMAS concentration, their effective mobility becomes anionic and then is depressed back by the ionic strength of the BGE to a lower, though anionic value as the HMAS concentration is further increased.

The third mobility pattern (bottom panel) is similar to the pattern for strongly binding bases observed in the aqueous measurements. The effective mobility of the enantiomers becomes anionic at a low HMAS concentration, then rapidly decreases at the higher HMAS concentrations due to increasing ionic strength. A discontinuity is observed in the separation selectivity patterns of both the moderately and strongly binding weak bases. The difference between the two is that the discontinuity occurs lower in the HMAS concentration range for the strongly binding weak bases and at some intermediate HMAS concentration for the moderately strongly binding weak bases.

Good peak resolution can be seen for several of the enantiomers in Figure 44. Weaker binding strengths in the methanolic BGE's combined with higher electric field strengths allowed for significantly faster run times, with most analytes passing the UV-
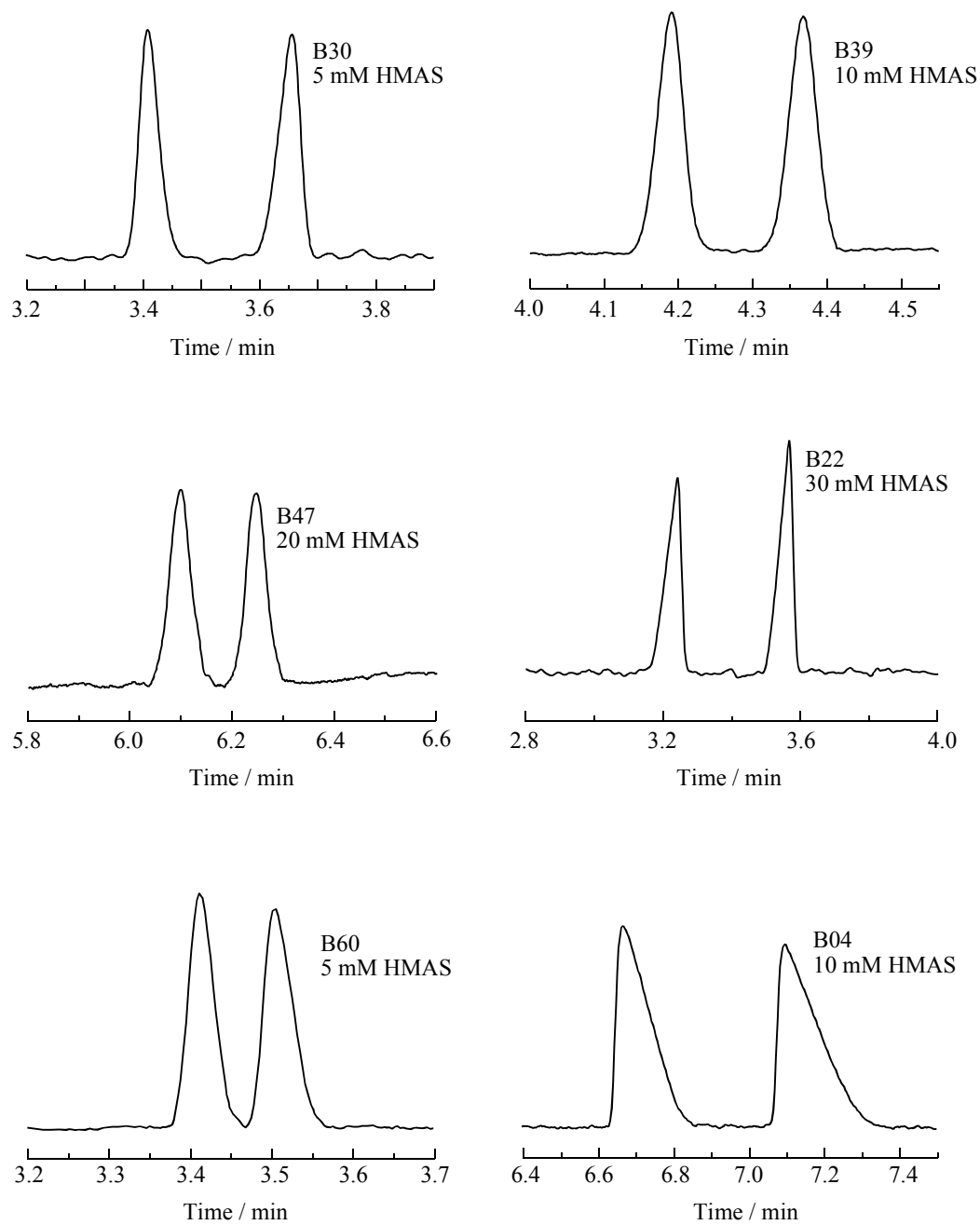
Figure 44. Typical electropherograms of weak base analytes in acidic methanol BGE with HMAS.
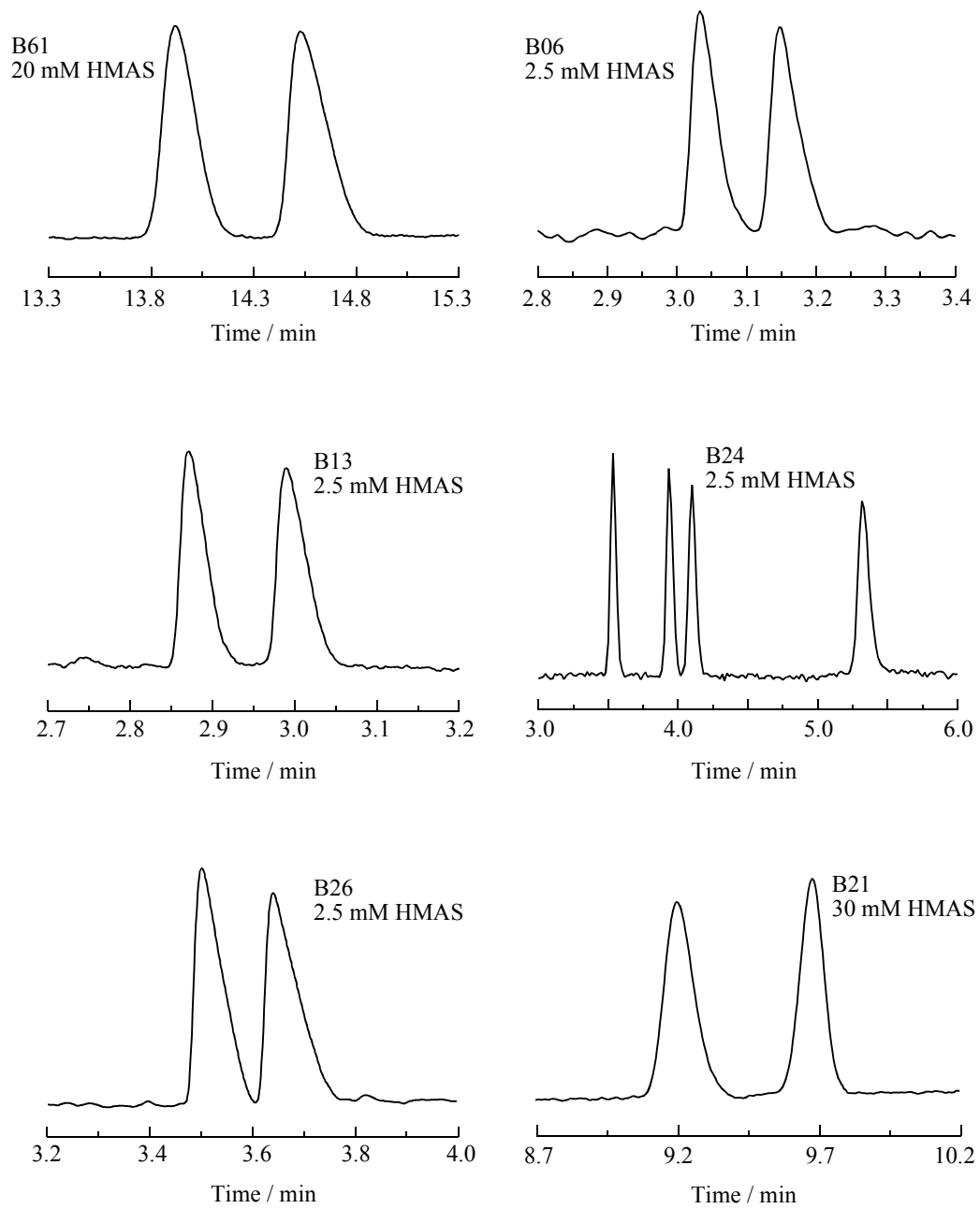
Figure 44. Continued.

detector in under five minutes. One notable separation is that of the stereoisomers of labetolol, B24, which possess' two chiral centers. The enantiomers of B24 were only poorly resolved in the aqueous BGE's but are baseline resolved in the methanolic BGE in under seven minutes.

3.4.1 Ionic Strength Effects in NACE Separations

Maynard et al. [51] predicted that in high ionic strength BGE's, like HMAS-containing BGE's, the effective mobility of weakly binding bases will show a cationic effective mobility minimum and that the separation selectivity will approach a maximum value after which, higher sulfated CD concentrations result in lower α values. Further, the authors predicted that strongly binding analytes will have an initially cationic effective mobility but, as the sulfated CD concentration is increased, the effective mobility will show an anionic maximum, approach the zero mobility line and become cationic again. The calculated separation selectivity plot for strongly binding analytes is shown in Figure 45, reprinted with permission from Ref. [51]. The α value is discontinuous at both zero mobility line crossovers, one at low sulfated CD concentration and one at higher SISCD concentration. The authors showed that the trends for a weakly binding analyte, 4-chloroamphetamine, followed closely those predicted by the model using HMDS as chiral resolving agent. However, no strongly binding analyte that crosses the zero mobility line twice has yet been found experimentally.

Figure 46 shows the effective mobility (top panel) and separation selectivity
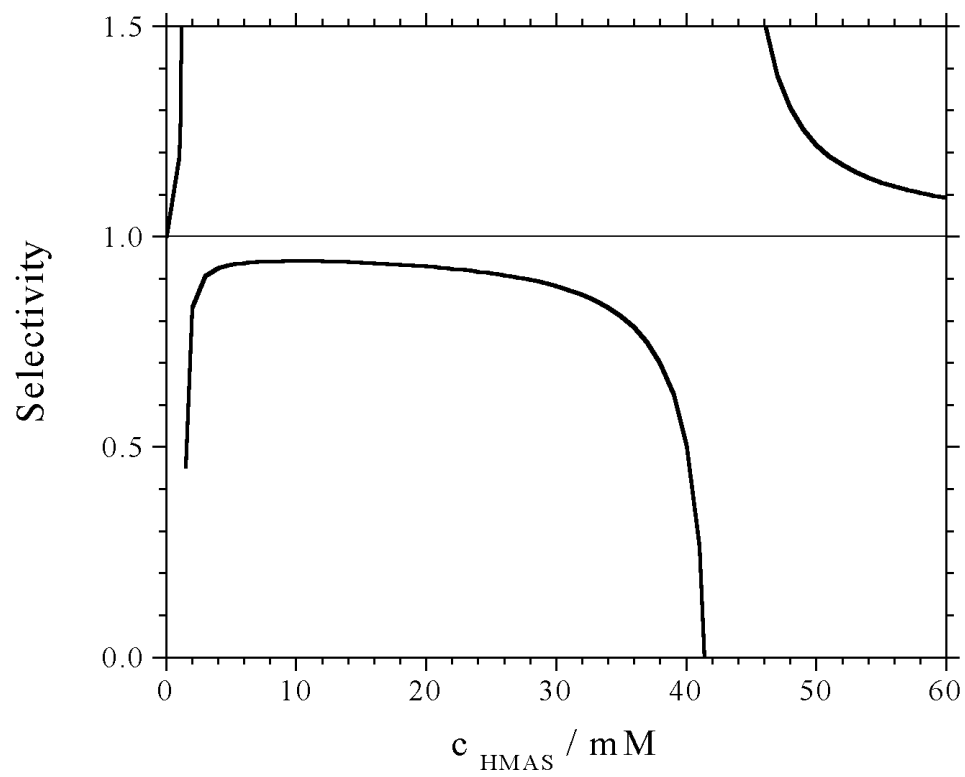
Figure 45. Predicted separation selectivity plot for strongly binding weak bases. Reprinted with permission from Ref. [51].
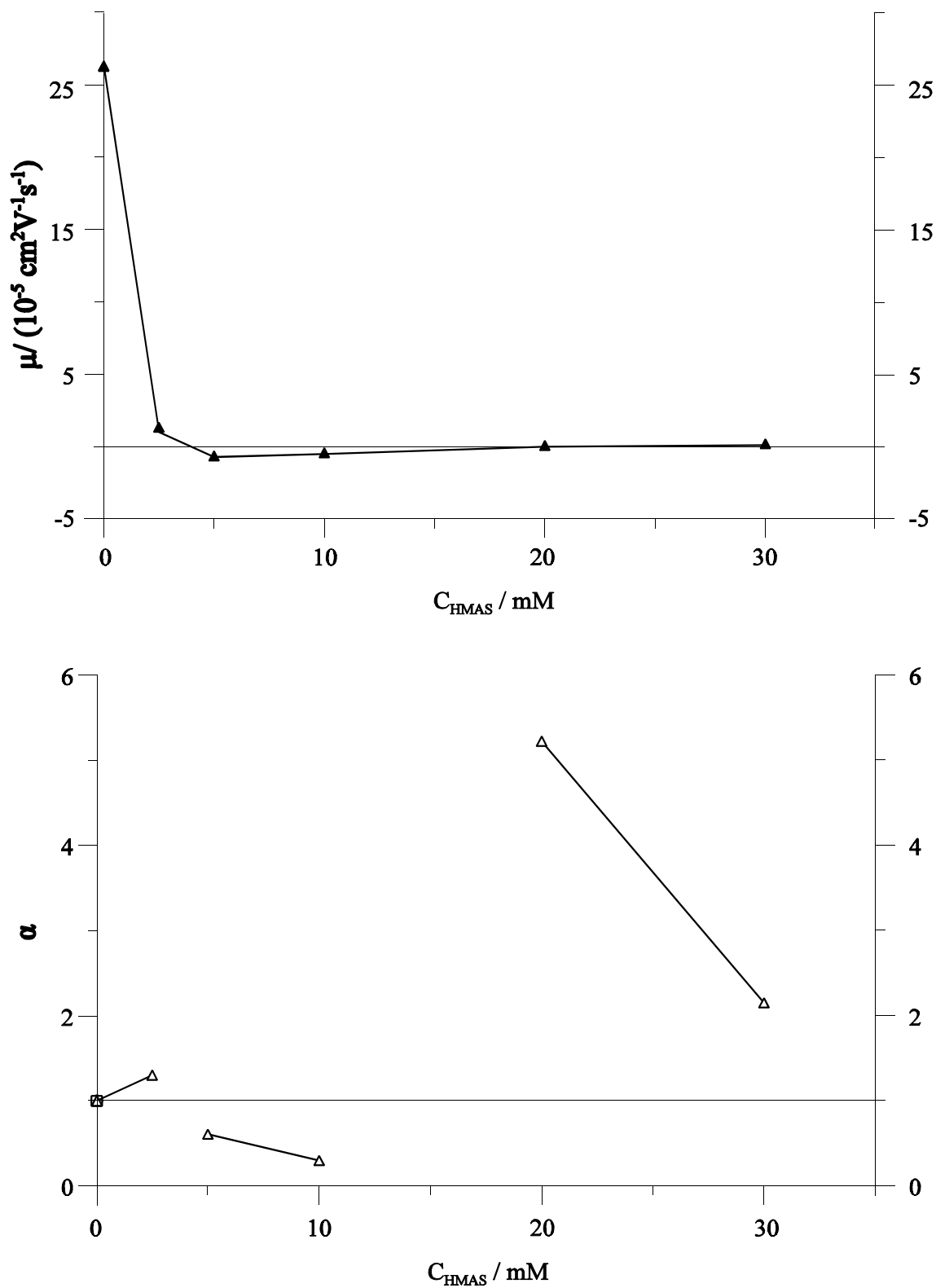
Figure 46. Effective mobility (top) and separation selectivity (bottom) curves for B60 measured in acidic methanol HMAS BGEs.

(bottom panel) of the strongly binding weak base, ephedrine, B60. The effective mobility of B60 is initially cationic, shows a local anionic maximum, then decreases and becomes cationic as the HMAS concentration is increased. The separation selectivity pattern shows that α is initially positive, becomes negative and approaches a local maximum. Finally, once the mobility is again cationic, the separation selectivity decreases to an α > 1 value as predicted in Ref. [51]. The two weakly binding weak bases B39 and B47 exhibited a cationic effective mobility minimum (see Table 2). Their separation selectivities approach a maximum near 10 mM HMAS and are lower at both 2.5 and 30 mM HMAS.

3.4.2 Comparison of Enantiomer Separations in Aqueous and Nonaqueous HMAS Containing BGE's

With the exception of B09, B14, B19 and B46, the binding strengths of all analytes were weaker in the acidic methanol BGE's compared to the pH 2.5 aqueous BGE's. Of these four analytes, only B14 showed separation selectivity in both the aqueous and methanolic BGE's. The other three showed no separation selectivity using either aqueous or methanolic BGE's.

Weaker analyte binding strengths in methanolic BGE's compared to aqueous BGE's are typical. Figure 47 shows the effective mobility and separation selectivity curves for B11, B13 and B14 using HMAS as chiral resolving agent in acidic aqueous and methanolic BGE's. Analytes B11 and B13 are strongly binding in aqueous BGE's but, are less anionic in the methanolic BGE's where B11 is only weakly binding.
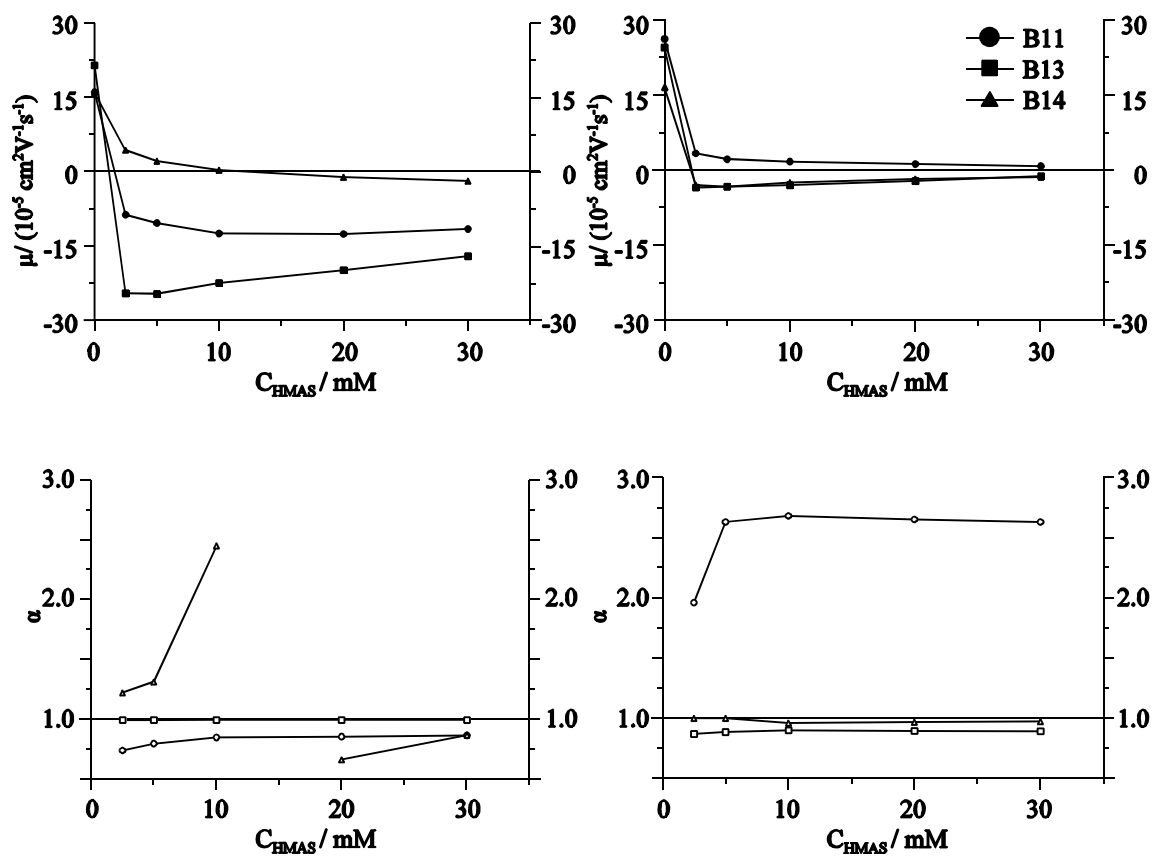
Figure 47. Effective mobility (top) and separation selectivity (bottom) of weak bases in low pH aqueous (left) and methanolic (right) HMAS BGE's.

Conversely, the effective mobilities for B14 show that it is moderately strongly binding

in aqueous but strongly binding in methanolic BGE's. The α values are improved for

both B11 and B13 in the methanolic BGE's vs. the aqueous BGE's. Better α values in

the methanolic BGE's allowed for baseline resolution of B13 even though the β values

were more favorable in the aqueous BGE's. Baseline resolution was achieved for B11 in

both BGE's despite poor α values in the aqueous BGE's. Resolution could not be

obtained for B14 in the methanolic BGE's but good α values in the aqueous BGE's

allowed baseline resolution in spite of poor β values.

The CHARM model [68] predicts that the effective mobility of an enantiomer is

dependent on the infinite dilution mobilities of the free and complexed forms of the

enantiomer, the enantiomer-HMAS complexation constant and the HMAS concentration.

Thus, the greater cationic character of weak bases in methanolic BGE's is most likely a

combination of smaller enantiomer-HMAS complexation constants and less anionic

effective mobilities of the complexed form of the enantiomer due to, perhaps, ion pairing

between HMAS and sodium.

3.5 Low pH Aqueous Separations Using HMS as Chiral Selector

The same set of 24 analytes were used to evaluate the utility of HMS as a chiral

resolving agent for CE as in the previous experiments that included HMAS as chiral

selector. All but 4 of the enantiomers showed at least some separation selectivity in the

pH 2.5 aqueous HMS-containing BGE's. Norephedrine, B34, scopolamine, B46,

chlorpheniramine, B56, and diltiazem, B57 remained unresolved despite favorable β

Table 3. Separations data in pH 2.5 aqueous HMS BGE's ((μ, in $10^{-5}cm^2$/Vs units).

[HMS]	0 mM*	2.5 mM			
U (kV)	14.8	14.8			
Analyte	μ	μ	α	β	Rs
B04	21.5	9.6	1.08	1.34	0.8
B06	22.1	10.3	1.05	1.21	<0.5
B09	16.5	-2.2	0.52	-5.8	2.3
B11	16.0	-4.8	0.81	-2.5	2.6
B13	21.4	-4.1	0.79	-3.0	1.6
B14	16.0	-10.5	0.70	-1.2	23
B19	17.0	2.3	1.55	4.9	3.0
B21	15.7	-1.2	-2.81	-9.5	5.9
B22	18.2	-1.1	0.17	-10	3.4
B23	15.4	-10.3	0.59	-1.1	180
B26	18.7	7.2	1.07	1.3	0.8
B28	20.1	10.2	1.04	0.99	0.5
B30	17.3	-21.9	0.68	-0.39	6.3
B34	21.4	6.7	1.00	1.5	0.0
B38	19.8	-19.5	0.75	-0.44	10
B39	23.5	14.6	1.00	0.63	0.0
B42	16.5	-14.9	0.85	-0.61	6.4
B46	16.0	4.1	1.00	2.5	0.0
B47	16.1	-23.6	0.81	-0.47	6.0
B56	16.2	-22.4	1.00	-0.40	0.0
B57	10.4	N/A			
B60	18.4	7.5	1.07	1.2	1.1
B61	20.8	3.2	1.5	3.8	1.5

Table 3. Continued

[HMS]	5 mM				10 mM			
U (kV)	13.4				11.1			
Analyte	μ	α	β	Rs	μ	α	β	Rs
B04	5.9	1.13	1.2	1.8	3.7	1.26	1.0	4.0
B06	6.3	1.10	1.1	1.4	4.3	1.15	0.84	2.0
B09	-11.3	0.87	-0.06	6	-12.2	0.90	-0.17	5.0
B11	-10.3	0.92	-0.05	3.5	-12.6	0.95	-0.37	4.5
B13	-7.5	0.88	-0.04	2.9	-10.3	0.92	-0.39	5.0
B14	-17.3	0.81	-3.9	7.6	-19.9	0.89	-0.12	8.5
B19	-1.6	0.20	-3.9	7.6	-6.0	0.70	-0.30	16
B21	-3.9	0.26	-1.7	12.5	-8.2	0.64	-0.49	20
B22	-7.3	0.81	-0.10	3.4	-11.5	0.92	-0.09	3.2
B23	-13.5	0.67	-0.11	19	-19.6	0.78	-0.03	11
B26	4.8	1.12	1.4	1.9	2.6	1.22	0.83	3.3
B28	7.7	1.05	0.83	1.4	5.0	1.08	0.54	2.1
B30	-25.3	0.79	-0.06	7.1	-23.3	0.83	-0.14	9.0
B34	4.9	1.00	1.3	0.0	2.2	1.00	0.96	0.0
B38	-21.3	0.83	-0.03	6.2	-21.4	0.88	-0.17	0.0
B39	11.0	1.03	0.59	0.9	9.1	1.03	0.33	1.0
B42	-18.1	0.91	-0.06	3.2	-18.7	0.94	-0.17	6.0
B46	-1.3	1.00	-5.0	0.0	-5.8	1.00	-0.17	0.0
B47	-24.7	0.83	-0.04	5.2	-24.3	0.88	-0.10	5.3
B56	-22.8	1.00	-0.12	0.0	-18.6	1.00	-0.08	0.0
B57	-9.2	1.00	-0.19	0.0	-12.9	1.00	-0.08	0.0
B60	4.1	1.14	1.6	2.2	1.2	1.60	5.5	3.6
B61	0.8	1.65	8.8	2.0	-2.7	0.63	-3.5	4.2

Table 3. Continued.

[HMS]	20 mM				30 mM			
U (kV)	8.9				7.4			
Analyte	μ	α	β	Rs	μ	α	β	Rs
B04	2.3	1.32	3.4	2.8	1.2	1.33	2.7	2.5
B06	2.0	1.2	1.3	2.0	1.8	1.22	3.1	2.4
B09	-11.7	0.94	-0.32	4.5	-10.8	0.92	-0.14	4.2
B11	-13.1	0.97	-0.23	2.4	-11.6	0.98	-0.11	2.0
B13	-9.8	0.92	-0.14	4.4	-8.1	0.91	-0.14	6.8
B14	-17.1	0.91	-0.16	8.7	-14.6	0.92	-0.07	7.5
B19	-5.8	0.72	-0.22	18	-5.6	0.71	-0.17	14
B21	-7.9	0.67	-0.31	17	-6.5	0.64	-0.11	25
B22	-11.8	0.93	-0.08	5.3	-10.4	0.94	-0.05	4.8
B23	-17.3	0.82	-0.04	12	-14.9	0.84	-0.05	12
B26	1.3	1.48	1.36	5.1	1.0	1.54	2.4	5.4
B28	3.2	1.23	0.91	1.9	1.5	1.43	1.9	4.5
B30	-20.2	0.86	-0.05	9.7	-16.8	0.89	-0.06	8.2
B34	N/A				N/A			
B38	-18.2	0.88	-0.12	11	-15.4	0.87	-0.03	12
B39	8.2	1.03	0.50	1.0	7.6	1.02	0.33	0.7
B42	-16.0	0.94	-0.13	6.1	-13.1	0.95	-0.03	5.0
B46	-6.1	1.00	-0.32	0.0	-5.4	1.00	-0.02	0.0
B47	-20.7	0.90	-0.09	10	-17.5	0.91	-0.06	9.3
B56	-9.8	1.00	-0.10	0.0	-8.2	1.00	-0.13	0.0
B57	-12.7	1.00	-0.15	0.0	-11.3	1.00	-0.09	0.0
B60	-1.7	0.43	-2.7	2.9	-2.8	0.57	-1.9	5.8
B61	-3.5	0.79	-0.26	10	-2.8	0.74	-0.18	29

* From Ref. [39].

values. Of the twenty that showed separation selectivity, phenylglycinonitrile, B39, was the only analyte not baseline resolved under the separation conditions used.

Table 3 lists the effective mobilities of the less mobile enantiomers, μ, the separation selectivities, α, the peak resolution, Rs, the normalized EOF mobility values, β, and the injector-to-detector potential drop, U values obtained in the low pH aqueous BGE's for the weakly basic enantiomers. An entry of N/A implies that a value could not be calculated because of overlap with a non-comigrating system peak or overlap with the neutral marker or anionic mobility marker.

The limiting applied potential values determined by the Ohm's Law plots were identical to those found for low pH aqueous HMAS-containing BGE's. The applied potential was 20 kV for the 2.5 mM HMS-containing BGE and decreased with increasing HMS concentration to 10 kV at 30 mM HMAS-containing BGE. Over the 2.5 to 30 mM HMS concentration range, the μ^{EOF} values were between 1 and 12 mobility units but were lower at greater HMS concentrations. Lower μ^{EOF} values at greater HMS concentrations are in accordance with expectations since higher viscosities and higher ionic strengths result from higher HMS concentration. Also, the lower μ^{EOF} values at higher HMS concentration indicate that HMS may adhere to the fused silica capillary wall to a lesser extent than HMAS. No studies were conducted to quantify the contribution to resolution from chromatographic retention of the analytes.

All three effective mobility and separation selectivity classes were also observed when HMS was used as the chiral resolving agent. The effective mobility and separation selectivity trends for a group of weak bases are shown in Figure 48. Weakly binding
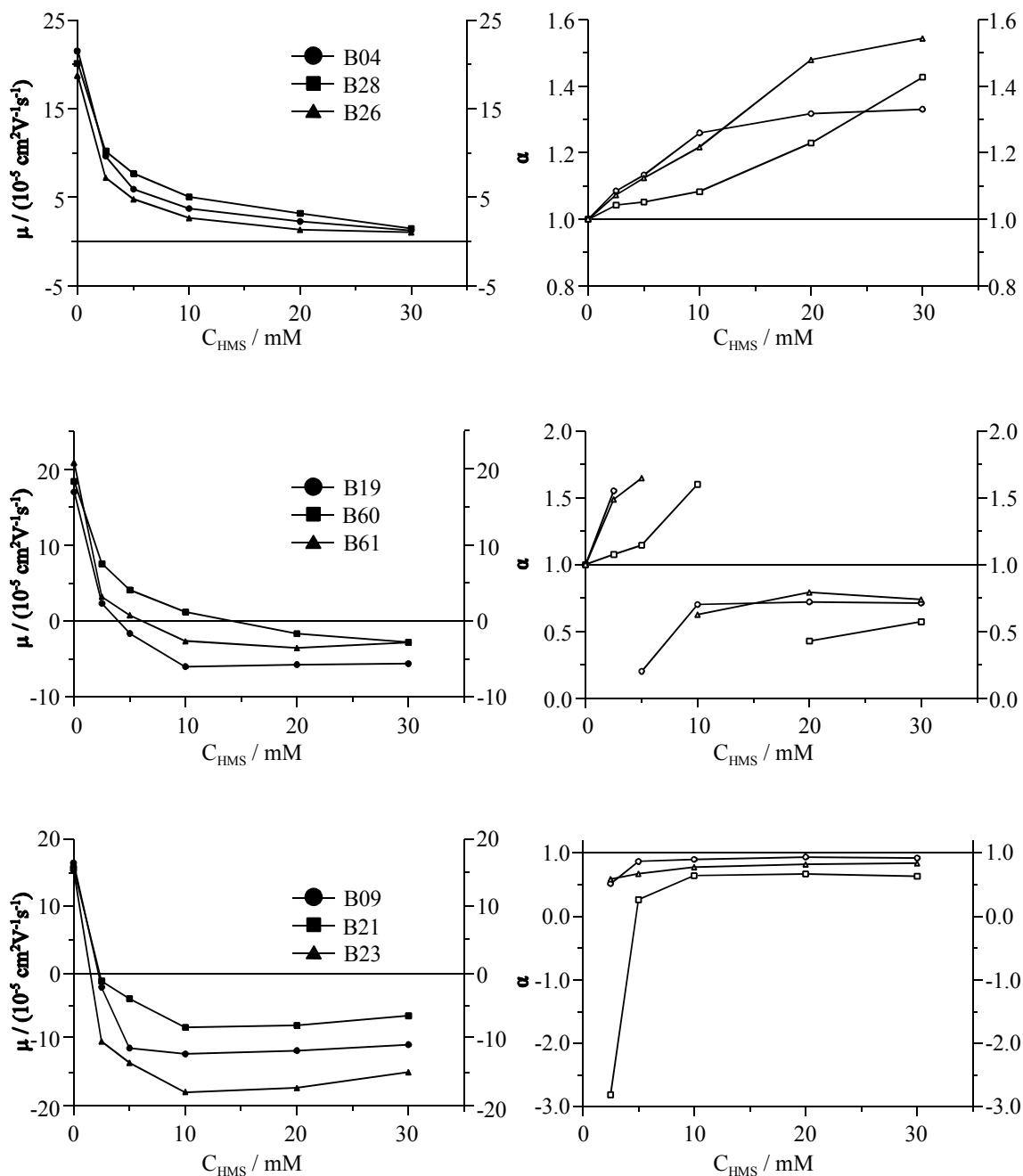
Figure 48. Effective mobilities (left panel) and separation selectivities (right panel) of weakly binding (top panel), moderately strongly binding (middle panel) and strongly binding (bottom panel) weakly basic analytes. Zero concentration effective mobility values as reported in Ref. [39].

bases (top panel) show the same trends as observed for the weak base separations in

HMAS-containing BGE's. Their effective mobilities remain positive over the entire

HMS concentration range. The separation selectivity values increase monotonically with

no discontinuity, in some cases to a limiting value.

The effective mobility and separation selectivity trends for the moderately

strongly binding weak bases (middle panel) shown in Figure 49 indicate that better

separation conditions occur at intermediate HMS concentrations where the effective

mobilities of the enantiomers cross the zero mobility line. Though α is highest in this

region of the mobility curve, faster, more robust enantiomer separations methods use

lower HMS concentrations at the expense of separation selectivity. Higher

concentrations see the α value pass a discontinuity in the curve and then increase to a

limiting value of $\alpha < 1$ where the effective mobility is anionic and run times are longer.

Strongly binding bases have effective mobilities that are anionic at the lowest HMS

concentration tested. The discontinuity in α observed for moderately strongly binding

bases occurs at HMS concentrations lower than included in this study.

Representative electropherograms for some of the weak base separations using

HMS as chiral resolving agent are included in Figure 49. Favorable β values and good

separation selectivities meant that most analytes could be separated at relatively low

HMS concentrations, with short analysis times. Two separations worth mentioning

include those of atropine, B09, and homatropine, B19, both of which were not resolved

in the HMAS-containing BGE's. Here, HMS is able to resolve these two analytes at 2.5

mM HMS in 4.5 and 27 minutes, respectively.
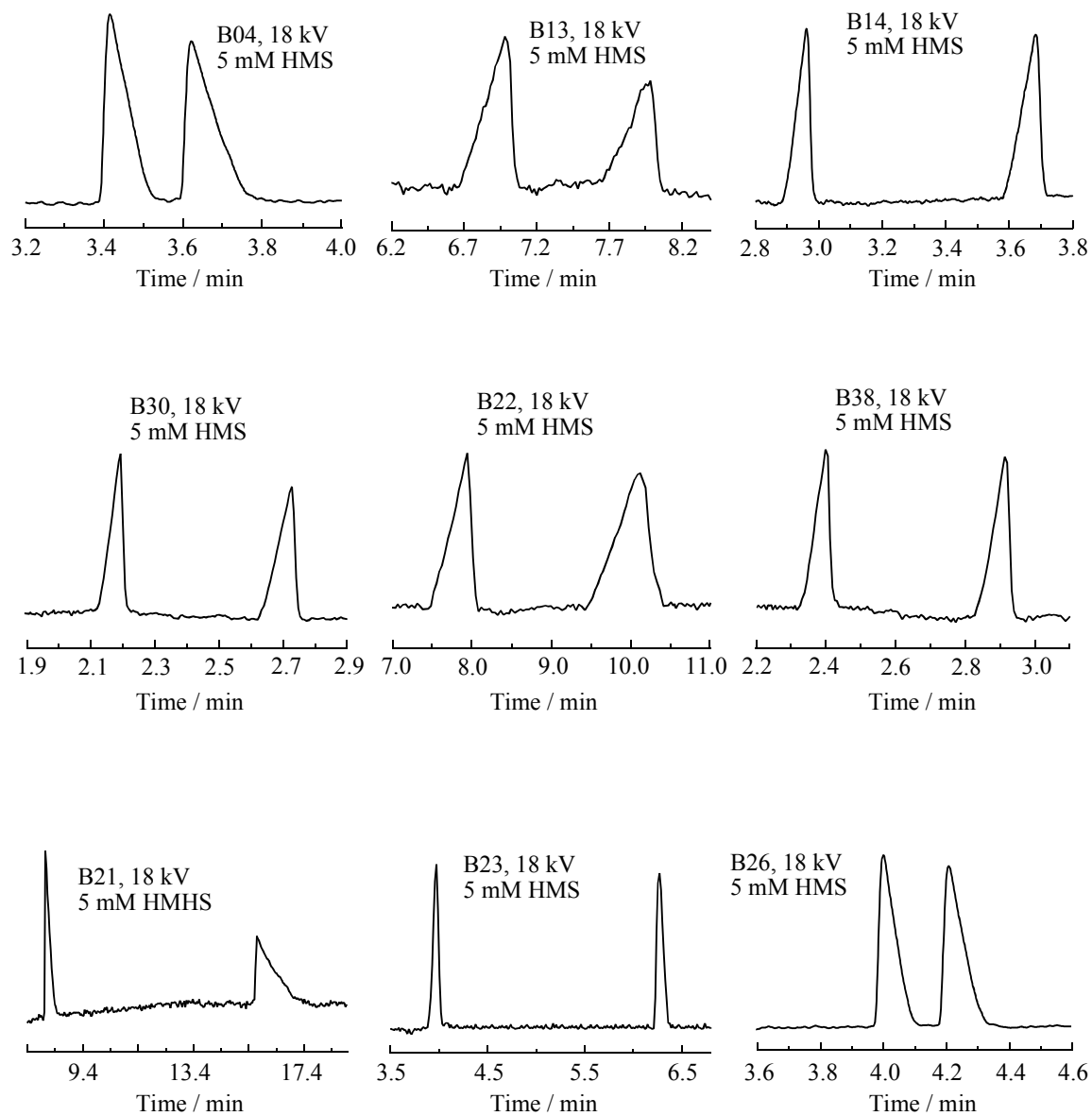
Figure 49. Typical electropherograms of weak base analytes in pH 2.5 aqueous BGE with HMS.
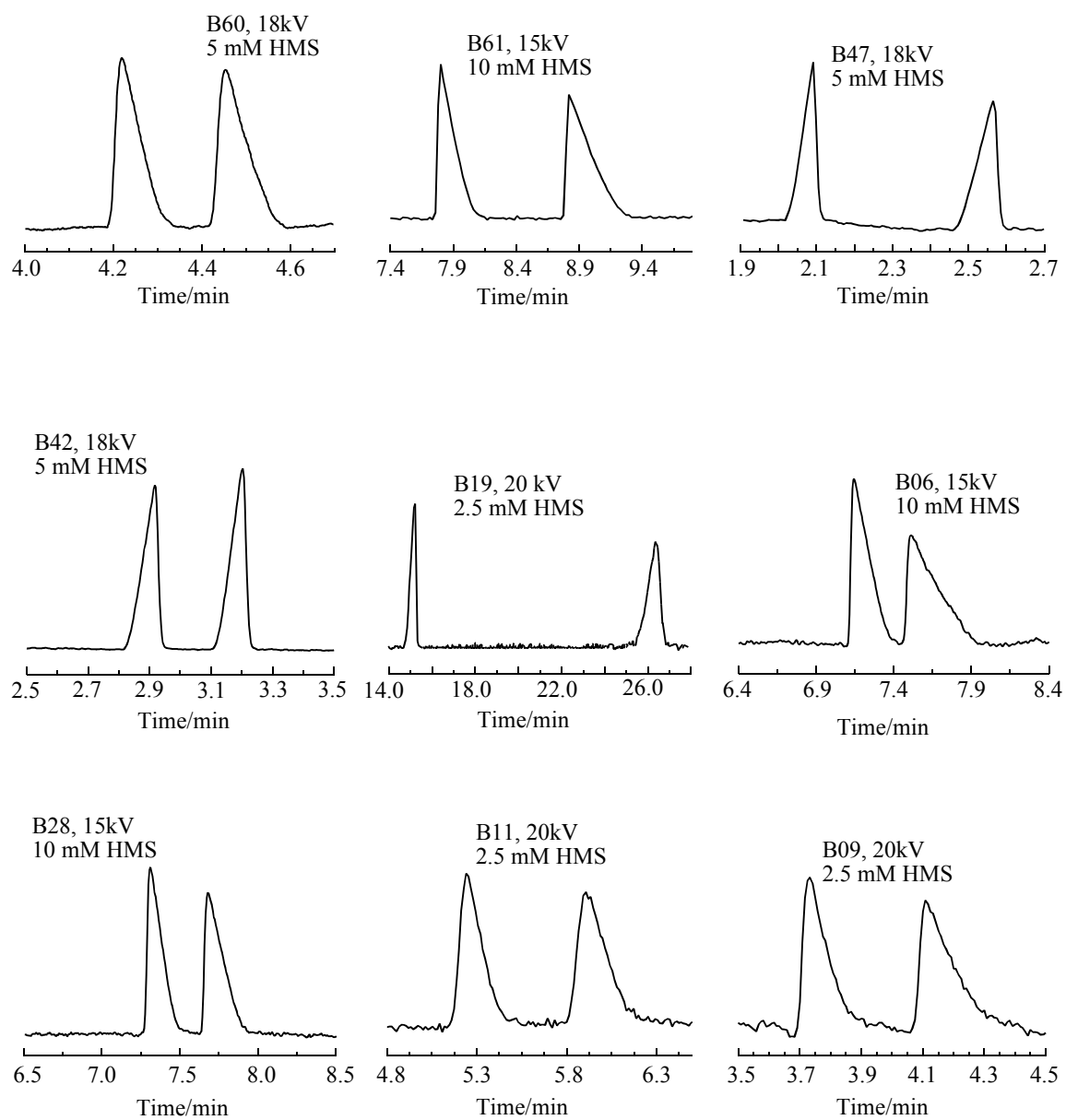
Figure 49. Continued.

3.5.1 Effects of Weak Base Structure on Aqueous Separations Using HMS

The effective mobility (top panel) and separation selectivity (bottom panel) of several structurally related weak bases used to evaluate the impact of analyte structure on separations using HMS are shown in Figure 50. They are the same group that was used for similar comparisons with HMAS as chiral resolving agent. The mobility curves show that these same analytes are less strongly binding in the HMS BGE's. The effective mobilities range between 5 to -25 mobility units at 5 mM HMS for B26 and B30, respectively. The order of binding strength is B30 > B47 >B21 > B60 > B26. All binding strengths are weaker compared to those observed in the HMAS BGE's.

All three effective mobility and separation selectivity classes are represented by the curves included in Figure 50. Metanephrine, B26, is weakly binding, ephedrine, B60, is moderately strongly binding while isoproterenol, B21, metaproterenol, B30, and terbutaline, B47, are strongly binding. Their separation selectivity patterns follow the same trends mentioned previously (see Section 3.5) but are better for the strongly binding analytes in HMS BGE's. Better separation selectivities are possible for B26 in low concentration HMAS BGE's but, more reproducible effective mobilities are obtained in HMS BGE's where small fluctuations in the chiral resolving agent concentration have less impact on the separation. The same is true for the separation of B60 enantiomers. High separation selectivities are available in both HMAS and HMS BGE's near the discontinuity in the α curve. However, since the discontinuity occurs at higher HMS concentration than with HMAS, more robust methods are obtained with HMS as chiral resolving agent.
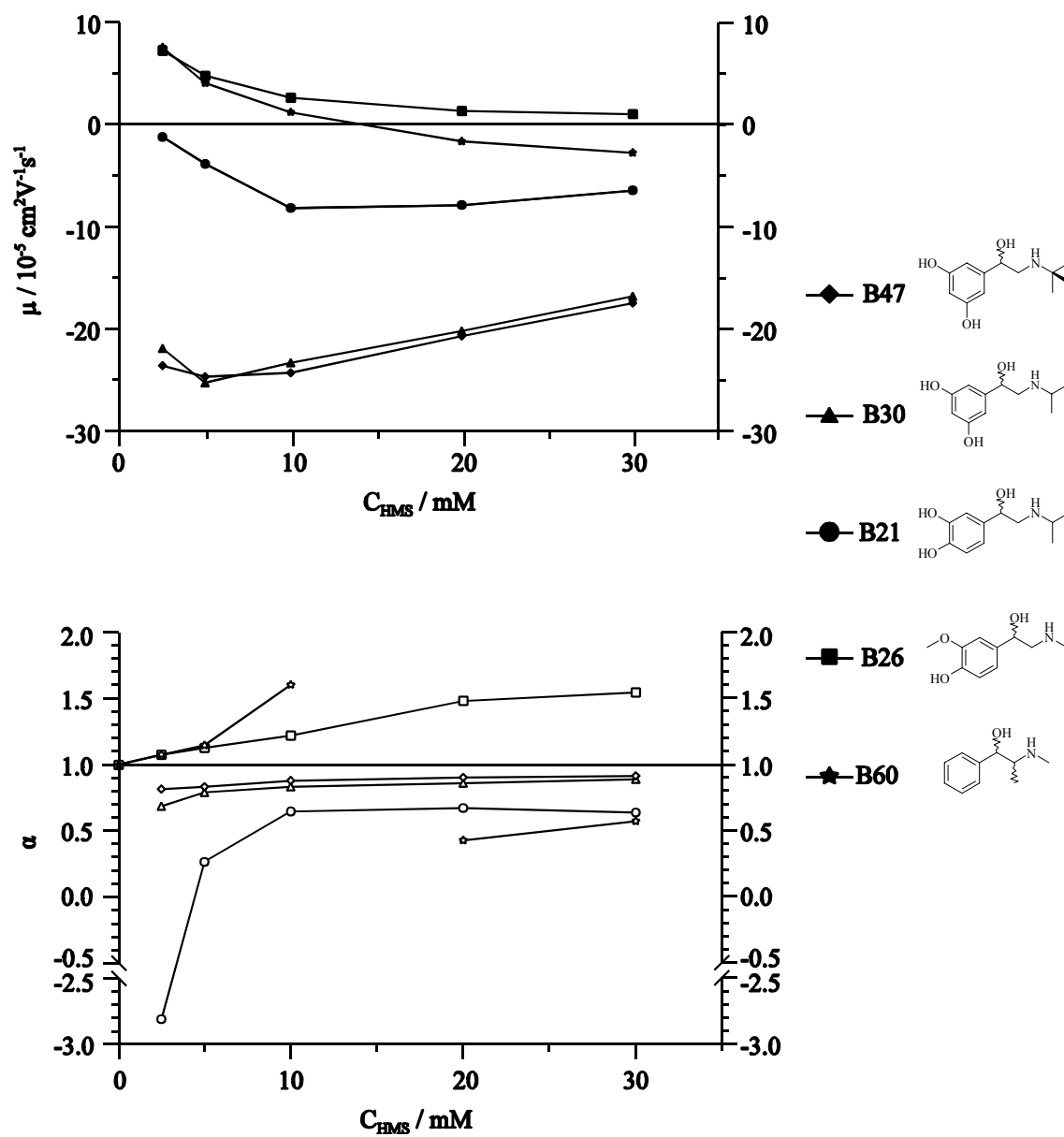
Figure 50. Effects of analyte structure on the effective mobilities and separation selectivities for weak bases B21, B26, B30, B47 and B60 obtained in pH 2.5 BGE using HMS.

3.6 Effects of C2 and C3 β-CD Substituents on Weak Base Aqueous Separations

The changes in the binding strength for a weak base due to differences in the functionalization at the C2 and C3 positions are represented in the effective mobility (top panel) and separation selectivity (bottom panel) curves shown in Figure 51 for piperoxan, B38, using HMAS, HMS, HS, HDAS and HDMS as chiral resolving agents. HDAS and HS values are from Ref. [55] and Ref. [56], respectively. The binding strengths follow the order HDAS > HS > HMAS > HMS > HDMS. The effective mobilities span the range -32 to -2 mobility units at low SISCD concentrations. The separation selectivity values are at all concentrations best when using HDMS as chiral resolving agent.

Typically, the trend is for the di-acetyl substituted CD's to exhibit stronger intermolecular interactions compared to the di-hydroxy substituted CD's which exhibit stronger intermolecular interactions compared to the di-methyl substituted CD's. HMAS and HMS are intermediate in the trend since they possess one acetyl or one hydroxy group and one methyl group. Exceptions to the trend are numerous with one example being terbutaline, B47. The effective mobility (top panel) and separation selectivity plots for B47 are shown in Figure 52 using HMAS, HMS, HS, HDAS and HDMS as chiral resolving agents. HDAS and HS values are from Ref. [55] and Ref. [56], respectively. Unlike the trend observed for B38, the binding strengths follow the order HMAS > HMS > HS > HDAS > HDMS. The effective mobilities span the ranged -26 to +8 mobility units at low SISCD concentrations. The separation selectivity values are good at low HMAS, HMS, HS and HDAS concentrations, but best at higher HDMS concentrations.
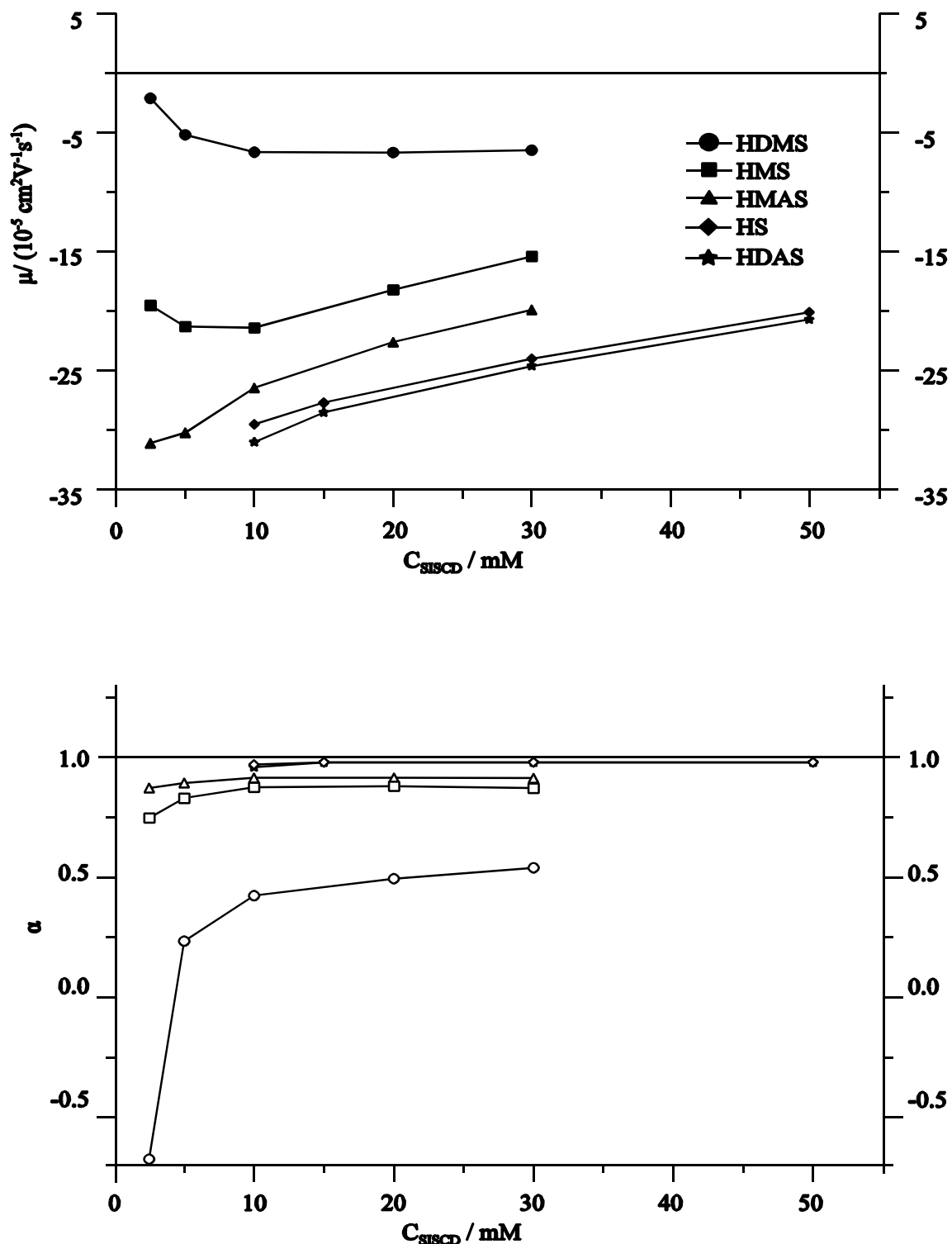
Figure 51. Effective mobilities (top) and separation selectivities (bottom) of B38 in pH 2.5 aqueous BGE's with HDAS (star), HS (diamond), HMAS (triangle), HMS (square) and HDMS (circle). Value in absence of SISCD is 19.4 mobility units but is omitted for clarity.
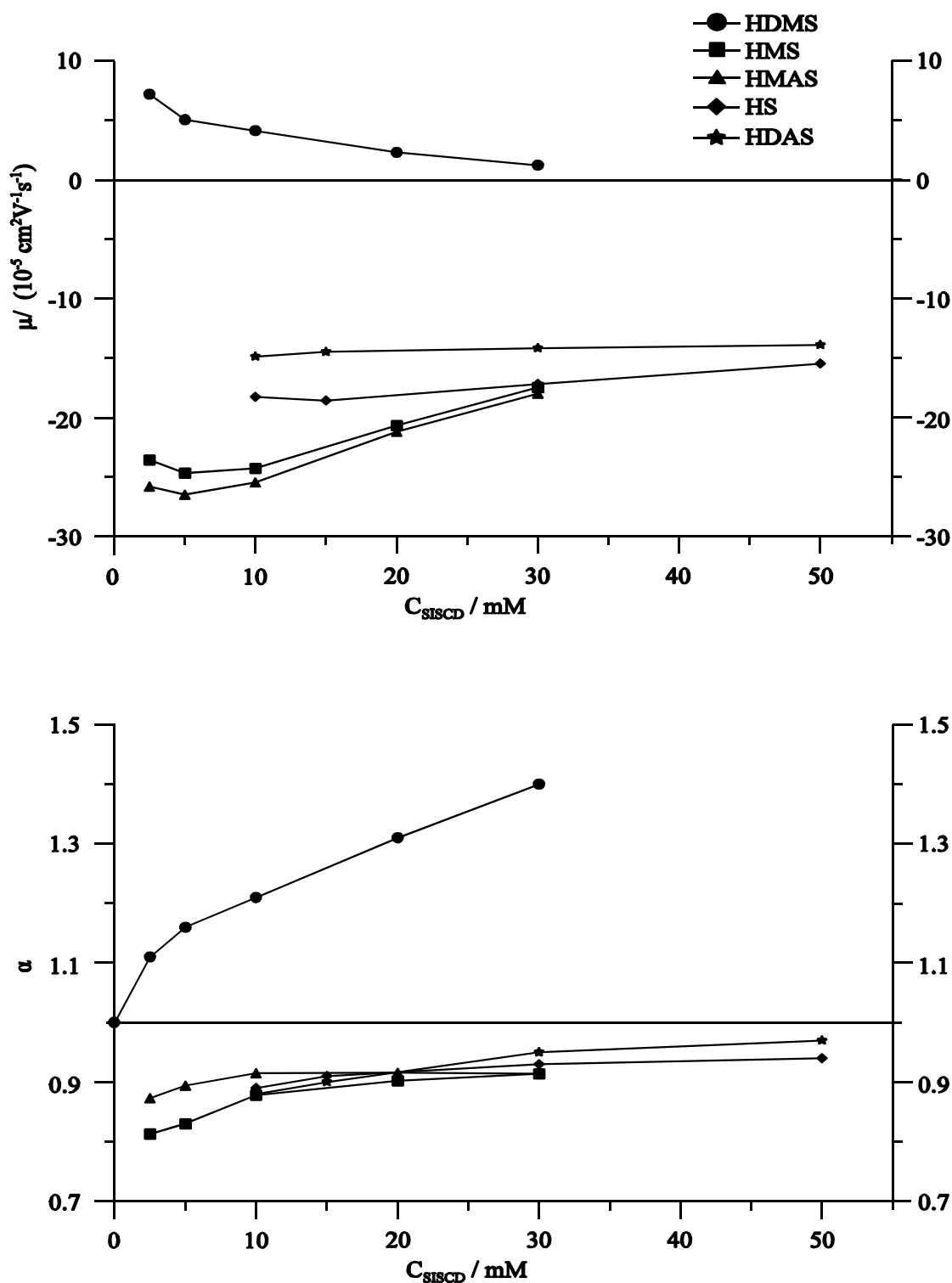
Figure 52. Effective mobilities (top) and separation selectivities (bottom) of B47 in pH 2.5 aqueous BGE's with HDAS (star), HS (diamond), HMAS (triangle), HMS (square) and HDMS (square). Value in absence of SISCD is 16.5 mobility units but is omitted for clarity.

Because of favorable β values and good separation selectivity, peak resolution values for the enantiomers of B47 were 6 and 2 at 2.5 mM HMAS and HMS, respectively.

3.7 Acidic Methanolic Separations Using HMS as Chiral Selector

The changes in effective mobilities and separation selectivities with changing BGE solvent is a compelling reason to conduct separations trials in both aqueous and methanolic BGE's despite the fact that sulfated cyclodextrins with non-acetylated and non-methylated C2 and C3 hydroxy groups do not work very well in methanol. Since HMS was available, studies were conducted to evaluate its utility in acidic methanolic BGE's. HMS-containing acidic methanolic BGE's were used to study the effective mobility and separation selectivity patterns obtained for the 24 weak base analytes. Only 12 of the analytes showed separation selectivity different from unity and four were baseline resolved including, B06, B09, B13 and B34. The useful HMS concentration range was only up to and including 10 mM HMS. Higher concentrations were found to produce solutions with viscosities too high to be useful as CE BGE's. In this respect, HMS proved ill-suited for resolving agent in acidic methanolic BGE's.

Table 4 lists the effective mobilities of the less mobile enantiomers, μ, the separation selectivities, α, the peak resolution, Rs, the normalized EOF mobility values, β, and the injector-to-detector potential drop, U values, obtained in the acidic methanolic BGE's for the weakly basic enantiomers. An entry of N/A implies that a value could not be calculated because of overlap with a non-comigrating system peak or overlap with the neutral marker or anionic mobility marker.

Table 4. Separations data in acidic methanol HMS BGE's (μ, in $10^{-5}cm^2/Vs$ units).

[HMS]	0 mM*	2.5 mM			
U (kV)	19.3	19.3			
Analyte	μ	μ	α	β	Rs
B04	23.0	1.1	1.00	106	0.0
B06	23.0	-12.8	0.81	-1.1	3.8
B09	21.2	-13.9	1.00	-10	0.0
B11	26.2	15.7	1.00	0.92	0.0
B13	24.5	-7.6	0.23	-1.8	2.1
B14	16.5	4.4	1.00	3.4	0.0
B19	14.0	-4.9	1.00	-3.0	0.0
B21	22.1	7.0	1.00	2.1	0.0
B22	25.6	12.8	1.00	1.1	0.0
B23	7.6	-5.4	1.00	-2.6	0.0
B26	19.3	1.2	1.00	10	0.0
B28	27.8	14.1	1.00	1.1	0.0
B30	18.3	7.3	1.00	2.2	0.0
B34	23.4	4.6	1.00	3.0	0.0
B38	19.3		N/A		
B39	26.5	0.5	2.02	29	0.0
B42	20.1	7.2	1.00	2.2	0.0
B46	16.1	-0.5	1.00	-30	0.0
B47	17.8	8.5	1.00	8.8	0.0
B56	14.4	1.6	1.00	8.8	0.0
B57	15.8	-1.2	1.00	-13.5	0.0
B60	26.3	9.6	1.00	1.7	0.0
B61	25.4	-1.4	0.28	1.6	-9.6

Table 4. Continued.

[HMS]	5 mM				10 mM			
U (kV)	19.3				19.3			
Analyte	μ	α	β	Rs	μ	α	β	Rs
B04	-2.4	1.00	-5.8	0.0	-3.3	1.00	-4.1	0.0
B06	-12.8	0.90	-1.1	7.7	-12.1	0.91	-1.2	3.0
B09	-2.7	1.00	-5.0	0.0	-4.0	0.81	-3.0	3.3
B11	13.5	1.00	1.0	0.0	12.7	1.00	1.2	0.0
B13	-7.7	0.39	-1.9	9.8	-7.8	0.38	-2.0	9.7
B14	3.6	1.00	3.8	0.0	3.4	1.00	4.4	0.0
B19	-4.9	1.00	-3.1	0.0	-4.2	0.94	-3.6	0.6
B21	6.5	1.00	2.3	0.0	5.3	1.00	2.7	0.0
B22	11.9	1.00	1.3	0.0	10.3	1.00	1.4	0.0
B23	-6.0	1.00	-2.4	0.0	-6.4	0.96	-2.1	0.8
B26	-3.9	0.76	-3.5	0.9	-2.6	0.76	-4.7	1.4
B28	10.4	1.00	1.4	0.0	8.5	1.05	1.5	<0.5
B30	5.3	1.00	2.8	0.0	4.3	1.00	2.9	0.0
B34		N/A			-1.4	0.52	-9.0	1.7
B38		N/A				N/A		
B39	-0.3	-2.08	2.6	-60	-0.6	-0.63	-24	3.9
B42	4.7	1.00	3.3	0.0	3.6	1.06	3.8	<0.5
B46	-1.6	1.00	-9.5	0.0	-3.2	1.00	-4.3	0.0
B47	6.6	1.00	2.3	0.0	5.4	1.00	2.6	0.0
B56	1.1	1.00	14	0.0	0.9	1.00	15	00
B57	-14.2	1.00	2.2	0.0	-2.1	1.00	-6.5	0.0
B60	6.7	1.00	2.2	0.0	4.8	1.00	2.8	0.0
B61	-7.8	0.74	-1.9	1.8	-7.6	0.84	-1.6	1.3

* From Ref. [47].

All separations were carried out within the linear region of Ohm's law with applied potentials at 26 kV in all of the HMS-containing BGE's. Over the 2.5 to 10 mM HMS concentration range, the μ^{EOF} was as high as 16 mobility units in the 2.5 mM HMAS-containing BGE's, but decreased with increasing HMS concentration to as low as 12 mobility units in the 10 mM HMS-containing BGE's. Decreasing EOF with increasing HMS concentration is as expected due to higher BGE viscosity.

The change in effective mobility of the weak bases with changing HMS concentration in acidic methanol BGE's showed weakly binding, moderately strongly binding and strongly binding trends. In general, binding strengths were much weaker in the methanolic HMS BGE's than in the aqueous HMS BGE's thus, β values were less favorable for resolution. Exceptions were the same four analytes that showed baseline resolution in the methanolic HMS BGE's. Trends in the α curves were similar to those observed previously for the 12 analytes showing some separation selectivity.

3.8 Summary

The first two unsymmetrically substituted single-isomer, sulfated β-CD's, the sodium salts of HMAS and HMS have been used to study the effective mobility and separation selectivity patterns of the enantiomers of 24 weak base pharmaceutical compounds in acidic aqueous BGE's. The study also included successful use of HMAS in acidic methanol BGE's, while HMS in the same BGE's proved far less useful. The trends observed in all cases followed closely the predictions of the CHARM model. Use of HMAS and HMS provided differences in effective mobility and separation

selectivities that were often complimentary to those for the same analytes using other

sulfated β-CD's. Finally, HMAS and HMS proved to be broadly useful to achieve

enantiomer resolutions of a combined 21 of 24 weak base analytes between the two.

CHAPTER IV

CONCLUSIONS

HMAS and HMS are SISCD's that are unsymmetrically substituted at the C2 and C3 positions of the glucopyranose subunits. The synthetic methodology used to produce these new derivatives utilized highly regioselective, orthogonally deprotectable, organosilicon chemistry to allow per-modification at the C2 positions only. This was made possible by first protecting the C6 positions with TBS followed by protection of the C2 positions with a TES group. The first step has long been used as a means to bi-functionalized SISCD's where the C2 and C2 positions are modified in a "one-pot" reaction with either methyl or acetyl groups. This technique has been applied to produce nine different SISCD's from three kinds of cyclodextrins, α-, β- and γ- CD's. The other three SISCD's are produced by hydrolysis of the acetyl group following sulfation of the C6 positions.

The TBS protecting group has long been a staple to those desiring new, useful cyclodextrin derivatives. Until now, other organosilicon protecting groups have received little attention because only the bulkiest offer the necessary regioselectivity. The problem of furthering cyclodextrin chemistry has been, in part, the lack of similarly highly regioselective deprotection methods that would distinguish between different, sterically hindered organosilicon protecting groups such as TES, TIPS (triisopropylsilyl), TBS and the diphenyl version, TBDPS. Development of novel reaction conditions utilizing imidazolium chloride to remove a TES protecting group at the C3 positions without

deprotection of the TBS protecting group at the C6 positions allowed for the first time per-modification of the C2 positions without concurrent modification of the C3 or C6 positions.

The TBS protection of C6, TES protection of C2, methylation of C2 (TES migrates to C3), and removal of the TES group to expose the C3 hydroxy groups have been scaled to 2 kg, 1 kg, 0.5 kg and 1 kg, respectively. Conversion rates for the TBS protection step were lowest at 83% with all others in excess of 96%. Yields after purification were lowest for the TBS protection and TES deprotection steps with 70% and 76%, respectively. All others were in excess of 90% yields with the TES protection step highest at 96% yield. Purification of each intermediate was accomplished using suitable recrystallization solvents.

Subsequent synthetic transformations began with acetylation of the C2 hydroxy groups, TBS deprotection and sulfation of the now exposed C6 hydroxy groups to produce HMAS. Hydrolysis of the C3 acetyl groups provided HMS. The acetylation reaction proceeded slowly with 96% conversion, the major impurity being a desilylation product as verified by MALDI-TOF MS. The deprotection, sulfation and deacetylation reactions were much faster and proceeded with 99% conversion for the deprotection step and > 97% for the sulfation and deacetylation reactions. Yields after purification were > 90% for all but the deacetylation reaction which gave only 65% yield after a costly recrystallization step. The TBS deprotection and sulfation products were purified by more efficient recrystallization methods. The acetylation product was purified using a counter-current DMF/hexanes extraction process.

Each synthetic product was characterized as to purity using either HPLC-ELSD for the non-ionic intermediates or indirect-UV CE detection for final ionic products, HMAS and HMS. One and two-dimensional ^{1}H and ^{13}C NMR and MALDI-TOF MS was used to structurally characterize each intermediate. Also, X-ray crystallography was used to confirm the expected substitution pattern.

HMAS and HMS were used to study the separation selectivity and effective mobility trends for a set of 24 pharmaceutically active weak base enantiomers. The BGE's were simple 25 mM phosphoric acid solution buffered to pH 2.5. The capillary was uncoated, bare fused silica and applied potentials were kept at maximums dictated by the linear region of Ohm's Law plots. The effective mobility trends for the weak bases agreed well with the predictions of the CHARM model as did the separation selectivity curves. All three categories of binding strengths described in the literature were observed. Most analytes fell into the strongly binding category in both aqueous and methanolic BGE's, though the binding strengths were consistently weaker in the methanolic BGE's.

Binding strengths were found to be highly dependent on the structures of the analytes and chiral resolving agent. A group of structurally similar catecholamines included in the test set showed that changes in substitution about the aromatic ring can result in dramatic changes in the both the effective mobility and separation selectivity trends. The effect was most prominent in the aqueous HMS-containing BGE's where effective mobilities of the analytes spanned the +5 to -25 mobility unit range at 5 mM HMS. The binding strengths were stronger in the aqueous HMAS BGE's and varied over

only -9 to -31 mobility units. Similar findings resulted from the comparison of the effective mobility and separation selectivity trends of piperoxan and terbutaline in acidic aqueous BGE's using numerous different single-isomer, sulfated β-cyclodextrins. The binding strength of the enantiomers of piperoxan was strongest for HDAS and HS and decreased in the order HDAS > HS > HMAS > HMS > HDMS. The binding strengths of the enantiomers of terbutaline were strongest for HMAS and decreased in the order HMAS > HMS > HS > HDAS > HDMS. The variation in such trends is a driving force for development of new single-isomer, sulfated CD's, since the new CD derivatives will undoubtedly offer different binding strengths and thus different separation selectivities.

In conclusion, the two new chiral resolving agents, HMAS and HMS proved broadly useful and in many cases, complimentary to other sulfated cyclodextrins used for CE separation of the enantiomers of weak bases. HMAS and HMS afforded fast separations with good resolution of 21 of the 24 analytes studied using either aqueous or methanolic BGE's, most in under 10 minutes. The three analytes for which no resolution was observed using either HMAS or HMS included diltiazem, scopolamine and chlorpheniramine. HMS gave poor separation selectivities for most of the analytes included in this study when used in acidic methanol BGE's with the exceptions of chlophedianol and phenylglycinonitrile. The separation selectivities for these two were highest in the methanolic HMS BGE's.

REFERENCES

[1] Schurig, V., *J. Chrom. A* 2001, *906*, 275-299.

[2] Breitinger, H., *Tet Lett.* 2002, *43*(35), 6127-6131.

[3] Mitchell, C., Desai, M., McCulla, R., Jenks, W., Armstrong, D., *Chromatographia* 2002, *56*(3-4), 127-135.

[4] Skrdla, P. J., Robertson, R., Antonucci, V., Lindemann, C., *J. Chrom. Sci.* 2003, *41*(3), 117-122.

[5] Porras, S., Sarmini, K., Fanali, S., Kenndler, E., *Anal Chem.* 2003, *75*(7), 1645-1651.

[6] Fanali, S., Desiderio, C., Olvecka, E., Kaniansky, D., Vojtek, M., et al., *J. High Res. Chrom.* 2000, *23*(9), 531-538.

[7] Gratz, S., Schneiderman, E., Mertens, T., Stalcup, A., *Anal. Chem.* 2001, *73*(16), 3999-4005.

[8] Glukhovskiy, P., Landers, T., Vigh, G.., *Electrophoresis* 2000, *21*(4), 762-766.

[9] Shave, E., Vigh, G., *J. Chrom A* 2003, *989*(1), 73-78.

[10] Schneiderman, E.; Stalcup, A., J. Chrom. B 2000, *745*(1), 83-102.

[11] Szejtli, J., *Chem. Rev.* 1998, *98*(5), 1743-1754.

[12] Bender, M. L., Komiyama, M., *Cyclodextrin Chemistry*, Springer-Verlag, Berlin, 1977, pg. 5.

[13] Williams, B. A., Vigh, G., *J. Chrom. A* 1997, *777*, 295-309.

[14] Vincent, J. B., Vigh, G., *J. Chrom. A* 1998, *817*, 105-111.

[15] O'Keefe, F., Shamsi, S. A., Darcy, R., Warner, I. M., *Anal. Chem.* 1997, *69*, 4773-4782.

[16] Schulte, G., Chankvetadze, B., Blaschke, G., *J. Chrom. A* 1997, *771*, 259-266.

[17] Wang, F., Khaledi, M., *Electrophoresis* 1998, *19*, 2095-2100.

[18] Francotte, E., Brandel, L., Jung, M., *J. Chrom. A* 1997, *792*, 379-384.

[19] Szeman, J., Ganzler, K., Salgo, A., Szejtli, J., *J. Chrom. A* 1996, *728*, 423-431.

[20] Schmitt, Ulrich, Ertan, Mevlut, Holzgrabe, Ulrike, *Electrophoresis* 2004, *25*(16), 2801-2807.

[21] Chankvetadze, B., Lomsadze, K., Bergenthal, D.,Breitkreutz, J., Bergander, K., et. al., *Electrophoresis* 2001, *22*, 3178-3184.

[22] Chankvetadze, B., Pintore, G., Burjanadze, N., Bergenthal, D., Bergander, K., et. al., *J. Chrom. A* 2000, *875,* 455-469.

[23] Sabah, S., Scriba, G., *J. Chrom. A* 1999, *833*, 261-266.

[24] Chankvetadze, B., Schulte, G., Blaschke, G., *Enantiomer* 1997, *2*, 157-159.

[25] Chankvetadze, B., Schulte, G., Blaschke, *J. Chrom. A* 1996, *732*, 183-187.

[26] Jicsinszky, L, Fenyvesi, E., *Cyclodextrin Derivatives in Comprehensive Supramolecular Chemistry*, Vol. 3, Cyclodextrins, Szejtli, J., Osa, T., Eds., Pergamon: Oxford, U.K. 1996, pg 87.

[27] Takeo, K., Uemura, K., Mitoh, H., *J. Carb. Chem.* 1988, *7*, 293-308.

[28] Takeo, K., Sumimoto, T., Kuge, T., *Staerke* 1974, *28*, 111-118.

[29] Kondo, Y., Takeo, K., *Carb. Res.* 1976, *52*, 232-234.

[30] Takeo, K., Kuge, T., *Staerke* 1976, *28*, 226-227.

[31] Takeo, K., Mitoh, H., Uemura, K., *Carb. Res.* 1989, *187*, 203-221.

[32] Fügedi, P., *Carb. Res.* 1989, *192*, 366-369.

[33] Fanali, S., *J. Chrom. A* 2000, *875*, 89-122.

[34] Li, S., Vigh, G., *Electrophoresis* 2004, *25*, 2657-2670.

[35] Cai, H., Nguyen, T., Vigh, G., *Anal. Chem.* 1998, *70*, 580-589.

[36] Vincent, J. B., Sokolowski, A. D., Nguyen, T., Vigh, G., *Anal. Chem.* 1997, *69*, 4226-4233.

[37] Vincent, J. B., Kirby, D. M., Nguyen, T., Vigh, G., *Anal. Chem.* 1997, *69*, 4419-4428.

[38] Li, S., Vigh, G., *J. Chrom. A* 2004, *1051*, 95-101.

[39] Busby, M. B., Maldonado, O., Vigh, G., *Electrophoresis* 2003, *23*, 456-461.

[40] Zhu, W., Vigh, W., *J. Chrom. A* 2000, *892*,499-507.

[41] Tacker, M., Glukhovskij, P., Cai, H., Vigh, G., *Electrophoresis* 1999, *20*, 2794-2798.

[42] Vincent, J. B., Vigh, G., *J. Chrom. A* 1998, *816*, 233-241.

[43] Cai, H., Vigh, G., *J. Chrom. A* 1998, *827*, 121-132.

[44] Li, S., Vigh, G., *Electrophoresis* 2004, *25*, 1201-1210.

[45] Li, S., Vigh, G., *Electrophoresis* 2003, *24*(15), 2487-2498.

[46] Cai, H., Vigh, G., *J. Micr. Col. Sep.* 1998, *10*, 293-299.

[47] Busby, M. B., Lim, P., Vigh, G, *Electrophoresis* 2003, *24*(3), 351-362.

[48] Zhu, W., Vigh, G., *Anal. Chem.* 2000, *72*, 310-317.

[49] Zhu, W., Wu, F., Raushel, F. M., Vigh, G., *J. Chrom. A* 2000, *895*, 247-254.

[50] Zhu, W., Vigh, G., *J. Micr. Col. Sep.* 2000, *12*, 167-171.

[51] Maynard, D. K., Vigh, G., *Electrophoresis* 2001, *22*, 3152-3162.

[52] Reibenspies, J., Maynard, D. K., Kovacs, A. D., Vigh, G., *Carb. Res.* 2000, *328*, 217-227.

[53] Cravotto, G., Palmisano, G., Panza, L., Tagliapietra, S., *J. Carb. Chem.* 2000, *19*, 1235-1245.

[54] Teranishi, K, Ueno, U., *Tet. Let.* 2003, *44* , 4843-4848.

[55] Icheln, D., Gercke, B., Piprek, Y., Mischnik, P., Koenig, W., et. al., *Carb. Res.* 1996, *280*, 237-250.

[56] Bansal, P., Francis, C., Hart, N., Henderson, S., Oakenful, D., et. al., *Aust. J. Chem.* 1998, *51*, 915-923.

[57] Mischnik, P., Lange, M., Gohdes, M., Stein, A., Petzold, K., *Carb. Res.* 1995, *277*, 179-187.

[58] Wren, S. A. C., *J. Chrom. A* 1993, *636*, 57-62.

[59] Wren, S. A. C., Rowe, R. C., *J. Chrom. A* 1993, *635*, 113-118.

[60] Wren, S. A. C., Rowe, R. C., *J. Chrom. A* 1992, *609*, 363-367.

[61] Wren, S. A. C., Rowe, R. C., *J. Chrom. A* 1992, *603*, 235-241.

[62] Rawjee, Y. Y., Staerk, D. U., Vigh, G., *J. Chroma. A* 1993, *635*, 291-306.

[63] Rawjee, Y. Y., Williams, R. L., Vigh, G., *J. Chrom. A* 1993, *652*, 233-245.

[64] Rawjee, Y. Y., Williams, R. L., Vigh, Gy., *J. Chrom. A* 1994, *680*, 599-607.

[65] Tavares, M., McGuffin, V., *Anal. Chem.* 1995, *67*, 3687-3696.

[66] Valkó, I., Sirén, H., Riekkola, M., *J. Micro. Sep.* 1999, *11*, 199-208.

[67] Rawjee, Y. Y., Vigh, G., *Anal. Chem.* 1994, *66*, 619-627.

[68] Williams, B. A., Vigh, G., *J. Chrom. A* 1997, *777*, 295-309.

[69] Zhu, W., Li, W., Raushel, F. M., Vigh, G., *Electrophoresis* 2000, *21*, 3249-3256.

[70] Zhu, W., Vigh, G., *Electrophoresis* 2000, *21*, 2016-2024.

[71] Zhu, W., Vigh, G., *Electrophoresis* 2001, *22*, 1394-1398.

[72] Reijenga, J. C., Kenndler, E., *J. Chrom. A* 1994, *659*, 417-426.

[73] Reijenga, J. C., Kenndler, E., *J. Chrom. A* 1994, *659*, 403-415.

[74] Reijenga, J. C., Verheggen, T., Martens, H., Everaerts, F., *J. Chrom. A* 1996, *744*, 147-153.

[75] Friedl, W., Reijenga, J. C., Kenndler, E., *J. Chrom. A* 1995, *709*, 163-170.

[76] Muzikar, J., Rozing, G., Van de Goor, T., Eberwein, C., Kenndler, E., *J. Chrom. A* 2002, *950*, 249-255.

[77] Muzikar, J, Van de Goor, T., Gas, B., Kenndler, E., *Anal. Chem.* 2002, *74*, 428-433.

[78] Muzikar, J., Van de Goor, T., Gas. B., Kenndler, E., *Electrophoresis* 2002, *23*, 375-382.

[79] Porras, S., Kenndler, E., *J. Chrom. A* 2004, *1037*, 455-465.

[80] Porras, S., Riekkola, M., Kenndler, E., *Electrophoresis* 2001, *22*, 3798-3804.

[81] Roy, K., Lucy, C., *Electrophoresis* 2003, *24*, 370-379.

[82] Sarmini, K., Kenndler, E., *J. Chrom. A* 1999, *833*, 245-259.

[83] Porras, S., Kenndler, E., *Electrophoresis* 2004, *25*, 2946-2958.

[84] Porras, S., Riekkola, M., Kenndler, E., *Electrophoresis* 2003, *24*, 1485-1498.

[85] Beckers, J. L., Ackermans, M. T., Bocek, P., *Electrophoresis* 2003, *24*, 1544-1552.

[86] Roy, K., Lucy, C., *J. Chrom. A* 2002, *964*, 213-225.

[87] Roy, K., Lucy, C., *Electrophoresis* 2002, *23*, 383-392.

[88] Roy, K., Lucy, C., *Anal. Chem.* 2001, *73*, 3854-3861.

[89] Porras, S., Marziali, E., Gas, B., Kenndler, E., *Electrophoresis* 2003, *24*, 1553-1564.

[90] Rathore, A. S., *J. Chrom. A* 2004, *1037*, 431-443.

[91] Muzikar, J., Van de Goor, T., Kenndler, E., *Anal. Chem.* 2002, *74*, 434-439.

[92] Tang, G. Y., Yang, C., Chai, J. C., Gong, H. Q., *Inter. J. Heat and Mass Trans.* 2003, *47*, 215-227.

[93] Palonen, S., Jussila, M. Porras, S., Hyotylainen, T., Riekkola, M., *J. Chrom. A* 2001, *916*, 889-99.

[94] Veraart, J. R., Gooijer, C., Lingeman, H., *Chromatographia* 1997, *44*, 129-134.

[95] Williams, B., Vigh, G., *Anal. Chem.* 1997, *69*, 4410-4418.

APPENDIX A

LETTER OF COPYRIGHT CREDIT

Sheik Safdar
14.01.2005 16:46

An: Claudia Jerke/VCH/Wiley@Wiley
Kopie: busby@mail.chem.tamu.edu
Thema: Fw: Republication/Electronic Request Form

Hi Claudia,

Please find below a request for you to handle.

Thanks.

Sheik Safdar
Administrative Assistant
John Wiley & Sons, Inc.
111 River Street/ Mail Stop: 3-05
Hoboken, NJ 07030
PH: 201.748.6512
FAX: 201.748.6008
www.wiley.com/go/permissions
----- Forwarded by Sheik Safdar/Corp/Hoboken/Wiley on 01/14/2005 10:45 AM -----

republication
<republication@wiley.com>
01/13/2005 06:20 PM

Please respond to
republication
<republication@wiley.com>

To <republication@wiley.com>

cc

Subject Republication/Electronic Request Form

A01_First_Name: Brent
A02_Last_Name: Busby
A03_Company_Name: Texas A&M University
A04_Address: Texas A&M University
A05_City: College Station
A06_State: TX
A07_Zip: 77843-3255
A08_Country: USA
A09_Contact_Phone_Number: 979-845-3777
A10_Fax: 979-845-4719
A11_Emails: busby@mail.chem.tamu.edu
A12_Reference:
A13_Book_Title: Electrophoresis
A40_Book_or_Journal: Journal
A14_Book_Author:
A15_Book_ISBN:
A16_Journal_Month:
A17_Journal_Year: 2001
A18_Journal_Volume: 22
A19_Journal_Issue_Number: 15
A20_Copy_Pages: 3160-botom right panel of figure 8
A21_Maximum_Copies: one time
A22_Your_Publisher: Teaxs A&M University
A23_Your_Title: Two new, single-isomer, sulfated beta cyclodextrins for use
as chiral resolving agents in CE
A24_Publication_Date: May 2005
A25_Format: print
A31_Print_Run_Size:
A41_Ebook_Reader_Type:
A26_If_WWW_URL:
A27_If_WWW_From_Adopted_Book: No
A28_If_WWW_Password_Access: No
A43_WWW_Professor_Name:
A44_WWW_Course_Name_Number:
A45_WWW_Users:

We hereby grant permission for the requested
use expected that due credit is given to the
original source. Please note that the author's
permission is also required.

WILEY-VCH, STM-Copyright & Licenses

C. Jerke

Weinheim, January 13, 2005

APPENDIX B

SYNTHESIS PROTOCOL FOR HMAS AND HMS

Heptakis(2-O-triethylsilyl-6-O-t-butyldimethylsilyl)cyclomaltoheptaose **(3)**.- To a mechanically stirred, sealed reaction vessel containing a solution of dry **(2)** (1.0 kg) and imidazole (284.5 g) in dry THF (2 L), then add drop-wise over a 4 hr period TESCl (600 g) in EtOAc (1 L). Add imidazole (5.1 g) to the THF/EtOAc mixture add drop-wise over a 10 min period TESCl (10.9 g) in EtOAC (20 mL). Repeat this last step until the relative area of the undersilylated side-product is lower than 0.5% as measured by RP-HPLC-ELSD (gradient elution 50:50 MeOH:EtOAc to 0:100 MeOH:EtOAC in 15 min at 2 mL/min). Filter the imidazolium chloride and wash with 2 x 250 mL EtOAc. Remove the solvent under reduced pressure to obtain a white solid. Slurry the crude product in refluxing acetone (5 L) for 1 hr. Allow to cool to room temperature and filter to obtain a white solid. Repeat the refluxing slurrying step two more times or until the isomeric purity is >99.5% as measured by RP-HPLC-ELSD. Dry the purified product in 100°C vacuum oven to a constant weight. Typical yield is 96%.

*Heptakis(2-O-methyl-3-O-triethylsilyl-6-O-t-butyldimethylsilyl)cyclomalto heptaose***(4)**.- To a mechanically stirred, sealed reaction vessel containing dry NaH (33.8 g) in THF (0.2 L) add, over a 45 min period, a solution of **(3)** (0.5 kg) and CH_3I (104 mL) in THF (1 L) and stir for 4 hr while monitoring completion of the reaction by RP-HPLC-ELSD (30:70 MeOH: EtOAc at 2 mL/min). Add anhydrous ethanol (50 mL) to quench. Allow the reaction mixture to stir for 30 min and add hexanes (85%, 1.2 L). Extract with 2 x1.2 L water. Back extract the water layers with 2 x 200 mL hexanes. Combine the hexanes layers and remove the solvent under reduced pressure. Slurry the crude product in refluxing acetone (3 L) for 30 min. Allow the slurry to cool to room

temperature and filter to obtain a white solid. Repeat the refluxing slurrying step 5-6

times or until the isomeric purity is >99.5 % as measured by RP-HPLC-ELSD. Dry the

product in an 80°C vacuum oven to a constant weight.

Heptakis(2-O-methyl-6-O-t-butyldimethyl)cyclomaltoheptaose **(5)**.- To a sealed,

mechanically stirred reaction vessel containing dry imidazolium chloride (413.5 g) in a

35% v/v MeOH in THF, prepared by mixing 3.6 L anhydrous MeOH and 6.7 L

anhydrous THF, add **(4)** (1 kg) and stir in a 60°C water bath for 4 hrs. Monitor the

reaction by RP-HPLC-ELSD (gradient elution 50:50 MeOH: EtOAc to 0:100

MeOH:EtOAc in 10 min at 2 mL/min). Typical reaction times are 6 hrs. Remove the

solvent under reduced pressure to obtain a white solid. Redissolve the crude in EtOAc (1

L) and filter the imidazolium chloride. Wash the filter cake with 2 x 250 mL EtOAc.

Combine with washes with the filtrate and in a magnetically stirring beaker add MeOH

(3 L). Allow to stir for 3 hr to complete recrystallization. Filter the white solid and repeat

the recrystallization step until isomeric purity is >99.5% as measured by RP-HPLC-

ELSD. Typical yields are 91%. Dry the product in a 110°C vacuum oven to a constant

weight.

Heptakis(2-O-methyl-3-O-acetyl-6-O-t-butyldimethylsilyl)cyclomaltoheptaose

(6).- To a sealed, magnetically stirred reaction vessel containing pyridine (0.5 L), add **(5)**

and continue to stir until it dissolves. Add acetic anhydride (325 mL) and stir for 30 hrs

suspended in a 50°C bath. Monitor the reaction using RP-HPLC-ELSD (45:55

MeOH:EtOAc isocratic mobile phase at 2 mL/min) and NP-HPLC-ELSD (95:5

$CHCl_3$:MeOH to 0:100 $CHCl_3$:MeOH in 7 min with 2 mL/min flow rate). Typical

reaction times are 48-52 hr. After the reaction period is complete, remove the solvent and acetic anhydride under reduced pressure to obtain the crude product. Extract in a counter-current process using 1% v/v water in DMF and hexanes (85%). The target will accumulate in the hexanes layer. Remove the hexanes from the product under reduced pressure to obtain the product with >99.5% isomeric purity. Typical yield is 90%. Dry the material in an 80°C vacuum oven to a constant weight.

Heptakis(2-O-methyl-3-O-acetyl)cyclomaltoheptaose (**7**).- To a sealed, magnetically stirred reaction vessel containing MeOH (1 L) add hydrofluoric acid (48% in water, 54.5 mL) and suspend in a 50°C bath. Add (**6**) (0.5 kg) and sodium fluoride (15.3 g). Not all NaF will dissolve. Monitor progress of the reaction using RP-HPLC-ELSD (gradient mobile phase 5:95 $THF:H_2O$ to 25:75 $THF:H_2O$ in 12 min then to 0:100 $THF:H_2O$ in 10 min at 2mL/min). Typical reaction times are 52-59 hr. After the reaction period, filter the excess NaF and remove the solvent under reduced pressure. Redissolve the white solid in dichloromethane (1.2 L) and filter the remaining sodium fluoride. Slurry the crude product in refluxing diethyl ether (1.5 L) for 1 hr. Filter the product and repeat the refluxing slurrying 4-5 times or until all TBS fluoride is removed as indicated by ^{1}H-NMR.

Heptakis(2-methyl-3-O-acetyl-6-O-sulfo)cyclomaltoheptaose (**8**).- To a sealed, magnetically stirred reaction vessel containing dimethylformamide (300 mL) and (**7**) (200 g) add sulfur trioxide-pyridine complex (175.1 g) and stir for 30 min. Monitor the reaction progress using indirect-UV CE (30 mM β-alanine titrated to pH=3.5 with para-toluenesulfonic acid, polarity is (+) to (-) at 20 kV, capillary is 46 cm long, 39 cm to

detector, detector at 214 nm). Typical reaction times are 1 hr. Slowly add a slurry of sodium bicarbonate (194 g) in water (200 mL). Remove the solvent under reduced pressure. Dissolve the crude product in MeOH (200 mL) and filter the Na_2SO_4 by-product. Precipitate the product by pouring the filtrate into diethyl ether (700 mL) and filter to obtain a white solid. Repeat the precipitation step 6-8 times or until DMF removal is complete as indicated by ^{1}H-NMR. Typical yield is 94%. Dry the product in an 80°C vacuum oven to a constant weight.

       Heptakis(2-O-methyl-6-O-sulfo)cyclomaltoheptaose **(9)**.- To a 1 L round bottom flask equipped with a magnetic stir bar containing **(8)** (100 g) in water (250 mL), add sodium hydroxide in water (32.6 mL), drop-wise, over a 30 min period. Stir for 1 hr. Monitor the reaction progress using indirect-UV CE (30 mM β-alanine titrated to pH=3.5 with para-toluenesulfonic acid, polarity is (+) to (-) at 20 kV, capillary is 46 cm long, 39 cm to detector, detector at 214 nm). Reduce the contents of the flask to approximately 100 mL in volume under reduced pressure. Precipitate the product by pouring the contents of the flask in isopropanol (500 mL). Filter the precipitate quickly, before the sodium acetate precipitates. Repeat the precipitation step 4 times or until CE indicates that all sodium acetate has been removed. Typical yield is 65%, with isomeric purity >98%.

VITA

Michael Brent Busby received his Ph.D. in chemistry from Texas A&M University in May 2005 where he attended as a graduate student under the direction of Dr. Gyula Vigh from 1998 to 2005. A portion of this time was spent working toward his Master of Science degree in chemistry, also under the direction of Dr. Vigh, which he earned in August 2002. Prior, Brent earned a Bachelor of Science degree in chemistry in May 1998, from the University of Texas at Tyler where he attended from 1995 to 1998. Also, he earned an Associate of Arts and Sciences degree from Tyler Junior College where he attended from 1991 to 1995.

Brent can be reached at his permanent address: 12360 Pioneer Dr., Tyler, TX 75704.